General Disclaimer

One or more of the Following Statements may affect this Document

- This document has been reproduced from the best copy furnished by the organizational source. It is being released in the interest of making available as much information as possible.

- This document may contain data, which exceeds the sheet parameters. It was furnished in this condition by the organizational source and is the best copy available.

- This document may contain tone-on-tone or color graphs, charts and/or pictures, which have been reproduced in black and white.

- This document is paginated as submitted by the original source.

- Portions of this document are not fully legible due to the historical nature of some of the material. However, it is the best reproduction available from the original submission.

DRA

FINAL REPORT OF RESEARCH

Performed Under NASA Grant No. NAGW-14

DEVELOPMENT OF A MERCURIC IODIDE SOLID STATE SPECTROMETER FOR X-RAY ASTRONOMY

September 1983

(NASA-CR-175330) DEVELOPMENT OF A MERCURIC IODIDE SOLID STATE SPECTROMETER FOR X-RAY ASTRONOMY Final Report (Massachusetts Inst. of Tech.) 139 p HC A07/MF A01 CSCL 03A

N84-16096

Unclas
G3/89 15150

FINAL REPORT OF RESEARCH

Performed Under NASA Grant No. NAGW-14

DEVELOPMENT OF A MERCURIC IODIDE SOLID STATE SPECTROMETER FOR X-RAY ASTRONOMY

Prepared for

NASA Headquarters

By

Dr. John B. Vallerga

For

Dr. George R. Ricker

INTRODUCTION

Since its beginning in 1962 with the discovery of Sco X-1, the science of X-ray astronomy has progressed by placing X-ray photon detectors above the atmosphere in rockets, balloons and satellites. This usually involves modifying the detectors to withstand extreme environments and payload constraints (size and weight). The goal has always been to increase the sensitivity of the detectors (signal to background ratio) either by increasing the effective collecting area and/or observing times while decreasing the background counting rate. Each new detector technology that is applied to X-ray astronomy must be reoptimized to achieve these goals using widely different strategies.

In the last few years, the balloon lab at the Center for Space Research at MIT has been studying mercuric iodide (HgI_2), a solid state room temperature X-ray detector, for use in hard X-ray astronomy. Its primary advantages are its good energy resolution at room temperatures and a large photon cross section. Much work has been done to characterize the properties of HgI_2 that affect the operation of these detectors for use in X-ray astronomy. The goal of this program has been to develop space and balloon qualified HgI_2 detectors.

Previous to this development effort, the balloon group flew large area balloon-borne arrays of scintillation detectors to observe hard X-ray astronomical sources. On May 8, 1980, a balloon gondola containing a 1500 cm^2 array of phoswich scintillation detectors was flown from Palestine, Texas. This gondola, built at MIT at the balloon lab in collaboration with the Cosmic Ray Working Group at Leiden University, was the most sensitive astronomical hard X-ray (20-240 keV)

detector in existence. After 16 hours of very high quality observations, the gondola free-fell from 38 kilometers and was destroyed (the data were telemetered to the ground and not lost). The destruction of this instrument was the impetus for accelerating the development of mercuric iodide for astronomical applications to replace the 1500 cm^2 array with an instrument of comparable sensitivity to faint hard X-ray sources.

The replacement gondola proposed was a collection of 4 Bragg diffraction X-ray concentrators that increase the effective area of 4 well-shielded, low background mercuric iodide detectors. Calculations show that this new gondola detector system can match the sensitivity of the old 1500 cm^2 array if the assumed background count rate at balloon float altitudes (crudely scaled from that of germanium detectors in orbit) is correct. In the work reported here a prototype detector inside a small balloon-borne gondola has been constructed and flown at balloon altitudes in order to test these calculations. The measured background count rate results were then used to confirm detector models that can be used to predict and optimize the background of future detector geometries.

DEVELOPMENT OF NEW TYPES OF DETECTORS FOR ASTRONOMICAL WORK

The ideal detector for hard X-ray astronomy would have excellent resolution, high efficiency, large area and be lightweight (including support equipment, i.e. cryogenics). This "dream" detector does not exist though most systems in use satisfy some of the requirements. The standard detector for astronomical hard X-rays has been large area NaI scintillation crystals that operate at ambient temperatures but with limited energy resolution (17% FWHM at 60 keV). The semiconductor detectors such as germanium have recently achieved respectable areas ($\sim$60 cm^2) yet their lower efficiencies require thicker detectors which increase the background counting rate. Also the requirement for cryogenic temperatures has limited their satellite lifetime to ~1 year.

Mercuric Iodide Detectors

Mercuric iodide (HgI_2) solid state X-ray detectors have many unique advantages in their application to X-ray astronomy. HgI_2 detectors operate at room temperature so that bulky and massive cryogenic coolers are not required. HgI_2 detectors also combine a high quantum efficiency with good energy resolution. Because of the excellent quantum efficiency (due to the high effective atomic number of HgI_2) background contributions which scale as the thickness of the detector (e.g. those due to neutrons and gamma rays) are lower than for other hard X-ray detectors with equivalent stopping power. At this time the largest area single detector that can be made is only 1 cm^2, so it is far from being ideal. Nonetheless, its properties are well matched to a scheme that increases the effective area using a Bragg diffraction concentrator.

Experimental Development for Astronomical Use

Mercuric iodide has been under development for ten years, and the balloon lab at the Center for Space Research at MIT has had a working experience with these detectors since 1979. The first use of HgI_2 in an astronomical instrument was a small array of 12 detectors with a combined area of 8 cm^2 constructed here at the balloon lab at MIT and flown in a small balloon-borne gondola in June, 1980. Though the background counting rate at float was high because of a less than optimum design, the instrument was able to set an upper limit to the hard X-ray flux of Cygnus X-1 in the "high state" (Ogawara et al 1982)

HgI_2 detectors can still be considered "experimental" in that they cannot be acquired commercially and each detector is in some way unique. In work carried out by the MIT balloon group, the HgI_2 crystals have been subjected to extensive field testing. They have been exposed to extreme variations in temperature, pressure, humidity, voltage, light level and handling. As might be expected with an experimental material, HgI_2 did not always pass with flying colors. However, from this experience, general procedures for handling and environmental limitations have been developed to extend the operating life and reproducibility of results necessary for a field detector.

Because of its relative softness, the direct handling of HgI_2 crystals that have been cleaved from the large 20 cm^3 parent crystal must be minimized. The "thick" crystals (~300-1000 microns) used at the balloon lab for hard X-rays have all been acquired from EG&G, Santa Barbara. The crystals are fabricated into detectors with evaporated palladium electrodes, mounted on ceramic or plastic substrates and

encapsulated with Dow Corning 3140 RTV. The typical area of these detectors is 1 cm^2 with energy resolution ranging from 2.8 to 15 keV FWHM at 60 keV. A typical energy resolution would be 4 keV at 60 keV. The area limitation requires many detectors in an array to achieve an astronomically useful collecting area (~100 cm^2). Such an array would also require 100 measurement chains (100 preamps + voltage amplifiers) as well as existing crystal growers to produce high resolution uniform detectors in quantity. Until the detector area can be made larger, some method of concentrating X-rays must be used to increase the effective area.

In the laboratory the detectors must be kept clean and dry. Small amounts of water and contaminants (dirt, solder flux, etc.) create current leakage paths that increase the overall RMS noise and small intermittent current pulses similar to a relaxation oscillator. Encapsulated detectors should not be exposed to vacuum because trapped air pockets will expand and strain the crystalline lattice, thus ruining the charge transport properties.

The temperature effects are striking for some crystals and unnoticeable with others. The mobility increases with lower temperatures for both electron and holes, but the mean lifetime of an electron or hole before it is trapped by the lattice decreases with decreasing temperature. These competing processes determine a temperature where the resolution is best (i.e. the mean free path, $\lambda=\mu\tau\xi$, is maximized) and is a function of the quality and purity of the crystal. Empirically, this temperature is between -20°C and 20°C, varying with detector (Ricker 1982). These temperatures are easily achieved at

balloon altitudes or on satellites by passive (radiative) or active (thermoelectric) techniques. Higher temperatures decrease the mobility and also produce a prohibitive leakage current which can saturate DC coupled preamplifiers.

The bias voltage across the HgI_2 must be applied slowly to avoid large induced currents. After the bias voltage is applied, the detector "warms up" over a time period of ~1 minute to 1 hour depending on the crystal. The pulse height for a given incident energy increases and the resolution improves. This can be interpreted as an increase in the depletion region as the deep traps (energy levels in the forbidden region caused by impurities) are emptied by the large electric field. Resolution usually improves with increasing electric field until the leakage current becomes too large. Also, high electric field strengths increase the chance for surface breakdown which intermittently injects current pulses into the preamp and shows up as low energy events. The frequency of occurrence of this "current injection noise" increases with applied voltage.

Many HgI_2 detectors perished in the balloon lab due to different types of abuse. However, by minimizing any handling that would stress the crystal and by keeping the detector in a clean, cool and dry assembly, it was possible to produce a stable and dependable operating HgI_2 X-ray detector.

RESULTS AND CONCLUSIONS

Previous to the research work described here, HgI_2 showed great theoretical potential for use in hard X-ray astronomy. The combination of high energy resolution at room temperature plus a high photon quantum efficiency seemed ideal for many balloon and satellite detector applications. Yet, experience in the field operation of HgI_2 was minimal and background count rate information at high altitudes did not exist. Development of HgI_2 specifically for use as an astronomical X-ray detector here at MIT over the last 4 years has changed this situation. Procedures for handling and packaging detectors have been developed that produce stable and dependable HgI_2 detectors for use in the field. HgI_2 detector assemblies have been constructed and flown at balloon altitudes and the detectors operated flawlessly on all occasions.

A major limitation to the application of HgI_2 in X-ray astronomy is the inability to fabricate individual detectors larger than ~1 cm^2. A scheme to overcome this limitation involves the use of X-ray concentrators to increase the effective area of a shielded, low-background HgI_2 detector. The concentrator consists of a paraboloid shell lined with lithium fluoride crystals that Bragg diffract on-axis incoming X-rays to the focus of the paraboloid, where a small area detector is located. To establish the expected sensitivity of this concentrator /detector design, the background counting rate of the shielded HgI_2 detector at balloon altitudes had to be determined. A balloon-borne gondola containing a prototype detector assembly was designed and constructed to measure this background rate. The prototype detector

consisted of thin HgI_2 detectors surrounded by a large bismuth germanate scintillator operated in anticoincidence. This gondola was flown twice in the spring of 1982 from Palestine, Texas.

The second flight of this prototype instrument established a background counting rate for a bismuth germanate-shielded mercuric iodide detector of $4.2 \pm 0.7 \times 10^{-5}$ counts/sec cm^2 keV over the energy range of 40-80 keV. This measurement was within 50% of the predicted value. The prediction was based on a Monte Carlo simulation of the detector assembly in the radiation environment at float altitudes (~40km). The Monte Carlo simulation can now be used to investigate the detector design parameters (geometry, discriminator levels, etc.) to attempt to lower the background rate even further.

Based on a background rate of 4.2×10^{-5} cts/sec cm^2 keV, calculations indicate that with 4 concentrators and 4 detector systems a celestial X-ray source with 1/100 the intensity of the Crab Nebula could be detected in 1.5 hours. This excellent sensitivity is achieved by simultaneously reducing the background by BGO shielding a HgI_2 detector, and increasing the effective area using hard X-ray concentrators.

The prescription for reducing the background rate by a factor of ~10 over previous balloon-borne hard X-ray detectors can be summarized very simply: use very high quantum efficiency detectors shielded by dense, high Z active scintillators. Because they are well suited to this experimental approach, HgI_2 and BGO are both likely to become major detector materials in X-ray astronomy. Furthermore, their ease of handling and improved performance at moderately reduced temperatures enhance their desirability for balloon and satellite use.

PUBLICATIONS

1. Ogawara, Y. et al, X-Ray Observations of the 1980 Cygnus X-1 "High State", 1982, Nature, 295, 675 A82-25479

2. Ricker, G. R. et al, New Measurement of the Fano Factor of Mercuric Iodide, 1982, Rev. Of Scientific Inst., 53, 5. p.700 A82-32721

3. Ricker, G. R., Vallerga, J. V., Wood, D. R., A Mercuric Iodide Detector System for X-ray Astronomy, 1983, Nucl. Inst. and Methods, Vol. 213, #1

4. Vallerga, J. V. et al, A Bismuth Germanate-Shielded Mercuric Iodide X-ray Detector for Space Applications, 1982, IEEE Trans. On Nucl. Sci., Vol. NS-29, #1, p. 151 A82-26111

5. Vallerga, J. V., 1982, "Studies of New Hard X-Ray Detection Methods and Observations of Cosmic X-Ray Sources," Ph.D. Thesis, M.I.T.

6. Vallerga, J. V., Vanderspek, R. K., Ricker, G. R., A Mercuric Detector System for X-Ray Astronomy, 1983, Nucl. Inst. and Methods, Vol. 213, #1

Submitted to Nature on 15 October 1981

X-RAY OBSERVATIONS OF THE 1980 CYGNUS X-1 "HIGH STATE"

Y. Ogawara and K. Mitsuda
Institute for Space and Aeronautical Science
4-6-1 Komaba, Meguro-ku
Tokyo, Japan

K. Masai
Department of Astrophysics, Nagoya University
Chikusa-ku, Nagoya, Japan

J.V. Vallerga, L.R. Cominsky, J.M. Grunsfeld, J.S. Kruper, and G.R. Ricker
Department of Physics and Center for Space Research
Massachusetts Institute of Technology
Cambridge, Massachusetts 02139

CSR-HEA-81-25

This work supported in part by NASA grants NGL-22-009-015 and NSG 7339.

Observations of intensity transitions in the X-ray emission from the black-hole candidate Cygnus X-1 (see reference 1 and references therein) were made by the Hakucho satellite[2] during the summer of 1980 and are reported here. In addition, we report the results of hard (20-120 keV) X-ray observations of Cyg X-1. These data were obtained during the "high" intensity state by balloon-borne mercuric iodide detectors, and are compared with data obtained at similar energies approximately one month earlier[3] during the "low" intensity state.

Cyg X-1 was observed to be in a "high state" by the Uhuru satellite[4] from December 1970 (its first observation of the source) to April 1971 and again during 1975 by the Ariel V[5-7], and OSO-8 instruments[8], as well as the Astronomical Netherlands Satellite[9]. Subsequent observations at many different X-ray energies have indicated that Cyg X-1 has been in an extended "low" state since early 1976. In his extensive review of Cyg X-1 (ref. 1), Oda has summarized the light curves and spectral information which were published as of 1977. During the transition to a "high" state, the soft (<10 keV) and hard (>10 keV) X-ray intensities appear to be anticorrelated, i.e., a "high" state below 10 keV is associated with a substantial decrease in the X-ray intensity above 10 keV.

For the work reported here, soft X-ray observations (1-30 keV) were made with the scanning Y-axis detectors on board the Hakucho satellite. The Y-axis detector system consists of a pair of Xenon-filled proportional counters (SFX-V1 and SFX-V2) with a 1°.7x32° FWHM field of view. Each of the two counters has an effective area of 32 cm^2. Only the SFX-V1 data was used in this analysis since the SFX-V2 field of view contained Cygnus X-3 during most of the observations. The satellite spins at 6 rpm, so that 3000 transits of a

given source are available during the 5 daily 10 minute passes above the tracking station at Uchinoura, Japan. The source transits are superposed and corrected for aspect transmission and Earth occultation. Background is also subtracted. (For further details on the Hakucho satellite see reference 10.)

Figure 1 shows a portion of the X-ray light curve obtained with the Hakucho Y-axis detectors during 1980. Each point represents the daily average X-ray intensity from Cyg X-1. Two "high" states are clearly visible. The first lasted at least fifteen days, and was followed by a decrease over approximately 25 days to the pre-transition level. A second increase was observed approximately four months later. This increase was quite brief, with the "high" state persisting for only two days. The erratic variability seen during the 1980 observations is similar to that observed in 1975 and reported by Holt et al. using the Ariel V All Sky Monitor[7].

Also indicated in Figure 1 are the dates when hard X-ray (20-200 keV) balloon observations of Cyg X-1 took place. The "low" state observations (8 May 1980) were performed by the MIT/Leiden Balloon Group and will be reported separately[3]. The "high" state observations (28 June 1980) constituted the first use of a mercuric iodide X-ray detector in an astronomical experiment. The detector consisted of 11 HgI_2 crystals with a total effective area of 7.6 cm^2. The detector assembly (crystals and preamps) was enclosed within a cylindrical NaI scintillator well (active anticoincidence shield) which rejected charged particles and gamma rays. The preflight energy resolution of the detectors ranged from 2-6 keV FWHM at 60 keV and remained stable during the 13-hour flight from Palestine, Texas. The gondola containing the detector was launched on an 11 x 10^6 ft^3 balloon at 0015 UT on 28 June 1980 and floated

west for 13 hours at an average altitude of 40 km ($\sim$ 2.9 gm cm^{-2}). Maximum exposure to Cyg X-1 occurred at 0830 UT 28 June 1980. The detectors were calibrated using an on-board Am^{241} source for two minutes out of every hour. The counts for each separate HgI_2 detector were binned in 64-second intervals in coarse energy channels, 10 keV wide. The detector counts were then summed to give the total counts per energy channel per 64 seconds.

Total exposure to the X-ray source was calculated as a function of time. The calculations took into account aspect (azimuth, latitude, sidereal time, and field of view of individual HgI_2 detectors), atmosphere and detector window transmission, detector efficiency, and dead time. The maximum exposure to Cygnus X-1 at transit was 37 percent over the 50-70 keV energy range. For each energy channel, an effective time on source, $t_{eff} = \sum_i t_i \varepsilon_i$, was calculated and used to convert observed counts to a photon flux at the top of the atmosphere. Here, t_i refers to an individual time bin and ε_i is the total exposure including atmospheric and aspect corrections as discussed above. There was less than a 2 sigma detection in all energy bands.

Cygnus X-1 passed through the field of view in 95 minutes resulting in 83 minutes of "on source" data (i.e., 5 minutes were occupied by calibrations and 7 minutes were lost due to telemetry dropouts). Forty minutes before and after this period were averaged and used as background.

Figure 2 shows the 2-sigma upper limits we have derived for the hard X-ray spectrum during the 28 June 1980 Cyg X-1 "high" state observation. Also indicated in Figure 2 are the results from the 8 May 1980 hard X-ray observations by Scheepmaker et al.[3] which were obtained when Cyg X-1 was in the "low" state, as well as representative hard X-ray measurements during the 1971 and 1975 "high" states. The 1-12 keV and 12-30 keV X-ray intensities

from the Hakucho observations have been averaged over the high state and low state. As can be seen in Figure 2 the hard X-ray intensity is anticorrelated with the soft X-ray intensity; the pivot point occurs for an energy below 30 keV. Using detectors on HEAO-3, Ling et al.[11,12] also recorded a continuous decrease in the hard X-ray intensity (48-183 keV) from 19 May 1980 until at least 2 June. The spectral anticorrelation reported here was also observed in previous low to high state transitions[8,13] and seems to be a consistent feature of the bimodal behavior of Cygnus X-1.

Previous observations have established that the spectrum varies with time during the different intensity states and is not well-represented by a simple relation (e.g., power law or exponential). This has led to the idea that the soft component of the spectrum may originate in the outer optically thick region of an accretion disk surrounding the central compact object, while the hard component arises in an optically thin, hot inner region[14]. The observed time scales for the transition to and decay from a "high" state are consistent with theoretical calculations for the evolution of a standard accretion disk[15], and suggest fluctuations in the accreted stellar wind or changes in the optical depth of the gas at the outer edge of the disk (see references 1 and 16 and references therein). Spectral anticorrelation has also been used to explain the energy dependence of the short term variability (msec to sec)[17]. A numerical model proposed by Ichimaru[18] shows that two physically distinct states can exist in the accretion disk depending upon whether the radiative loss is smaller than or larger than the viscous heating near the outer boundary (i.e. a transition is expected to occur for $\dot{M}/T^2 \sim 5\times10^3$ gm s^{-1} K^{-2} where $\dot{M}$ is the accretion rate and T is the gas temperature at the outer edge of the disk). Thus, the middle part of the disk may become optically thick (high state) or optically thin (low state).

In conclusion, we have established that Cygnus X-1 returned to its high state in 1980 after an apparent 4.5 year interval in the low state. It is interesting to note that this time period is similar to the 4 year interval between the first and second observed transitions[4,5]. We have established that the soft and hard X-ray intensities are anticorrelated in the transition between the two distinct states and we believe that any theoretical model of the bimodal behavior of Cygnus X-1 must account for this spectral anticorrelation.

ACKNOWLEDGEMENTS

The authors thank all the members of the Hakucho team for their contributions to the observations. The assistance of Drs. H. Inoue, K. Makishima and T. Murakami in the data analysis and preparation of the manuscript is also acknowledged. The authors are also grateful for the assistance of: Robert Kubara and the launch crew at the National Center for Atmospheric Research; Dick Lynn, Carol Ortale, Wayne Schnepple, and John Warren at the Advanced Measurements Laboratory at EG&G (Santa Barbara). A. Scheepmaker kindly provided data from the MIT/Leiden 1980 balloon flight in advance of publication. L.C. acknowledges support from Zonta International during part of this work. This research was sponsored in part by the National Aeronautics and Space Administration under grants NGL-22-009-015 and NSG7339.

REFERENCES

1. Oda, M. Space Science Reviews, 20, 757-813 (1977).

2. Oda, M. and the Hakucho Team, IAU Circular No. 3491 (1980).

3. Scheepmaker, A. et al. manuscript in preparation.

4. Tananbaum, H. et al. Astrophys. J. 177, L5-L10 (1972).

5. Holt, S.S. et al. Nature 256, 108-109 (1975).

6. Sanford, P. et al. Nature 256, 109-111 (1975).

7. Holt, S.S. et al. Nature 261, 213-215 (1976).

8. Dolan, J.F. et al. Astrophys. J. 236, 551-557 (1979).

9. Heise, J. et al. Nature 256, 107-108 (1975).

10. Kondo, I. et al. Space Science Instrumentation, 5, 211 (1981).

11. Ling, J.C. et al. B.A.A.S. 13, No. 2, p. 549.

12. Ling, J.C. (private communication).

13. Matteson, J.L. et al. in X-Ray Binaries, eds, E. Boldt and Y. Kondo (NASA SP-389), 407-424 (1975).

14. Thorne, K.S. and Price, R.H., Astrophys. J. 195, L101-L105 (1975).

15. Lightman, A.P. Astrophys.J. 194, 419-427 (1974).

16. Eardley, D.M. et al. Comments on Astrophysics (1978).

17. Doi, K., Nature, 287, 210-212 (1980).

18. Ichimaru, S., Astrophys.J., 214, 840-855 (1977).

FIGURE CAPTIONS

Figure 1: Soft X-ray (1-12 keV) light curve of Cyg X-1 obtained with the Hakucho satellite. Two "high" states are evident. The first began before 10 June 1980 and the second transient event occurred in November 1980. Also shown are the dates of simultaneous observations in hard X-rays by balloon-borne instruments.

Figure 2: X-ray spectra taken before and after the "high" state transition of Cyg X-1 in late May/early June 1980. Data points were obtained with the Hakucho satellite and with balloon borne hard X-ray detectors. The Hakucho data points for high and low states are averages over 12 June - 17 July, 1980 and 1-19 May 1980, respectively. Also included are representative hard X-ray spectra taken during previous high states.

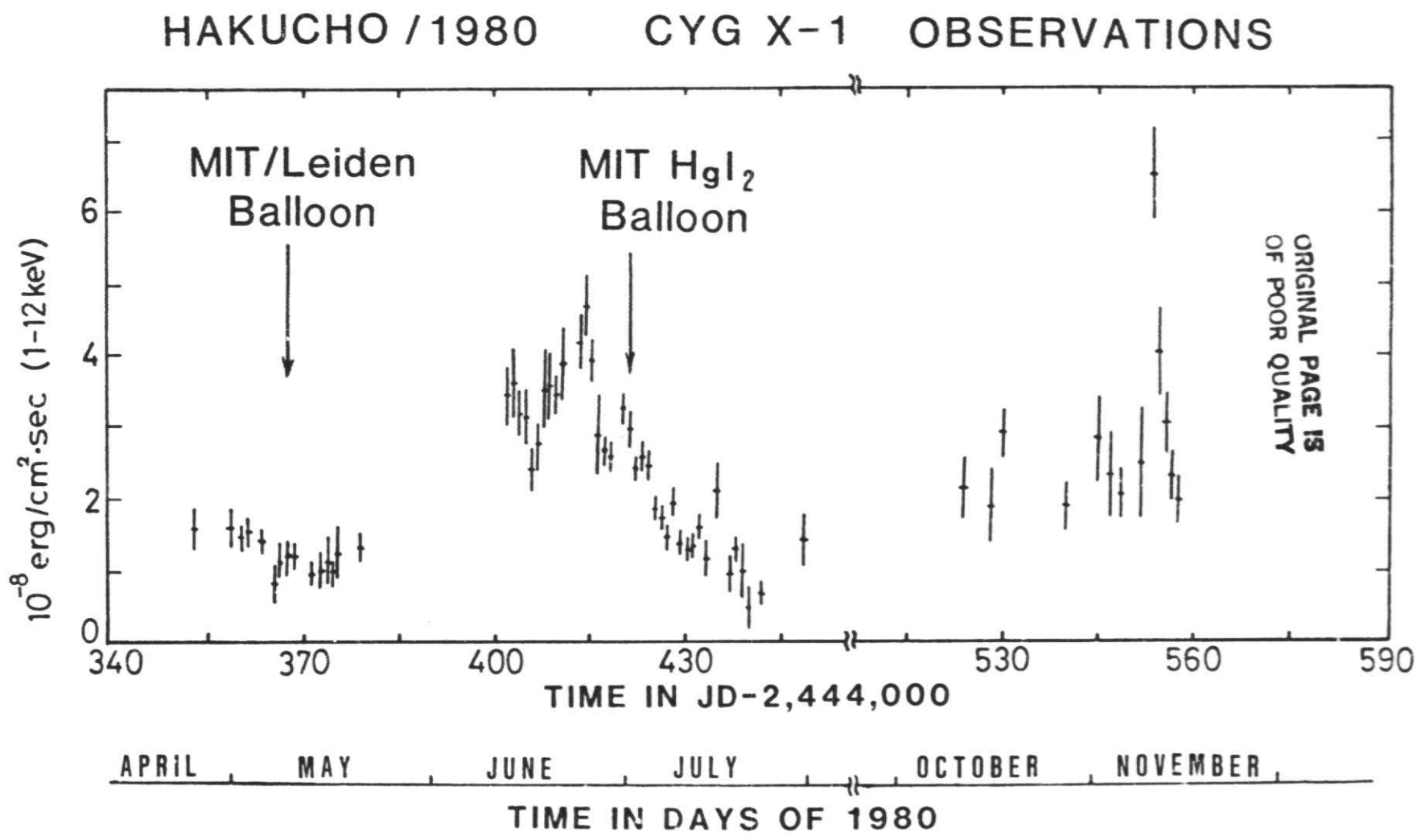
HAKUCHO / 1980 CYG X-1 OBSERVATIONS
MIT/Leiden Balloon
MIT HgI_2 Balloon
ORIGINAL PAGE IS OF POOR QUALITY
10^{-8} erg/cm^2·sec (1-12 keV)
0
2
4
6
340
370
400
430
530
560
590
TIME IN JD-2,444,000
APRIL
MAY
JUNE
JULY
OCTOBER
NOVEMBER
TIME IN DAYS OF 1980

Figure 1

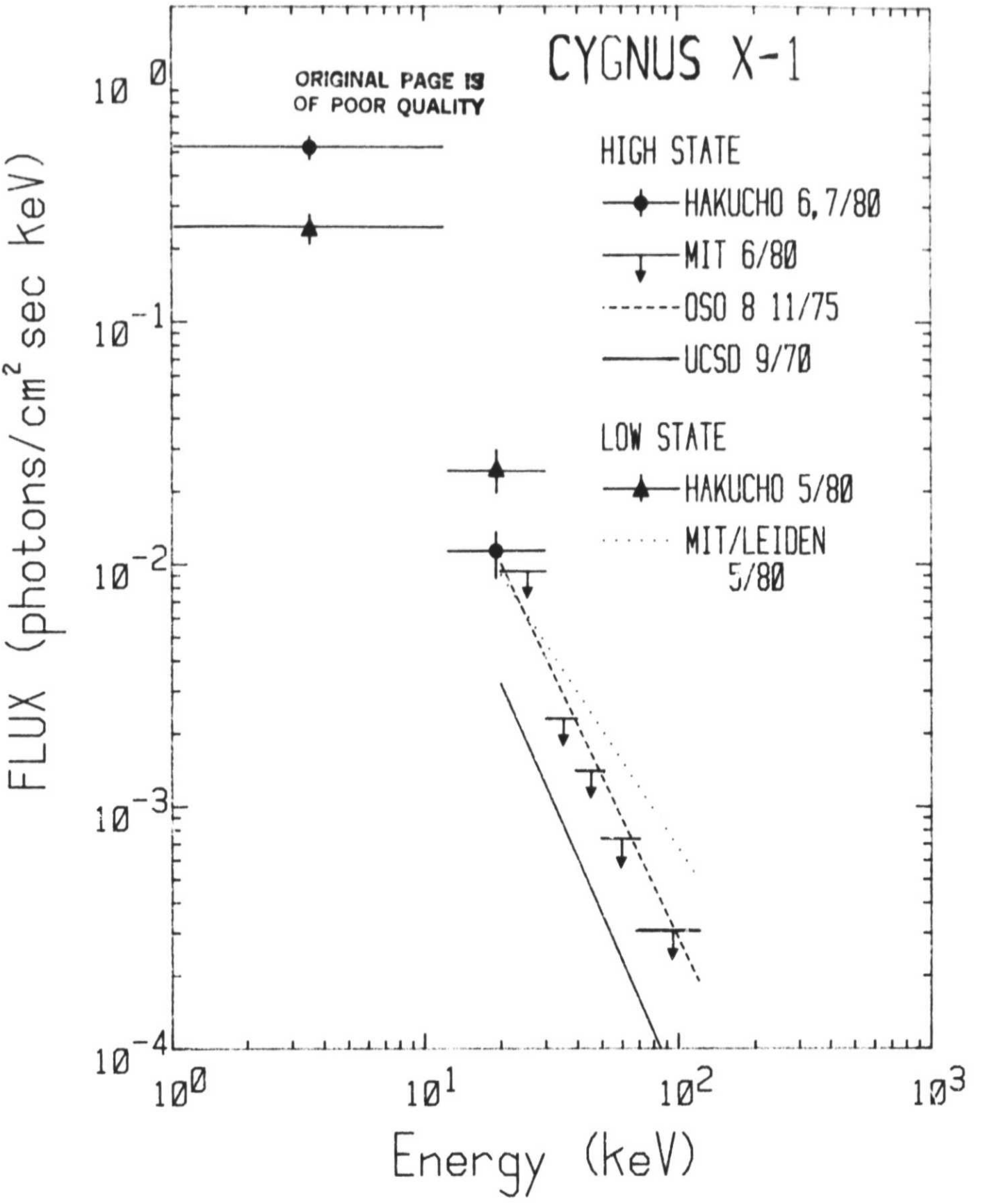
CYGNUS X-1
ORIGINAL PAGE IS
OF POOR QUALITY
HIGH STATE
HAKUCHO 6,7/80
MIT 6/80
OSO 8 11/75
UCSD 9/70
LOW STATE
HAKUCHO 5/80
MIT/LEIDEN
5/80
FLUX (photons/cm² sec keV)
Energy (keV)
10⁰
10⁻¹
10⁻²
10⁻³
10⁻⁴
10⁰
10¹
10²
10³

STUDIES OF NEW HARD X-RAY DETECTION METHODS

AND

OBSERVATIONS OF COSMIC X-RAY SOURCES

by

JOHN VINCENT VALLERGA

Submitted to the Department of Physics on August 19, 1982
in partial fulfillment of the requirements for the
Degree of Doctor of Philosophy in Physics

ABSTRACT

To establish the expected sensitivity of a new hard X-ray telescope design, an experiment was conducted to measure the background counting rate at balloon altitudes (40 km) of mercuric iodide, a room temperature solid state X-ray detector. A balloon-borne gondola containing a prototype detector assembly was designed, constructed, and flown twice in the spring of 1982 from Palestine, Texas. The prototype detector consisted of thin mercuric iodide (HgI_2) detectors surrounded by a large bismuth germanate ($Bi_4Ge_3O_{12}$) scintillator operated in anticoincidence. The bismuth germanate shield vetoed most of the background counting rate induced by atmospheric gamma-rays, neutrons and cosmic rays.

The second flight of this instrument established a differential background counting rate of $4.2 \pm 0.7 \times 10^{-3}$ counts/ sec cm^2 keV over the energy range of 40 to 80 keV. This measurement was within 50% of the predicted value. The prediction was based on a Monte Carlo simulation of the detector assembly in the radiation environment at float altitude.

Two results are also presented on the hard X-ray (20-200keV) observations of the COS-B gamma-ray source, CG 135+01, and the Galactic Center using a balloon-borne array of phoswich detectors with a total active area of 1200 cm^2. The observations took place during a high altitude balloon flight on May 8, 1980 from Palestine, Tx. CG 135+01 was detected with a 4 sigma level of significance while upper limits were placed on the flux from the Galactic Center, confirming the reported variability.

Thesis Supervisor: Dr. George R. Ricker

Title: Principal Research Scientist

Dedicated to Helene

ACKNOWLEDGMENTS

I first wish to thank my advisor, George Ricker, who taught me the art and science of high altitude ballooning. I also want to thank those people who helped in the construction and preparation of the many balloon gondolas: Jim Ballintine, Darren DePoy, John Doty, Doug Franklin, Dan Griscom, John Grunsfeld, John Kruper, Pete Tappan, Roland Vanderspek, and Darien Wood. I also would like to thank Wayne Schnepple and Carol Ortale for all their help with mercuric iodide. Robert Kubara and the crew at the National Scientific Balloon Facility did an outstanding job launching our payloads. I am also grateful for Brenda Parsons' help in producing this and many other documents.

TABLE OF CONTENTS

Page

LIST OF FIGURES

LIST OF TABLES

1.0 INTRODUCTION

Since its beginning in 1962 with the discovery of Sco X-1, the science of X-ray astronomy has progressed by placing X-ray photon detectors above the atmosphere in rockets, balloons and satellites. This usually involves modifying the detectors to withstand extreme environments and payload constraints (size and weight). The goal has always been to increase the sensitivity of the detectors (signal to background ratio) either by increasing the effective collecting area and/or observing times while decreasing the background counting rate. Each new detector technology that is applied to X-ray astronomy must be reoptimized to achieve these goals using widely different strategies.

In the last few years, the balloon lab at the Center for Space Research at MIT has been studying mercuric iodide (HgI_2), a solid state room temperature X-ray detector, for use in hard X-ray astronomy. Its primary advantages are its good energy resolution at room temperatures and a large photon cross section. Much work has been done to characterize the properties of HgI_2 that affect the operation of these detectors for use in X-ray astronomy. The goal of this program has been to develop space and balloon qualified HgI_2 detectors.

Previous to this development effort, the balloon group flew large area balloon-borne arrays of scintillation detectors to observe hard X-ray astronomical sources. On May 8, 1980, a balloon gondola containing a 1500 cm^2 array of phoswich scintillation detectors was flown from Palestine, Texas. This gondola, built at MIT at the balloon lab in collaboration with the Cosmic Ray Working Group at Leiden University, was the most sensitive astronomical hard X-ray (20-240 keV)

detector in existence. After 16 hours of very high quality observations, the gondola free-fell from 38 kilometers and was destroyed (the data were telemetered to the ground and not lost). The destruction of this instrument was the impetus for accelerating the development of mercuric iodide for astronomical applications to replace the 1500 cm^2 array with an instrument of comparable sensitivity to faint hard X-ray sources.

The replacement gondola proposed was a collection of 4 Bragg diffraction X-ray concentrators that increase the effective area of 4 well-shielded, low background mercuric iodide detectors. Calculations show that this new gondola detector system can match the sensitivity of the old 1500 cm^2 array if the assumed background count rate at balloon float altitudes (crudely scaled from that of germanium detectors in orbit) is correct. In the work reported in this thesis a prototype detector inside a small balloon-borne gondola has been constructed and flown at balloon altitudes in order to test these calculations. The measured background count rate results will be used to confirm detector models that then can be used to predict and optimize the background of future detector geometries.

This thesis begins (Section 2) by describing the currently popular detectors used in hard X-ray astronomy. Section 3 goes into detail concerning the two new materials used in the prototype detector: mercuric iodide, the primary solid state X-ray detector; and bismuth germanate, a scintillator with a very large photon cross section, which is used as an anticoincidence shield. In section 4, two of the most significant results from the 1980 flight of the 1500 cm^2 gondola are

discussed. These results show the potential of a new gondola design that can achieve this excellent sensitivity. The design considerations for the new gondola detector are explained in Section 5 while Section 6 is a detailed description of the detector prototype gondola and associated electronics. The prototype detector model used in predicting the background count rate due to gamma rays, neutrons and charged particles is described in Section 7. The results of two balloon flights of this prototype detector are compared with predictions in Section 8. A summary and conclusion is presented in Section 9.

2.0 ASTRONOMICAL HARD X-RAY DETECTORS IN CURRENT USE

Detectors used to count photons from celestial X-ray sources differ greatly from their laboratory counterparts. In general, high sensitivity to faint sources is the goal in astronomical detector design. Because the atmosphere is opaque to hard X-rays (20-200 keV) for column densities greater than $20 gm/cm^2$, studies of cosmic sources must be carried out from satellites or high altitude balloons. Thus, weight and volume of the instrument are at a premium. The detectors should have large areas and a high quantum efficiency to collect as many source photons as possible and also be well shielded to reject background events induced by primary cosmic rays and their secondaries. Good energy resolution increases the sensitivity to features in a source spectrum and can "resolve out" line features in the background. Some of these goals are incompatible and cannot all be found in one type of detector. The final choice is usually determined by the scientific objective of the observation. For example, timing observations of X-ray pulsars require large areas to acquire many photons from the source and can tolerate a somewhat higher background rate because of the time signature of the source. On the other hand, energy resolution might have a higher priority in observations of possible cyclotron line features in magnetized neutron stars.

It takes an appreciable detector mass to stop hard X-rays. The most sensitive hard X-ray telescopes have been flown from high altitude balloons where payload weights can reach 2000 kg with sensitive areas of 3000 cm^2. A typical long balloon flight lasts only ~30 hours, so that satellite-borne hard X-ray experiments can make up for reduced

areas with longer observing times. The most common astronomical X-ray detectors used on satellites and balloons have been proportional counters, scintillators and cooled solid state detectors. A detailed review of these detectors can be found in Peterson (1975) and references therein. What follows is a summary of the properties of various detectors, emphasizing the advantages and disadvantages of each type for use in X-ray astronomy.

2.1 Proportional Counters

A proportional counter consists of a gas filled chamber traversed by thin anode wires (~.01 mm diameter) carrying a potential of several thousand volts. A photon entering the chamber may interact with the gas liberating a photoelectron that ionizes the gas, producing additional electrons and ions. As the electrons move toward the anode they can further ionize the gas resulting in a "gas multiplication" of $\sim 10^3$ to 10^5. This electron charge pulse is collected at the anode and is proportional to the energy of the X-ray. The most quantum efficient counters contain xenon (Z=54) with mixtures of a "quench" gas such as methane or carbon dioxide to absorb UV radiation and de-excite metastable states of the positive ions.

Xenon proportional counters require a large thickness to achieve reasonable efficiencies and have mostly been used for energies below 60 keV (Clark et al. 1973). The photon mean free path in xenon at STP at 50 keV is ~15 cm. The small efficiencies of proportional counters at high energies can be somewhat compensated by the very large areas that can be constructed and deployed such as the High Energy Detectors (HED) of the A2 experiment on the first High Energy Astronomical Observatory

(HEAO 1) (2500 cm^2 geometric area, Rothschild et al. 1979).

Background reduction is accomplished by using ground plane wire grids that section a common gas volume into many elements, each with its own anode. This makes the "wall-less" counters with the outer elements operated in anticoincidence (Serlemitsos 1971). Non-local interactions, such as high energy charged particles, can be rejected because of simultaneous signals in many anodes.

The method of charge collection in proportional counters can be used to advantage in locating the position of the photon interaction. A charge pulse produced locally flows in two directions along the anode wire and the ratio of the charge collected at both ends can give the one dimensional position of the interaction along the wire. Multiwire counters using this position sensitive technique can be used to determine the two dimensional position of interaction. These position sensitive detectors are used at the focus of grazing incidence X-ray focusing telescopes such as the Imaging Proportional Counter (IPC) on the HEAO 2 (Einstein) satellite (Giacconi et al. 1979).

Though large areas can be constructed in a straightforward manner, proportional counters have not been very effective in hard X-ray astronomy above 60 keV because of the very low quantum efficiencies at these energies for reasonable volume detectors.

2.2 Scintillators

A photon interacting in an inorganic scintillator will release an energetic electron that excites elevated lattice states by collision. These states de-excite to the ground state by emitting optical or ultraviolet photons. The number of photons released is proportional to

the energy of the incident X-ray (deviations from linearity in light yield vs. energy do exist; a complete description of the theory and experimental techniques of scintillators can be found in Birks, 1964). The optical photons that exit the crystal impinge on the photocathode of a photomultiplier tube. The photocathode releases photoelectrons which are multiplied by the dynodes producing a charge pulse proportional to the X-ray energy deposited in the crystal.

Inorganic scintillators such as sodium iodide (NaI) and cesium iodide (CsI) have been the "work horses" of hard X-ray astronomy because of their high stopping power. (The mean free path for a 100 keV photon in NaI is 1.8 mm.) Organic scintillators, made up mostly of hydrogen and carbon, are almost transparent to hard X-rays yet can detect charged particles very efficiently. Thus, they are frequently used as anticoincidence shields to reject cosmic rays because of their relatively low cost and availability in all sizes and shapes.

The properties of some scintillators are shown in Table 2.1. Thallium doped NaI is popular because it has the highest light yield of all scintillators and large areas can be acquired. NaI(Tl) is hygroscopic and brittle, so it must be hermetically sealed and handled gently. The high light yield of NaI(Tl) gives it the best energy resolution of all scintillators: approximately 11 keV full width at half maximum (FWHM) at 60 keV (Ballintine 1981). Sodium doped CsI has had more use as an anticoincidence shield, either as a large shield with a "well" for the primary detector or as the shield crystal in a "phoswich" detector (Peterson 1975). Bismuth germanate, ($Bi_4Ge_3O_{12}$ or "BGO"),is a recent addition to the scintillator family. Its most

Table 2.1*

Properties of Commonly Used Scintillators

	INORGANIC			ORGANIC
	NaI(Tl)	CsI(Na)	$Bi_4Ge_3O_{12}$	Plastic (NE102)
Light Output (relative to NaI)	100	85	10	28
Density (gm/cm^3)	3.67	4.52	7.13	1.03
Decay Time Constant (nanoseconds)	230	630	300	2.4
Wavelength of Maximum Emission (nanometers)	415	420	480	423
Index of Refraction	1.85	1.8	2.2	1.6
Thickness Required to Attenuate 500 keV photons by 90% (centimeters)	6.7	5.3	2.4	23

*Adapted from Farukhi (1978)

outstanding characteristic is its photon stopping power due to a high effective atomic number and density (see section 3.2).

2.2.1 Phoswich Detectors

A "phoswich" detector (phosphor sandwich) consists of two dissimilar scintillators such as NaI and CsI optically coupled together and viewed by a single photomultiplier (Fig. 2.1). It takes advantage of the different luminescence decay times of the two crystals so that a decay time discriminator can differentiate between pulses originating in the NaI or CsI. It is an efficient background rejection scheme providing "4π" sterradians shielding of penetrating radiation as well as removing the phototube mass (and its associated background production) away from the primary detector.

To achieve a low background in a phoswich configuration the shield crystal (usually CsI(Na)) must be quite thick (~3 cm) while the primary crystal thickness is determined by the energy range of interest. The HEAO A4 experiment (Matteson,1978) contained 3 phoswich detectors optimized for 3 energy ranges (10-200 keV, 80-2000 keV, 300-10,000 keV) with effective areas of 220 cm^2, 170 cm^2 and 120 cm^2, respectively. To date, this instrument has been the most sensitive broad band hard X-ray detector in orbit.

Larger area phoswich systems have been flown from balloons by groups from UCSD, Max Planck Institute and here at MIT. The Balloon Group at the Center for Space Research in collaboration with the Cosmic Ray Working Group at the University of Leiden, designed, constructed and flew a 1500 cm^2 phoswich array. This instrument (see Section 4 and Ballintine 1981) was the most sensitive (per unit time) astronomical

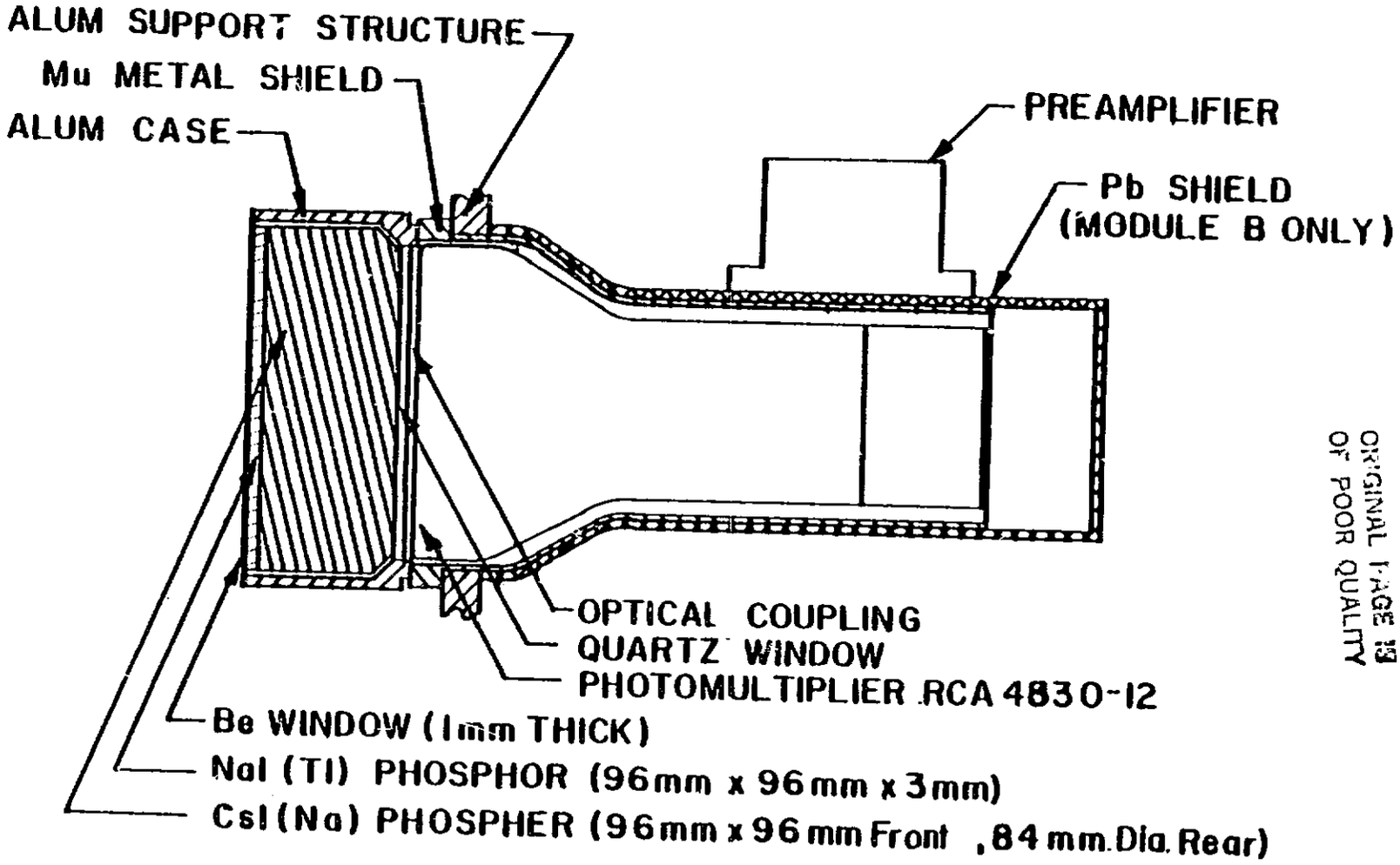

Figure 2.1 Phoswich assembly. This sectional view shows the construction of an individual phoswich detector (16 were used in the MIT 1500 cm² instrument last flown in May 1980). See section 2.2.1 for a description of its operation.

hard X-ray detector until its demise in May 1980.

2.3 Solid State Detectors

The application of silicon and germanium solid state detectors to X-ray astronomy has occurred only recently due to the slow progress in growing large volume crystals. Such a solid state detector can be thought of as a solid ionization chamber in which incoming radiation produces energetic electrons that ionize the lattice and raise electrons from the valence band to the conduction band. These conduction electrons (and the corresponding holes) diffuse under an applied electric field to the electrodes and are collected as a charge pulse proportional to the energy deposited in the crystal. Due to the lack of competing energy loss mechanisms and the small band gap, most of the deposited energy goes into electron-hole production, giving many charge carriers and a correspondingly smaller relative statistical variance (see Section 3.1.2). This small variance in generated charge gives the solid state detector its excellent energy resolution (0.5 keV FWHM at 60 keV, Knoll 1979 pg. 500), which is limited by the preamplifier electronics.

The advantage of good energy resolution is the ability to resolve possible features in an energy spectrum that would be lost in the continuum using a broad band instrument such as NaI. Possible features expected in astronomical observations include nuclear gamma ray lines from radioactive decay of elements produced in supernova explosions, a positron annihilation line from the Galactic Center, and cyclotron lines from magnetized neutron stars. Though it is possible to deconvolve the monoenergetic response of a broad band detector, the

stability and the number of photons required is prohibitive in most astronomical hard X-ray observations.

The properties of various solid state detectors are listed in Table 2.2. Germanium has been the usual choice for hard X-ray astronomy because of the materials available in large sizes, it has the highest photon stopping power. The most important limitation of germanium detectors is the requirement that they be operated at liquid nitrogen temperatures to reduce thermally-generated leakage current. This involves massive and bulky cryogenic equipment and, on satellites, a limited operating life. The gamma ray spectrometer on HEAO 3 (Mahoney et al. 1980) made with 4 Ge detectors (effective area, 64 cm^2, and sensitive from 45-10,000 keV) had a planned operating life of 1 year. Of all the other detector materials listed in Table 2.2, only HgI_2 combines a high photon stopping power with satisfactory room temperature operating ability. Room temperature solid state detectors such as HgI_2 work because of a large bandgap that suppresses thermally generated leakage current. Cadmium telluride's smaller bandgap results in larger room temperature leakage currents that degrade the energy resolution. Gallium arsenide (GaAs) has a bandgap similar to CdTe (1.43eV) and therefore suffers from the same leakage current problems at room temperature. The development of GaAs as an X-ray detector is not as advanced as is the development of the materials listed in Table 2.2, with a maximum detector thickness limited to 100 microns. Silicon can be made to work at room temperature with suitably doped contacts, yet its hard X-ray stopping power is insufficient. Since the development of "flight qualified" HgI_2 detector system is a major focus

Table 2.2*

Properties of Commonly Used Solid State Detectors

	Si (300°K)	Ge (77°K)	HgI_2 (300°K)	CdTe (300°K)
Atomic Number	14	32	80-53	48-52
Density (gm/cm^3)	2.3	5.3	6.4	6.0
Band Gap (eV)	1.12	0.66	2.13	1.47
Energy Required per electron-hole pair (eV)	3.6	3.0	4.2	4.4
Thickness Required to Attenuate 60 keV by 90% (mm)	57	2.1	0.6	0.6

*Adapted from Whited (1979)

of this thesis, extensive details of mercuric iodide as a detector are discussed fully in Section 3.

3.0 DEVELOPMENT OF NEW TYPES OF DETECTORS FOR ASTRONOMICAL WORK

The ideal detector for hard X-ray astronomy would have excellent resolution, high efficiency, large area and be lightweight (including support equipment, i.e. cryogenics). This "dream" detector does not exist though most systems in use satisfy some of the requirements. The standard detector for astronomical hard X-rays has been large area NaI scintillation crystals that operate at ambient temperatures but with limited energy resolution (17% FWHM at 60 keV). The semiconductor detectors such as germanium have recently achieved respectable areas (64 cm^2, Mahoney et al. 1980) yet their lower efficiencies require thicker detectors which increase the background counting rate. Also the requirement for cryogenic temperatures has limited their satellite lifetime to ~1 year.

3.1 Mercuric Iodide Detectors

Mercuric iodide (HgI_2) solid state X-ray detectors have many unique advantages in their application to X-ray astronomy. HgI_2 detectors operate at room temperature so that bulky and massive cryogenic coolers are not required. HgI_2 detectors also combine a high quantum efficiency with good energy resolution. Because of the excellent quantum efficiency (due to the high effective atomic number of HgI_2, see fig. 3.1) background contributions which scale as the thickness of the detector (e.g. those due to neutrons and gamma rays) are lower than for other hard X-ray detectors with equivalent stopping power. At this time the largest area single detector that can be made is only 1 cm^2, so it is far from being ideal. Nonetheless, its properties are well matched to a scheme that increases the effective area

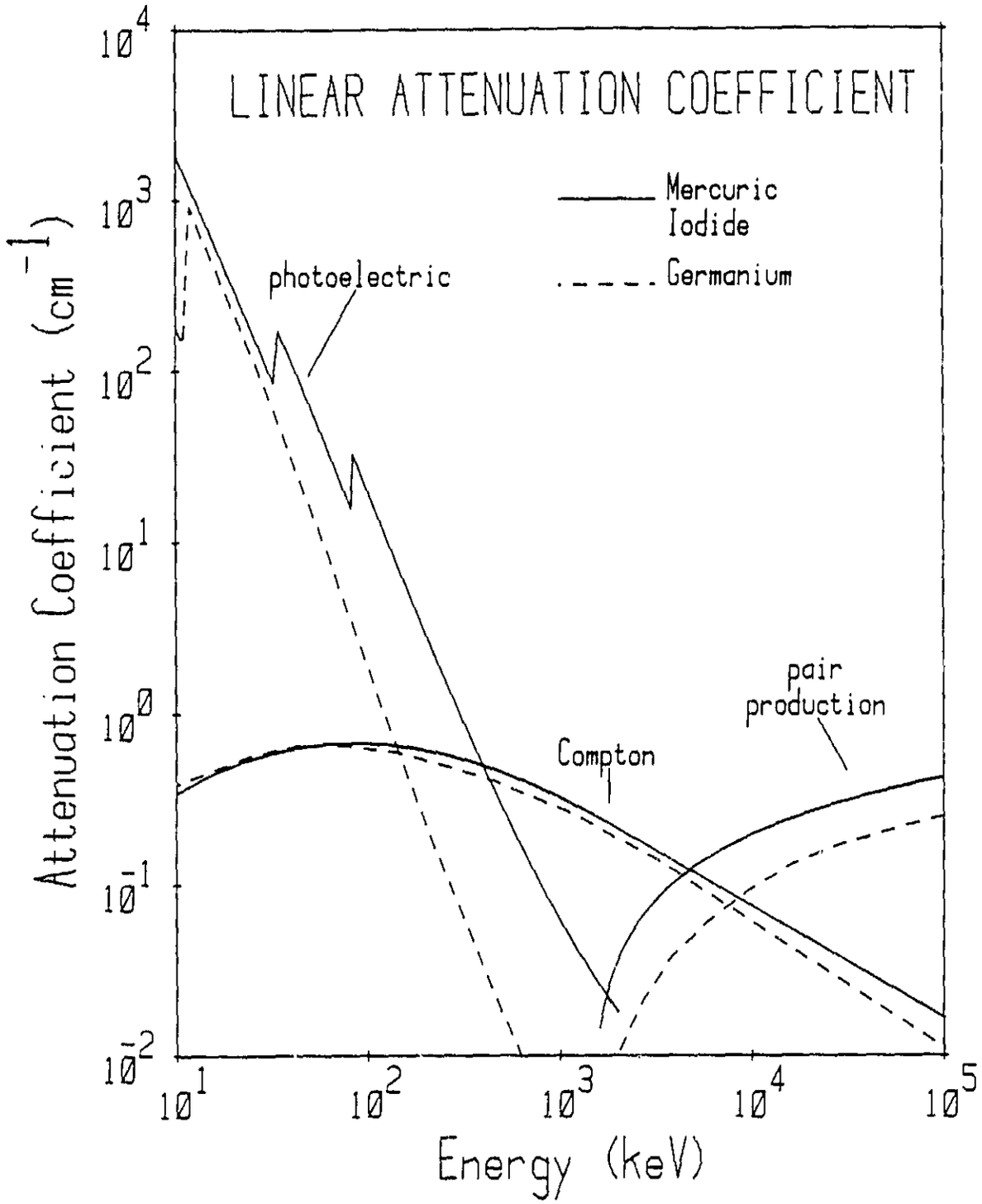

Figure 3.1 Linear attenuation coefficient vs. energy for mercuric iodide and germanium. For energies above 33 keV, the thickness of a detector required to stop a given percentage of incident photons is much less for mercuric iodide than germanium.

using a Bragg diffraction concentrator (described in more detail in Section 5.2).

3.1.1 Detector Production and Characterization

Mercuric iodide is a recent development in the search for high Z room temperature solid state detectors. The first real energy spectrum presented using HgI_2 as a detector was of the radioactive ource ^{241}Am in 1972 (Malm 1972). In the last ten years many international groups have been growing HgI_2 crystals but the major efforts have been at EG&G's Department of Energy laboratories in Santa Barbara and at the Hebrew University of Jerusalem, Israel (Whited 1979; Van den Berg 1978). Detectors studied at MIT have either been grown here or acquired from Santa Barbara.

Mercuric iodide must be grown using vapor growth techniques because it undergoes a destructive phase change at 127°C when the room temperature red colored tetragonal structure transforms reversibly to the yellow orthorhombric structure. This temperature is below the 250°C melting point of HgI_2, preventing growth through solidification. The most widely used growth technique is the temperature gradient reversal process (Van den Berg 1977) producing crystals of ~20 cm^3 from which thin (.05 cm x 1 cm^2) detectors are then cleaved.

Recently, a new method of growing crystals has been developed using an organic polymer (Faile 1981). This method produces thin crystals that can be directly fabricated into detectors thereby bypassing the cleaving process that might damage the soft HgI_2. Detectors fabricated from crystals grown with the Faile organic polymer method show excellent charge transport properties. The reasons for

such good performance have not yet been established. One hypothesis (Burger 1982) is that the polymer affects the stoichiometry of the final crystal (ratio of iodine to mercury) decreasing the number of trapping centers. At this time crystals grown with the Faile process are too thin (~50-100 microns) to be of use in hard X-ray astronomy. However, as low energy X-ray (1-10 keV) astronomical detectors, they show great promise.

3.1.2 Physics of Detectors

Radiation interacting with semiconductor detectors converts most of its energy into electron-hole pairs by exciting electrons into the conduction band of the crystal. This charge is collected by applying a constant electric field across the detector. The resulting current pulse is proportional to the energy deposited in the crystal. The energy required to produce an electron-hole pair in HgI_2 and Ge is 4.2 eV and 3.0 eV, respectively (e.g. a 42 keV X-ray will produce an average of 10,000 electron-hole pairs in HgI_2). To see these small charge pulses, the statistical variation in the leakage (DC) current and therefore the current itself must be small. For example, a 500 picoampere current corresponds to 3120 electrons per microsecond with a statistical fluctuation of $(3150)^{1/2}$ or 55 electrons. If the charge generated by the 42 keV X-ray is collected in 1 microsecond then the variation in the collected charge is dominated by the statistical variation in the generated charge and not the statistical variation of the leakage current. Because of its relatively large bandgap (2.13 eV) the HgI_2 leakage current at toom temperature is typically in the range of 10-500 picoamperes. This allows room temperature operation in

contrast to germanium (bandgap .66 eV) which requires liquid nitrogen temperatures to achieve these low leakage currents.

In the absence of quantum statistics, electronic noise, and variations in the efficiency with which charge is collected, discrete mono-energetic events should give a delta function line spectrum. In actuality, all these effects act to broaden the line. Due to the stochastic nature of the charge generation process, the variance of the number of electron hole pairs is:

$$\sigma^2 = FE/\varepsilon$$

where σ^2 is the variance in the number of pairs generated

ε is the energy required to create an electron-hole pair

F is the Fano factor

E is the energy deposited in the crystal

The Fano factor is introduced as an adjustment factor to relate the actual variance with the Poisson predicted variance (Knoll 1979, pg. 373). It is determined empirically, although qualitative models do exist that attempt to explain the non-unity value (Klein 1968). In semiconductor detectors and gas counters, the statistical variation is smaller than expected if the lattice ionization events are uncorrelated (Poisson, F=1). Of course, the ionization events are correlated (electrons are excited into the conduction band by other electrons) and it is the random nature of competing energy loss mechanisms (phonons) that determine the variance. The smaller the Fano factor, the better the energy resolution. Upper limits to the Fano factor are determined

by accounting for all other line broadening mechanisms and assuming the residual line width is due to charge generation statistics alone. Recently, a new lower value for the HgI_2 Fano factor of .19±.03 was determined at the balloon lab at MIT (Ricker et al. 1982a; see appendix). This continued the trend of decreasing the measured Fano factor that was also observed in silicon and germanium as crystal growing and fabrication techniques improved (Knoll 1979, pg. 374). The full width at half maximum (FWHM), ΔE, due to charge generation statistics is given by:

$$\Delta E = 2.355\ (F \epsilon E)^{1/2}$$

For F=.19, the formal value of ΔE in HgI_2 is .5 keV FWHM at 60 keV. This energy resolution represents a theoretical intrinsic limit which has yet to be observed.

A further limit to energy resolution is imposed by the fact that the efficiency of charge collection does not equal 100 percent for typical detectors of ~500 microns thickness. The mean free drift length, λ, of an electron (hole) can be expressed as:

$$\lambda = \mu \tau \xi$$

where ξ is the electric field

μ is the electron (hole) mobility

τ is the mean free time before the electron (hole) is "trapped" (i.e. removed from the conduction band by defects or impurities in the lattice.)

The drift length characterizes the mean distance a charge carrier will travel before being lost or "trapped" by the lattice. For good collection efficiency these lengths should be large compared to the

thickness of the detector. Expressed in terms of λ_e and λ_h, the charge collection efficiency, η, as a function of the position x of the initial ionization in the crystal is given by:

$$\eta(x) = \frac{\lambda_e}{d}\left(1-\exp(-x/\lambda_e)\right) + \frac{\lambda_h}{d}\left(1-\exp(-d+x)/\lambda_h\right)$$

where d is the thickness of the detector (Day 1967). Table 3.1 lists the charge transport parameters of good HgI_2 crystals, as well as germanium crystal parameters for comparison. Two points must be made. First, the electric field cannot be increased indefinitely (thereby increasing λ) because electrical breakdown of the crystal at high voltages will result in the destruction of the detector. Typical voltages used in the lab are ~1000 V for a 500 micron detector, giving electric fields of 2×10^4 V/cm. Second, the large ratio of the $\mu\tau$ product for electrons and holes (~100) creates an asymmetry in the collection ability of the detector. If the incident radiation ionization sites are distributed uniformly throughout the detectors (high energy gamma rays) then the spread in pulse heights for monoenergetic radiation is the difference between η_{max} and η_{min}. If the radiation interacts closer to one electrode (low energy X-rays) the polarity of the electric field should be applied in such a way as to make the distance the holes must travel as small as possible. Fig. 3.2 shows the result of a simulation of a 390 micron thick HgI_2 detector irradiated with monoenergetic beams of 20, 60 and 150 keV photons. The charge collection parameters of Table 3.1 and an applied electric field of 16000 V/cm were used as well as a 2 keV FWHM Gaussian folding

Table 3.1*

Charge Transport Parameters for HgI_2 at Room Temperature and Ge at Liquid Nitrogen Temperature

	HgI_2 (300°K)	Ge (77°K)
Mobility, μ in cm^2/volt-sec		
electrons	90	3.6×10^4
holes	3	4.2×10^4
Mobility-lifetime product, $\mu\tau$, in cm^2/volt		
electrons	5×10^{-4}	$>5 \times 10^{-2}$
holes	5×10^{-6}	$>5 \times 10^{-2}$
Maximum electric field	50,000 V/cm	2000 V/cm

*Adapted from Iwancyzk (1981)

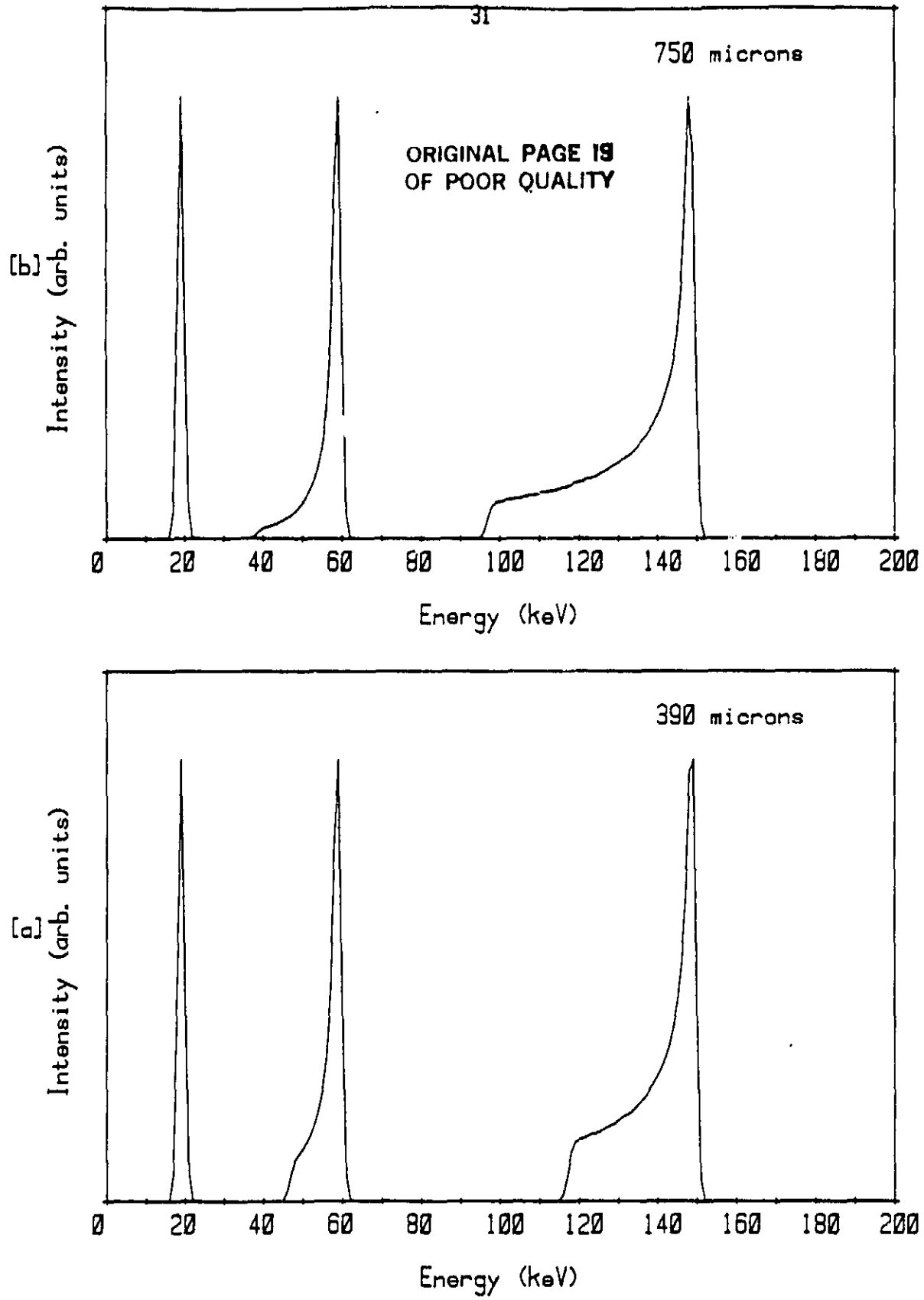

Figure 3.2 Mercuric iodide charge collection efficiency simulation. Shown are the resulting simulated energy spectra for two different thicknesses of detector: a) 390 microns and b) 750 microns. Both detectors were irradiated with three different beams of monoenergetic X-rays with energies of 20, 60, and 150 keV. The "low energy tails" of the higher energy peaks is due to the small mean free path of the holes resulting in incomplete charge collection for interactions far from the negative electrode.

routine to simulate the electronic noise. The high energy interactions have the characteristic "low energy tail" due to incomplete charge collection. For high resolution spectrometers, hole trapping is the major limitation of detector thickness. A thicker (fig.3.2b) and thus more efficient detector of X-rays must sacrifice some of the energy resolution of the detected radiation. The energy at which this trade-off occurs is a function of the quality of the detector.

Besides charge generation and charge collection efficiency, the electronic noise introduced by the preamplifier can broaden mono-energetic line features. At low energies (<6 keV) electronic noise is the dominant noise source and much progress has been made at room temperature with low noise preamplifiers ($\Delta E_{electronic}$ ~225 eV FWHM) (Iwanczyk, 1981). At higher energies, preamplifiers with an electronic noise contribution of 1 keV FWHM are common and the line width is dominated by the charge collection efficiency, especially since the uncorrelated noise sources add in quadrature.

3.1.3 Experimental Development for Astronomical Use

Mercuric iodide has been under development for ten years, and the balloon lab at MIT has had a working experience with these detectors since 1979. The first use of HgI_2 in an astronomical instrument was a small array of 12 detectors with a combined area of 8 cm^2 constructed here at the balloon lab at MIT and flown in a small balloon-borne gondola in June, 1980. Though the background counting rate at float was high because of a less than optimum design, the instrument was able to set an upper limit to the hard X-ray flux of Cygnus X-1 in the "high state" (Ogawara et al 1982; see Appendix).

HgI_2 detectors can still be considered "experimental" in that they cannot be acquired commercially and each detector is in some way unique. In work carried out by the MIT balloon group, the HgI_2 crystals have been subjected to extensive field testing. They have been exposed to extreme variations in temperature, pressure, humidity, voltage, light level and handling. As might be expected with an experimental material, HgI_2 did not always pass with flying colors. However, from this experience, general procedures for handling and environmental limitations have been developed to extend the operating life and reproducibility of results necessary for a field detector.

Because of its relative softness, the direct handling of HgI_2 crystals that have been cleaved from the large 20 cm^3 parent crystal must be minimized. The "thick" crystals (~300-1000 microns) used at the balloon lab for hard X-rays have all been acquired from EG&G, Santa Barbara. The crystals are fabricated into detectors with evaporated palladium electrodes, mounted on ceramic or plastic substrates and encapsulated with Dow Corning 3140 RTV. The typical area of these detectors is 1 cm^2 with energy resolution ranging from 2.8 to 15 keV FWHM at 60 keV. A typical energy resolution would be 4 keV at 60 keV. The area limitation requires many detectors in an array to achieve an astronomically useful collecting area (~100 cm^2). Such an array would also require 100 measurement chains (100 preamps + voltage amplifiers) as well as existing crystal growers to produce high resolution uniform detectors in quantity. Until the detector area can be made larger, some method of concentrating X-rays must be used to increase the effective area. (An X-ray concentrating technique using Bragg diffrac-

tion is described in Section 5.)

In the laboratory the detectors must be kept clean and dry. Small amounts of water and contaminants (dirt, solder flux, etc.) create current leakage paths that increase the overall RMS noise and small intermittent current pulses similar to a relaxation oscillator. Encapsulated detectors should not be exposed to vacuum because trapped air pockets will expand and strain the crystalline lattice, thus ruining the charge transport properties.

The temperature effects are striking for some crystals and unnoticeable with others. The mobility increases with lower temperatures for both electron and holes ($\mu_e \sim T^{-.9}$; $\mu_h \sim T^{-1.7}$; Minder 1974) but the mean lifetime of an electron or hole before it is trapped by the lattice decreases with decreasing temperature. These competing processes determine a temperature where the resolution is best (i.e. the mean free path, $\lambda = \mu\tau\xi$, is maximized) and is a function of the quality and purity of the crystal. Empirically, this temperature is between -20°C and 20°C, varying with detector (Ricker 1982a, Grunsfeld 1980). These temperatures are easily achieved at balloon altitudes or on satellites by passive (radiative) or active (thermoelectric) techniques. Higher temperatures decrease the mobility and also produce a prohibitive leakage current which can saturate DC coupled preamplifiers.

The bias voltage across the HgI_2 must be applied slowly to avoid large induced currents. After the bias voltage is applied, the detector "warms up" over a time period of ~1 minute to 1 hour depending on the crystal. The pulse height for a given incident energy increases and the resolution improves. This can be interpreted as an increase in

the depletion region as the deep traps (energy levels in the forbidden region caused by impurities) are emptied by the large electric field. Resolution usually improves with increasing electric field until the leakage current becomes too large. Also, high electric field strengths increase the chance for surface breakdown which intermittently injects current pulses into the preamp and shows up as low energy events. The frequency of occurrence of this "current injection noise" increases with applied voltage.

Many HgI_2 detectors perished in the balloon lab due to different types of abuse. However, by minimizing any handling that would stress the crystal and by keeping the detector in a clean, cool and dry assembly, it was possible to produce a stable and dependable operating HgI_2 X-ray detector.

3.2 Bismuth Germanate as Active Shielding

A recent development in scintillation crystals is bismuth germanate ($Bi_4Ge_3O_{12}$ or "BGO") (Nestor 1975). BGO is a clear, inert, non-hygroscopic scintillator with a light output ~10% that of NaI. Because it contains bismuth (Z=83) and has a density of 7.1 gm/cm^3, it has a large attenuation coefficient for photons (Fig. 3.3). These characteristics make it ideal as an anticoincidence shield where stopping power is more important than energy resolution.

The stopping power of BGO is at least a factor of ~2 greater than CsI, another scintillator commonly used as an anticoincidence shield (Fig. 3.3). The shield geometries can be more compact, enabling the use of smaller photomultipliers. Another advantage of a smaller size is a decrease in the count rate, leading to reduced dead times. Since BGO

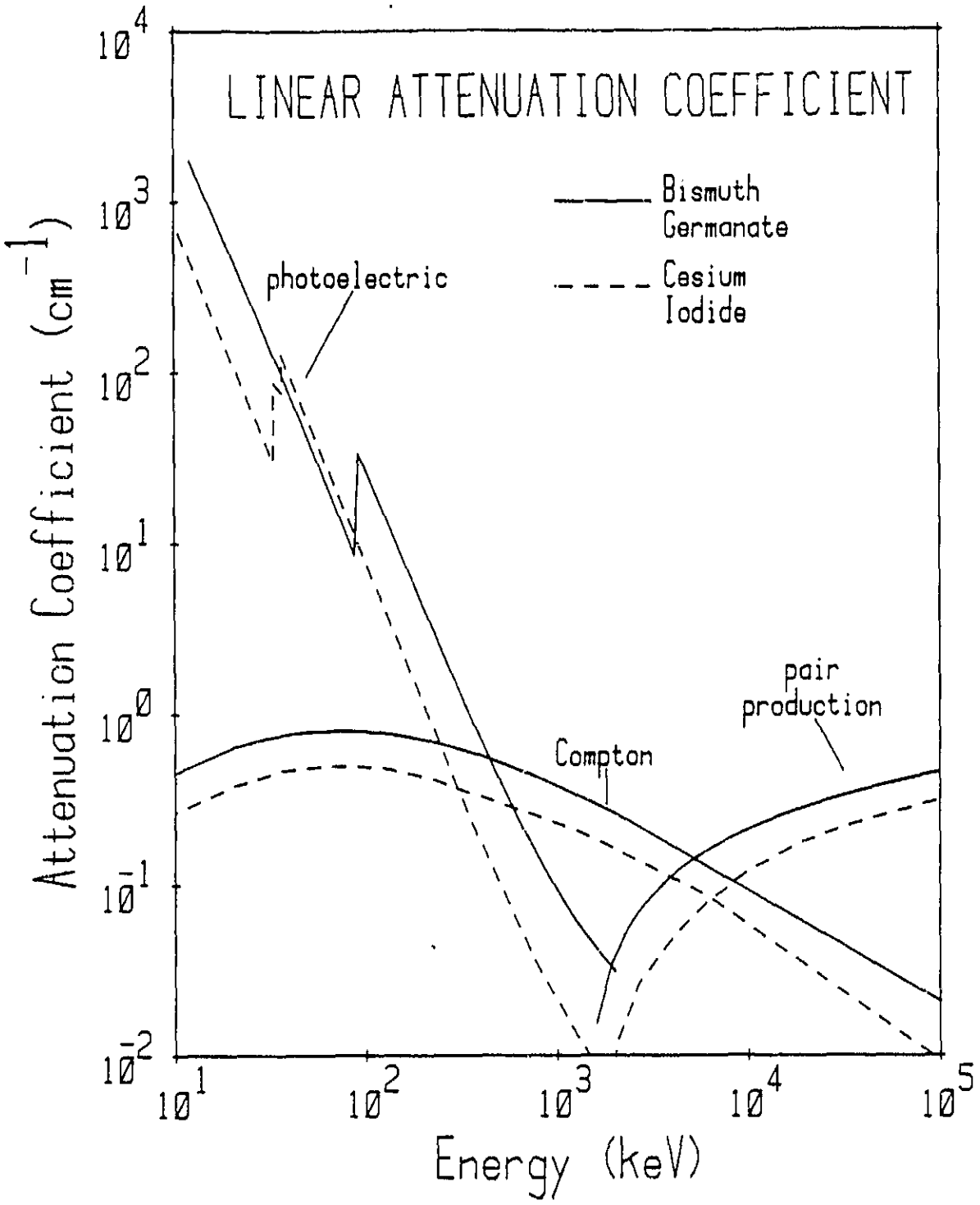

Figure 3.3 Linear attenuation coefficient vs. energy for bismuth germanate and for cesium iodide, a more commonly used anticoincidence shield.

is non-hygroscopic, it does not need to be hermetically sealed. This allows a simpler, less expensive container that can be modified and repaired in the laboratory. Unlike NaI, BGO is very hard and rugged and can be machined like glass. It is also resistant to thermal shocks.

Even with all these advantageous properties, BGO will probably not be used as a primary detector for astronomical hard X-rays because of its low light output (as compared to NaI) which determines its energy resolution (30 keV FWHM at 60 keV). What is more important for use as an anticoincidence shield is the minimum detectable energy above the photomultiplier noise so that the anticoincidence lower level discriminator can be set as low as possible. In the laboratory the BGO crystal/photomultiplier combination described in Section 6 can detect 6 keV X-rays. The light output of BGO increases with decreasing temperatures (Piltingsrud 1979) by 25% from 30°C to 0°C. This fact combined with the lower noise characteristics of photomultiplier tubes at low temperatures argues for a slightly cooled BGO shield (0°C), easily achieved at balloon altitudes.

4.0 RESULTS FROM MAY 1980 BALLOON FLIGHT OF A LARGE AREA (1500 cm^2) PHOSWICH DETECTOR

Until its demise on May 8, 1980, one of the most sensitive hard X-ray telescopes existing was the balloon-borne 1500 cm^2 phoswich array constructed at MIT by the Balloon Group in collaboration with the Cosmic Ray Working Group, University of Leiden, the Netherlands.

A detailed description of the orientation system, phoswich detectors and associated electronics has previously been reported (J. Ballintine 1981) and a short summary follows. Observations of two celestial objects using this telescope will be reported: the COS B gamma ray source CG 135+1 and a drift scan across the Galactic Center. These observations have been analyzed as part of the investigations leading to this thesis. The exceptional sensitivity of these observations motivates the search for a replacement instrument, an example of which is described in later sections of this thesis.

4.1 Instrument

The gondola flown on May 7 and 8, 1980, basically consisted of a detector system with associated electronics and an orientation system that could point the detectors at any celestial hard X-ray source above the horizon. The data telemetered back to ground included: detector events (energy, time, pulse shape); redundant aspect information of the azimuth and elevation of pointed detectors vs. time measured by various sensors and detectors (including a charge-coupled device (CCD) television camera aligned with the X-ray axis and a sun sensor); and general housekeeping information (voltages, currents, temperatures, etc.).

The detector assembly consisted of an array of passively collimated phoswich scintillation crystals sensitive to 20-240 keV X-rays. The sixteen 92 cm^2 square detectors were divided into 2 groups of 8, module A and module B, each surrounded by plastic scintillators to veto high energy charge particle events. The phoswich assembly (Fig. 2.1) had as the primary X-ray detector a 9.6 cm x 9.6 cm x 0.3 cm thallium activated NaI crystal bonded to a 9.6 cm x 9.6 cm x 3.8 cm sodium activated CsI crystal. The crystal was heremetically sealed in an aluminum case with a 1 mm beryllium entrance window and a 3 mm quartz window optically coupled to a photomultiplier tube. Only events occurring in the NaI crystal (as determined by the risetime) were considered valid events.

In front of the detector were a pair of slat collimators that defined the field of view. Each collimator consisted of flat parallel plates made up of layered metal. The horizontal collimator restricted the field of view in elevation and the vertical collimator restricted the field of view in azimuth. The slat collimators had a triangular response to off axis X-rays. Module A had a field of view of 3°x3° FWHM while Module B had 3° elevation x 1.5° azimuth FWHM field of view. The finite geometric size of the collimators reduced the sensitive area of 1475 cm^2 to 1125 cm^2 effective area for on-axis X-rays. The vertical collimators were mounted in such a way as to be rocked right and left by 4.5° relative to the nominal viewing direction. This allowed a background measurement to the right and left of a faint X-ray source without moving the entire gondola. For faint sources where half the observation was spent on background, the collimators pointed two

minutes on the source, two minutes to the left of the source, two minutes source, two minutes right, and the cycle repeated. This "chopping" of the field of view reduced systematic errors in background subtraction due to long term variations in the background counting rate. For drift scans the collimators were left in the neutral (on-axis) position, and the source was allowed to drift through the field of view as the earth rotated.

The aspect determination of the gondola is important in determining the exposure of the detectors to a celestial source. Once the position on the celestial sphere of the collimator axis and the X-ray source itself is determined, then the collimator transmission function, T, can be calculated using:

$$T = \frac{\cos(\text{El source})\ (3-|\text{El}_{\text{source}}-\text{El}_{\text{axis}}|)\ (F-|\text{Az}_{\text{source}}-\text{Az}_{\text{axis}}|)}{3xF}$$

where $(\text{Az}_{\text{source}}, \text{El}_{\text{source}})$ and $(\text{Az}_{\text{axis}}, \text{El}_{\text{axis}})$ are the azimuth and elevation of the X-ray source and collimator axis respectively. F is a constant equal to 3 for module A and 1.5 for module B.

The method of establishing the X-ray axis of the collimators during flight are described in detail elsewhere (Ballintine 1981). The aspect during the galactic center drift scan came from two independent sources: the "coarse" aspect based on the orientation system (angle of elevation axle, azimuth of magnetometer, roll and pitch sensors); and a direct measurement with the "star TV", a CCD camera whose optical axis is calibrated against the X-ray collimator axis on the ground. The star TV has an accuracy of ~.1° (calibration error) though the coverage

of the drift scan is incomplete due to lack of bright stars in the field of view of the CCD (3°x4°). The coarse aspect is complete throughout the flight though its accuracy is only ~.3°. The CG 135+01 observation occurred during the day so the coarse aspect was used along with an azimuth-sensitive sun sensor accurate to .1°. Based on the collimator transmission function, an error of 0.3 degrees in either azimuth or elevation is a 10% error in intensity for module A and a 20% error in intensity for module B if the error is in the azimuthal direction. These errors in absolute intensity are small compared to the statistically determined errors of faint sources such as CG135+01 and the Galactic Center.

4.2 The 1980 Flight

The gondola was launched at 00:30 UT on May 8, 1980. The 1.2×10^6 m^3 balloon from which it was suspended reached an average float altitude of 38 km (~4 gm/cm^2 atmospheric column density). Sources observed during the flight included NRAO 140, Her X-1, Cyg X-1, 3C273, Crab Nebula, CG 135+1 and the Galactic Center. Results on the first five have been reported elsewhere (Scheepmaker 1981; Ricker 1981). Two drift scans of the Galactic Center were made during the period 08:25 UT to 9:21 UT on May 8, 1980. The X-ray detectors were pointed at ~180° azimuth and 29° elevation (gondola position: 31.3°N latitude and 94.3°W longitude). The source drifted across the field of view at ~.2°/min. The 2 hour observation of CG 135+1 began at 13.06 UT on May 8. The collimators were pointed at the most recent COS B error circle (Swanenburg 1981) and the chopping collimator technique was used. The average atmospheric column density to the source was 9.2 gm/cm^2 for the

Galactic Center and 4.25 gm/cm for CG 135+01.

4.3 Detection In Hard X-rays of the COS-B Gamma Ray Source CG 135+1

With the publication of the second COS-B catalogue (Swanenburg et al. 1981) only 4 of the 25 detected gamma ray (E>100 MeV) sources had been positively identified with sources at other wavelengths. Two are associated with the Crab and Vela pulsars through their timing signatures and the other two are identified by positional coincidences with the quasar 3C273 and the cloud complex ρ Oph. Because of the large error circles of COS-B (radius ~1°) and the fact that most of the COS-B sources lie on the galactic plane, the identification of additional sources with lower energy counterparts is ambiguous at best.

The two "best" candidate sources that have been proposed as the lower energy counterparts to CG135+1 are the QSO 0241+62 discovered by Apparao et al. (1978) in soft X-rays and the radio star GT0236+61 (LSI+61°303) discovered by Gregory and Taylor (1978) in a survey of variable radio sources in the Galactic plane. LSI+61°303 is also a soft X-ray source and has been observed by the Einstein HRI and IPC instruments (Bignami 1980). Recently a 26.5 day period was observed in the radio emission of the radio star (Taylor 1982) and has been interpreted as a binary period of a compact object orbiting a B0-B0.5 main sequence star. Since the only identified 100 MeV gamma ray sources are the Crab and Vela pulsars, the QSO 3C273, and the cloud complex ρ Oph, the QSO 0241+62 and the radio star system LSI+61°303 are both strong contenders for the identification with CG 135+01. Fig. 4.1 shows the location of these 2 candidates with respect to the COS-B error circle.

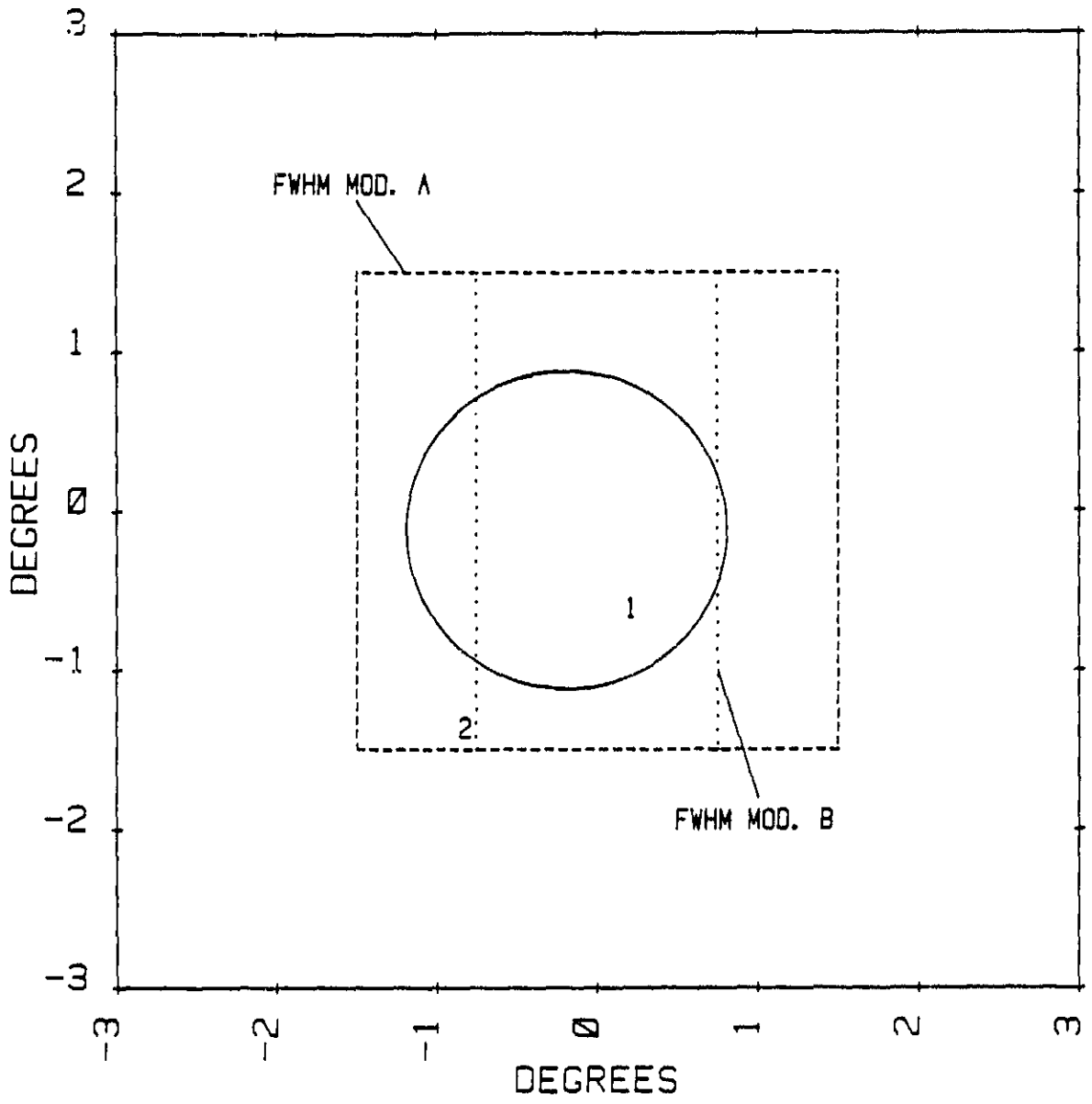

1 LSI 61 303
2 QSO 0241+62
CG 135+01 ERROR CIRCLE

Figure 4.1 The sky near the COS B gamma-ray source CG 135+01. Shown are the positions of two soft x-ray sources proposed as X-ray counterparts, as well as the COS B 90% confidence circle for the gamma-ray source. Also shown is the average field of view of the slat collimators over the 1500 cm^2 phoswich array. The FWHM of the triangular response is plotted for both Module A (3°x3°) and Module B (1.5°x3°).

Note that the QSO 0241+62 is just outside the reported 90% confidence contour (Swanenburg 1981).

The observation on May 8 detected a hard X-ray source with a 4.1 sigma level of significance from the region of the sky containing the gamma ray source CG135+01. Both candidates, the QSO 0241+62 and the radio star LSI+61°303 were in the field of view of the detectors (Module A: 3°x3° FWHM; Module B: 1.5°x3° FWHM) and therefore it cannot be positively determined from which source the X-rays were detected (Fig. 4.1). The intensity can be determined assuming it was one source or the other and that intensity can be compared with previous observations carried out by other observers in different (sometimes overlapping) energy bands.

Figure 4.2 shows the hard X-ray spectrum plotted two ways. In 4.2 the source of emission was assumed to be the QSO 0241+62, which was on the average ~1.6° away from the center of the field of view; while in 4.2b the source assumed was LSI+61°303, which was 0.65° away from the center. Thus, due to aspect corrections, the intensity for the source in (a) is greater than in (b). This intensity difference is due to the triangular response of the slat collimators. Plotted along with these measurements are results reported in the literature from previous observations of this region (OSO 8, Worrall et al. 1980; OSO 7, Marachi et al. 1978; SAS-3 Apparao et al. 1978; MISO, Perrotti et al. 1980; MPC on HEAO 2, Halpern 1982).

As can be seen in Fig. 4.2a, if the hard X-ray source is the QSO 0241+62 then the intensity in the range 20-50 keV (overlap with OSO 8) has increased by a factor of ~5 over a timescale of ~2 years. This

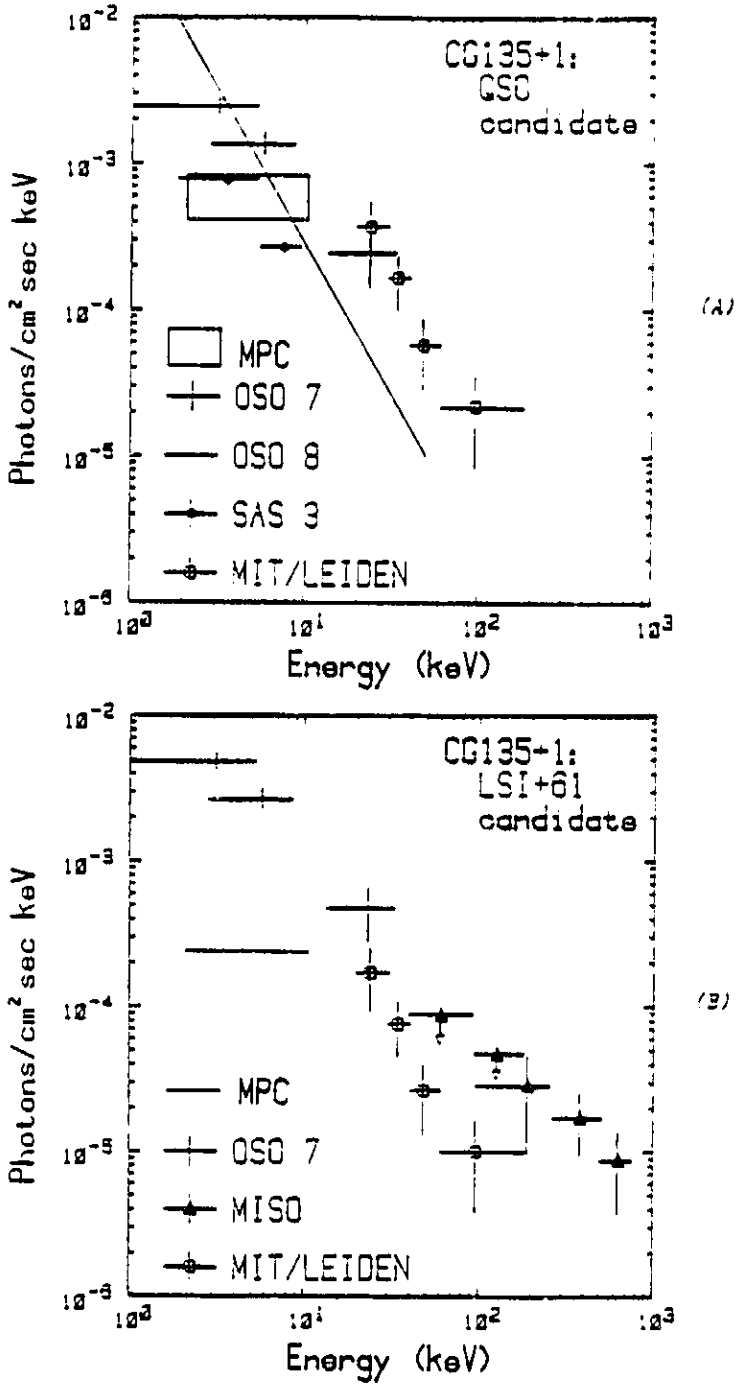

Figure 4.2 X-ray spectra for two possible candidates for the gamma-ray source CG 135+01. The MIT/Leiden points are plotted assuming the source is either the QSO 0241+62 [upper panel (A)] or the radio star LSI+61°303 [lower panel (B)]. For further details see text.

QSO is known to be highly variable in both the radio and optical bands (Feldman 1980). There is also evidence for variability in X-rays by approximately this same factor based on the OSO 7, OSO 8 and SAS-3 data points. The box shown for the MPC on the Einstein Observatory covers the range of fluxes measured in 4 separate observations over a period of 7 months (Feb. to July, 1979).

Plotted in Figure 4.2b are the MIT/Leiden data points assuming the observed hard X-ray source was the radio star LSI+61°303. Of the previous results plotted for this source, only the MPC instrument has a small enough field of view to avoid contamination from the QSO. The OSO-7 data points have been corrected for aspect assuming the radio star was the soft X-ray source although the 1 sigma error box does not contain the radio star (Markert 1982). Based on the factor of ~20 lower flux measured by the MPC, the OSO-7 points are more consistent with the QSO interpretation of their origin. The MISO points also suffer from possible source confusion (collimators: 3°x3° FWHM). The points are plotted only for the radio star because the QSO lies just outside their 1-sigma error region determined from their drift scan results. An extrapolation of the MIT/Leiden data points is inconsistent with the MISO points in the .2-1 MeV range by a factor of 12. Also the MIT/Leiden data do not require a spectral break in the power law extrapolation to explain the COS-B gamma ray intensity as do the MISO points (Perotti 1980). A low energy extrapolation would also seem to be inconsistent with the very low flux measured by the MPC.

The parameters of a power law fit to the hard X-ray data are shown in Table 4.1 for both assumed sources. The hard X-ray luminosities

TABLE 4.1

FLUX AND DERIVED LUMINOSITIES FOR TWO POSSIBLE CG135+01 CANDIDATES

ASSUMED SOURCE	MIT/LEIDEN POWER LAW FIT *		DISTANCE (H_o=75km/s per Mpc)	DERIVED SOURCE LUMINOSITY (ergs/sec)		
	A	Γ		MIT/LEIDEN (20-80keV)	HEAO 2 MPC ** (2-10keV)	COS B *** (100-1000MeV)
QSO 0241+62	1.0×10^{-4}	2.4 (+1.2, -1.0)	z=.044	1.7×10^{45}	4×10^{44}	1.5×10^{45}
				OR		OR
LSI 61 303	4.6×10^{-5}	2.4 (+1.2, -1.0)	2.3kpc	1.3×10^{35}	7×10^{33}	2.6×10^{35}

* $dN/dE = A*(E/40)^{-\Gamma}$ photons/cm^2 sec keV

** Monitor Proportional Counter, Halpern (1982)

*** Swanenburg (1981)

derived from this flux are similar to the measured gamma ray (100 MeV-1 GeV) and soft X-ray (2-10 keV) luminosities for the QSO. Other quasars (e.g. 3C273) also exhibit luminosities in this range throughout the spectra from radio to gamma rays. Models accounting for this energy generation in quasars are usually based on accretion disks around supermassive black holes (Eardley et al. 1978) where the X- and gamma-rays are created by inverse Compton scattering of photons off reletivistic electrons.

A similar process (inverse Compton scattering) for producing high energy photons in the LSI+61°303 system is proposed by Marachi and Treves (1981). Their model proposes a young pulsar losing energy in a relativistic wind at a rate of 10^{37} ergs/sec. The wind is randomized in a shock region at the interaction boundary of the pulsar and stellar winds. The stellar photons are inverse Compton scattered to X- and gamma-ray energies. This model produces relativistic electrons continuously while competing accretion disk models can modulate the production to better explain the perodic synchrotron radio emission (Taylor and Gregory 1982). The radio emission peaks between the phases 0.3 to 0.8 of the 26.52 day period (phase 0.0=JD 2443366.775) and so should the hard X-ray and gamma rays if particle acceleration is linked to an accretion process. The MIT/Leiden observations occurred at the radio phase ~0.75. The MISO observation occured at the radio phase ~0.01, inconsistent with this interpretation of the radio emission. The MISO derived luminosity, L (.2- 1MeV) ~10^{37} erg/sec, also pushes the Marachi and Treves model to its limit requiring 100% conversion of rotational energy into 1 GeV electrons. There is also a large discrepancy with

the MPC soft X-ray luminosity.

Although this detection of CG 135+1 in the energy range 20-180 keV cannot with certainty determine the low energy counterpart to the gamma ray source, it does extend the knowledge of this source region into another spectral decade. Whether it shows variability of the quasar 0241+62 or establishes a hard X-ray flux for LSI+61°303, this detection should be helpful in unravelling this interesting part of the sky.

4.4 Upper Limits on the Hard X-ray Flux of the Galactic Center

In the study of astrophysical processes near galactic nuclei, the closest example, our own galactic nucleus, has been hidden at optical wavelengths due to intervening gas and dust in the galactic disk (visual extinction ~27 magnitudes). The ~10 kpc distance to the nucleus is a factor of 60 smaller than the distance to the nucleus of M31. The galactic nucleus is, however, observable both in the infrared and radio bands and also at X-ray energies above about 2 keV.

A review by Oort (Oort 1977) summarizes the principle features of the galactic center region observed in radio and infrared. Within the central 30 arc min of the galactic center (100 pc at 10 kpc) the mass density distribution, inferred from the infrared light distribution, shows an increase from 100 M_0 pc^{-5} at R=100 pc to $4x10^5$ M_0 pc^{-3} at R=1 pc. Radio observations show large H II regions and molecular cloud complexes. The radio source Sgr A West is thought to be coincident with the dynamical center. Contained in Sgr A West is a compact non-thermal radio source (Balick and Brown 1974) with VLBI determined scale sizes at 3.6 cm of 0".015 (150 A.U.) (Lo et al. 1981). The 2.2μm

infrared source IRS16 is commonly accepted as the counterpart to the non-thermal radio source. This position is also the dynamical center of a group of compact clouds seen in Ne II infrared fine structure emission (Lacy 1980). Recently, deep exposures of this region using charge-coupled devices have discovered a far red (9200A) source close to the reported location of the non-thermal radio source (Ricker 1982b).

Detection of X-rays (1-10 keV) from the Galactic Center began with the UHURU satellite which found evidence for an extended source (or source complex) about the galactic center designated GCX (Kellogg 1971). Many instruments using modulation collimators and coded masks produced images of the galactic center with angular resolutions from 2.5 arc min to 15 arc min (see Skinner for summary of results, Skinner 1979). Six sources were discovered within 1.5° of the galactic center. The brightest, A1742-289, was a transient source with a peak luminosity of 4×10^{38} ergs/sec (1-10 keV) in February 1975, though it faded to 2×10^{36} ergs/sec by June 1976. The source is 1 arc min from the galactic center and is considered a typical X-ray transient not necessarily associated with the nucleus (Skinner 1979).

The second High Energy Astronomical Observatory, HEAO-2 or Einstein Observatory, observed the galactic center region in 1979 using a focussing X-ray telescope over the energy range .5 to 4.5 keV (Watson et al. 1981). They found 12 point sources and diffuse emission within 0.5° of the galactic nucleus. One of the sources was coincident with the galactic center (1 arc min resolution) and had a luminosity of 1.5×10^{35} ergs/sec. This luminosity may be in error by as much as a

factor of 10 due to assumptions about the spectral shape and low energy cutoff that are used in converting measured counts to source luminosity. The variability was less than 2% over 6 months. The Einstein MPC also detected a flux (2 to 6 keV) from the galactic center region (Watson et al. 1981) although the field of view contained all of the 12 point sources as well as the diffuse emission. The measured flux is consistent with UHURU results for GCX and is plotted in Fig. 4.3.

In the hard X-ray regime, source confusion due to large fields of view has been the main hindrance to observational progress. Balloon observations with 1.5° angular resolution discovered several sources (20-50 keV) within 10° of the galactic center (Ricker et al. 1976) though emission from the galactic center was not definitely observed since GX1+4 was also in the field of view. The OSO-8 hard X-ray detector with a 5° angular resolution detected a strong source in September 1978 whose 95% confidence contour contained the galactic center (Dennis et al. 1980). A photon power law spectrum from 21 to 197 keV is best fit to their data with a power law photon index of -2.3±.3.

The low energy detector (LED) on the A4 experiment on the HEAO-1 satellite observed the galactic center region 3 times separated by ~6 months. Using data fitting procedures on the 1.6° angular resolution scanning exposures, a source located within 0.5° of the galactic center was detected on all three observations in the energy band 13-100 keV (Matteson 1982). This source had the hardest spectral index of all sources within 10° of the nucleus, accounting for 14% of the flux in the 13-50 keV energy band and 23% of the total flux from 50-100 keV for

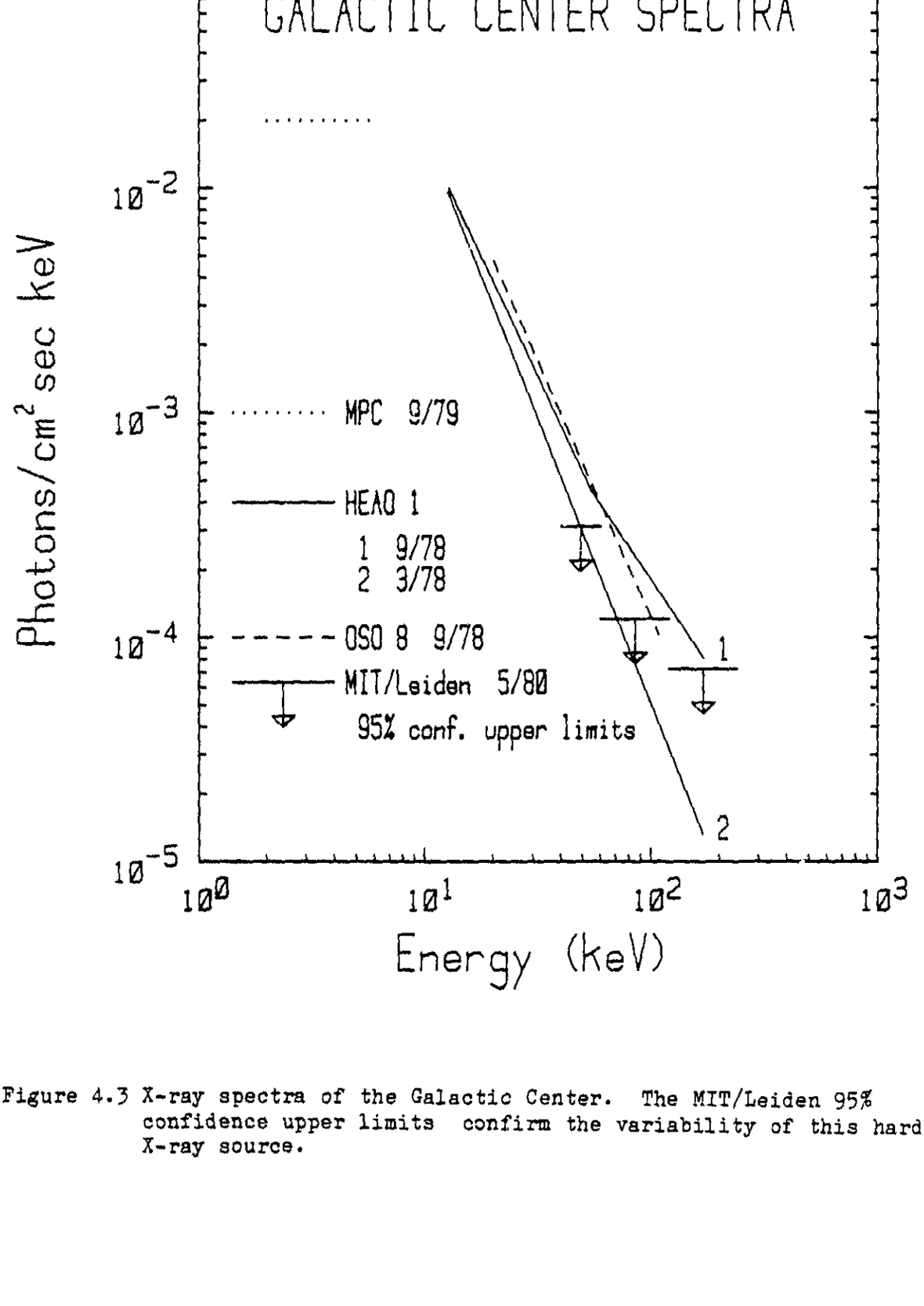

Figure 4.3 X-ray spectra of the Galactic Center. The MIT/Leiden 95% confidence upper limits confirm the variability of this hard X-ray source.

the observation in September 1977. The spectral fits for two observations from HEAO-1 are shown in Fig. 4.3 along with the OSO-8 results. The variability in the higher energies over the 6 month time period are apparent. The variation at 100 keV is a factor of 3 while only 15% at 20 keV. The luminosity from 10 to 100 keV for the 9/78 HEAO 1 observation is 7×10^{37} ergs/sec.

At energies above 100 keV most observations have very large fields of view containing many X-ray sources. At 300 keV HEAO-1 and HEAO-3 showed variability of a factor of 4 and 8 decrease over 6 months, respectively (Riegler et al. 1981). Although this cannot be positively identified with the lower energy Galactic Center source, the large variability implies a strong single emitter with a peak luminosity of $\sim 3 \times 10^{38}$ ergs/sec (Matteson 1982) in the 100 to 1 MeV range or 30 times the Crab Nebula luminosity.

4.4.1 May 1980 Drift Scan

The MIT/Leiden gondola scanned across the galactic center region twice on May 8. Because the Galactic Center only reaches an elevation angle of ~30° at transit, the atmospheric column density to the source was 9.2 gm/cm^2 which gives an atmospheric transmission of 25% in the 60-120 keV band.

The response function of the collimators vs. time, R(t), was calculated based on the gondola aspect (azimuth, elevation, longitude, latitude, roll, and pitch); the source (RA, Dec, time); and the calibrated collimator axes with respect to the gondola. The response of Module A and B to the galactic center is shown in Fig. 4.4 (the collimator response is normalized such that an on-axis source has a resp-

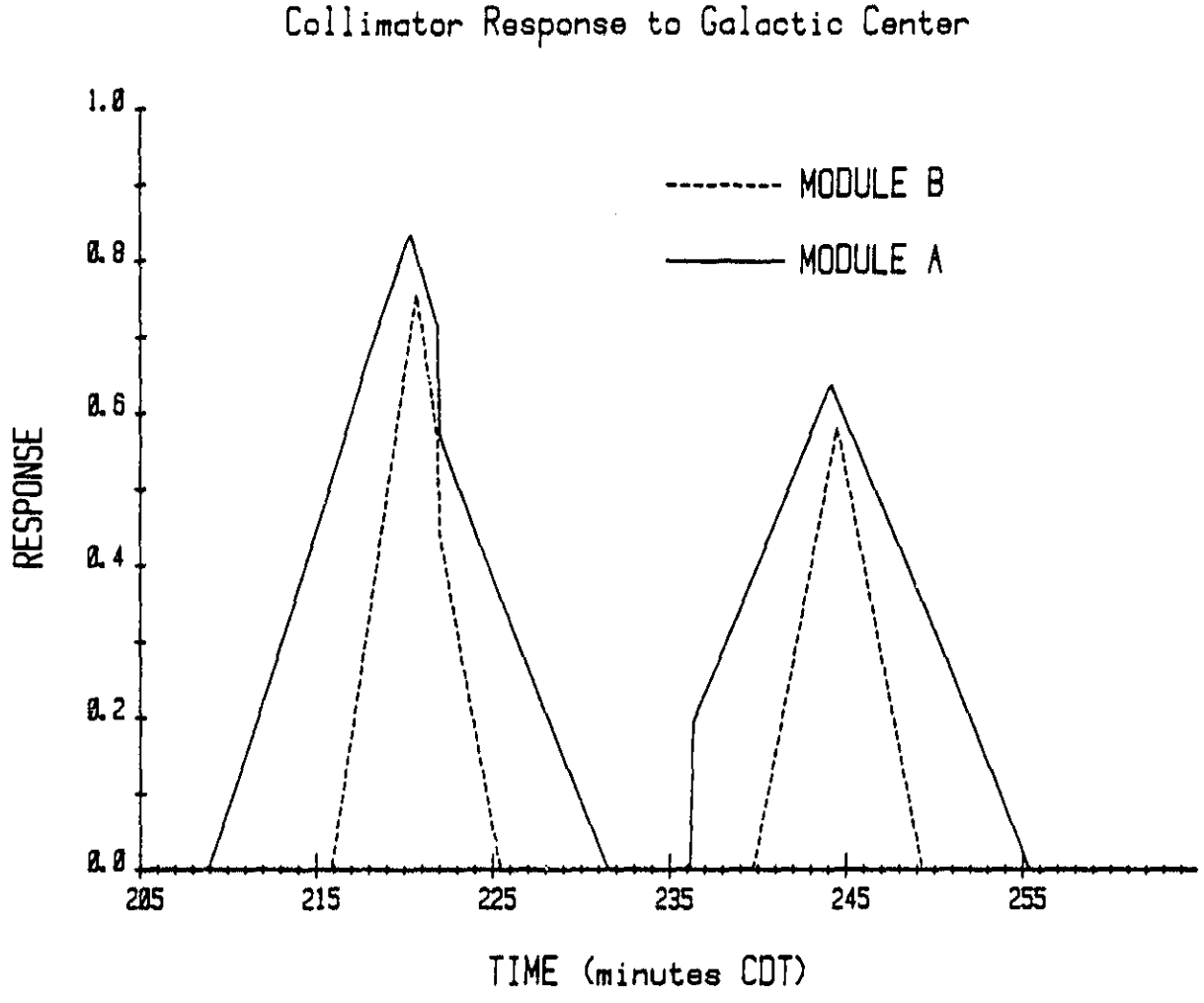

Figure 4.4 The 1500 cm^2 phoswich array collimator response vs. time during 2 drift scans across the Galactic Center. The response is normalized such that an on-axis source with a response of 1 would be observed with 592 cm^2 effective area. The glitch at minute 222 was due to the elevation drive suddenly moving 0.2°.

onse of 1 with the effective area equal to 592 cm^2).

The measured count rate vs. time, F (counts/minute), for each module was fit with two free parameters: a constant background rate B(cts/min); and a constant source flux A (cts/min) times the independent variable R(t).

$$F(t)=B + A * R(t)$$

A chi-squared minimizing technique was used for 3 energy bands: 40-60 keV; 60-120 keV; 120-200 keV. The source flux was then corrected for detector and window efficiency and atmospheric transmission resulting in a source photon flux at the top of the atmosphere (Ballintine 1981). Though small positive detections occurred in the 2 lower energy bands for both modules A and B, the data were consistent with a source flux equal to zero. Upper limits (95% confidence) to a source at the galactic center are plotted in Fig. 4.3. The 95% confidence limits were determined using the χ^2 minimum + 3.8 criterion as described by Avni (1976).

This observation indicates a continued variability of the hard X-ray source near the Galactic Center. The variability is at least a factor of 2 at 60 to 120 keV over a period of 1.6 years. This strengthens the identification of this 10-100 keV source with the (>100 keV) highly variable source. The next logical step of identifying this bright, variable hard X-ray source with the Galactic Center is on less firm ground. The best argument is based on extragalactic observations of active galactic nuclei (Seyferts, quasars, N galaxies) where highly luminous objects vary on short time scales and are located close to the dynamical center of the galaxy. The identification with the Einstein

source at the galactic center that has a constant luminosity in soft X-rays cannot be proven, though the HEAO-1 A-4 results vary less with time at lower energies. Qualitative source models have beer proposed (Matteson 1982) in which high temperature (10^{10}K), high luminosity ($\sim 10^{38}$ erg/sec), short timescale (6 months), energy outbursts occur in a central region providing the hard X-ray flux. Outer regions (which are heated to only 10^{7}K, have luminosities $\sim 10^{35}$ ergs/sec, and lifetimes of years) provide the constant soft X-ray luminosity which is the integrated effect of many impulsive events.

The above results indicate that what appears to be a stable low intensity source in one energy band might be a highly variable and luminous object in another energy band. Sensitive hard X-ray telescopes with good angular resolution are needed to resolve the candidate Galactic Center sources and monitor their variability. Such an instrument is described in Section 5.

5.0 DESIGN CONSIDERATIONS FOR A NEW HARD X-RAY TELESCOPE

After the demise of the 1500 cm^2 balloon-borne hard X-ray telescope due to a free-fall from float altitude, the design of a completely new telescope became necessary. Though starting from scratch was not desired, it did allow a rare freedom to rethink and redesign all major systems in a future gondola, especially the main X-ray detectors. The constraints imposed upon a design for a balloon-borne detector are considerable. The goal was to match the sensitivity of the 1500 cm^2 detector in hard X-rays with a gondola that would weigh less than 400 kgs. This would allow possible long duration balloon flights (~30 days) at higher altitudes.

5.1 Sensitivity

Signals from cosmic X-ray sources are received as photons and counted individually by the detector. The limitations of measuring observable properties such as intensity, location and spectra are statistical in nature and X-ray telescope parameters are optimized to minimize statistically determined errors. The basic parameters of an X-ray telescope are: collecting area, A, in cm^2; differential background counting rate, B (counts/cm^2 sec keV); energy bandwidth, ΔE, in keV; observation time, t; and detection efficiency ε (including atmospheric transmission). The number of signal counts, N_s, from a source with differential photon flux, F (photons/cm^2 sec keV), observed with a counter of effective area, A, efficiency ε, over a time t, bandwidth ΔE is:

$$N_s = FAt\Delta E\varepsilon$$

During this same time the number of background counts, N_B, observed is:

$$N_B = BAt\Delta E$$

(B is measured at the detector so $\epsilon=1$)

The total number of counts observed is N_s+N_B so a separate measurement of the background of length t must be made and then subtracted to yield the signal counts:

$$N_s=(N_s+N_B)-N_B$$

and the variation:

$$\Delta N_s=(\Delta(N_s+N_B)^2+\Delta N_B^2)^{1/2}$$

assuming F and B are uncorrelated and that changes, ΔB, in the background rate are small compared to statistical fluctuations. (Changes in the background counting rate with time is a major problem and many techniques have been developed to reduce this systematic error. See Section 4.1.)

For a faint source (i.e., $\epsilon F<B$) the statistical fluctuations in B dominate the error. For $N_B>>N_s$:

$$\Delta N_s = \sqrt{2}\ \Delta N_B = \sqrt{2N_B} = \sqrt{2BAt\Delta E}$$

(This is just the standard deviation of a Poisson distributed count rate.) The minimum detectable flux, F_{min}, can be defined as that flux where the signal counts are a certain number, S, of standard deviations above the background

$$S = \frac{N_s}{\Delta N_s} = \frac{F_{min}At\epsilon\Delta E}{\sqrt{2BAt\Delta E}}$$

$$F_{min} = \frac{S}{\epsilon}\sqrt{\frac{2B}{At\Delta E}}$$

The number used for S depends on the number of separate measurements of

length t and the significance required. A "four sigma detection", (S=4), has a probability of randomly occuring once in 30,000 measurements (Bevington 1969).

To make F_{min} as small as possible (i.e. sensitive to very faint sources), the goal in designing a hard X-ray detector is a large effective area of efficient, low background detectors that can observe for a long time. Because these goals are sometimes incompatible, tradeoffs among the design parameters must be made. For example, to take advantage of a satellite's long observing time, effective area (and its corresponding mass) is usually sacrificed. Large areas are also difficult to shield so higher background rates are reluctantly accepted.

The formula for F_{min} does disguise the fact that A is the photon collecting area, not the detector area, while B refers to the background counts observed at the detector divided by the collecting area. Thus, if the collecting area could be increased with X-ray mirrors or concentrators while keeping the detectors the same size, not only would A increase but B would decrease and F_{min} would be proportional to A^{-1} rather than $A^{-1/2}$. (This is not true if the background, B, is dominated by diffuse sky flux. In that case an increase in collecting area would increase the background and F_{min} would be proportional to $A^{-1/2}$).

This technique of separating the collecting area from the detector has been used in optical astronomy since Galileo (Galileo 1610) and recently has been applied to all of the electromagnetic spectrum up to and including the soft X-ray (1-5 keV) imaging telescope of the Einstein Observatory (HEAO-2) (Giacconi 1979).

5.2 Bragg Diffraction Concentrator

In the energy regime accessible with balloon-borne detectors (greater than 20 keV), grazing incidence reflection of X-rays does not work (reflection efficiencies <<1%). But X-rays of this energy can be Bragg diffracted with reasonable efficiencies using thin crystals of lithium fluoride (Lytle 1969). The angle of diffraction has a finite spread ("rocking curve" ~.2° for LiF) so any focal point would be "blurred" and concentration of X-rays to a single detector rather than imaging would be the result. However, the inability to image X-ray sources using a Bragg diffraction concentrator relaxes some construction and pointing accuracy constraints. A concentrator need not be perfectly rigid with arc-second tolerances and can be made relatively lightweight and inexpensive.

5.3 Low Background Balloon-Borne Telescope Design

The preceding design considerations have lead to the concept of a hard X-ray diffraction telescope consisting of a lithium fluoride lined paraboloid that concentrates hard X-rays onto a small, well-shielded HgI_2 detector (Figs. 5.1 and 5.2). This design has been accepted as the basis for the Hard X-ray Diffraction Telescope (HXDT) to be flown on a future Space Lab mission. The size and shape of the paraboloid determines the energy bandwidth of the photons concentrated to the detector at the focus. On-axis X-rays entering the aperture will Bragg diffract from the LiF crystals and proceed to the focus only if their energies are correct for that position on the paraboloid. The Bragg diffraction serves only to concentrate on- or near-axis X-rays; no fine energy resolution is derived from the concentrator, just the solid

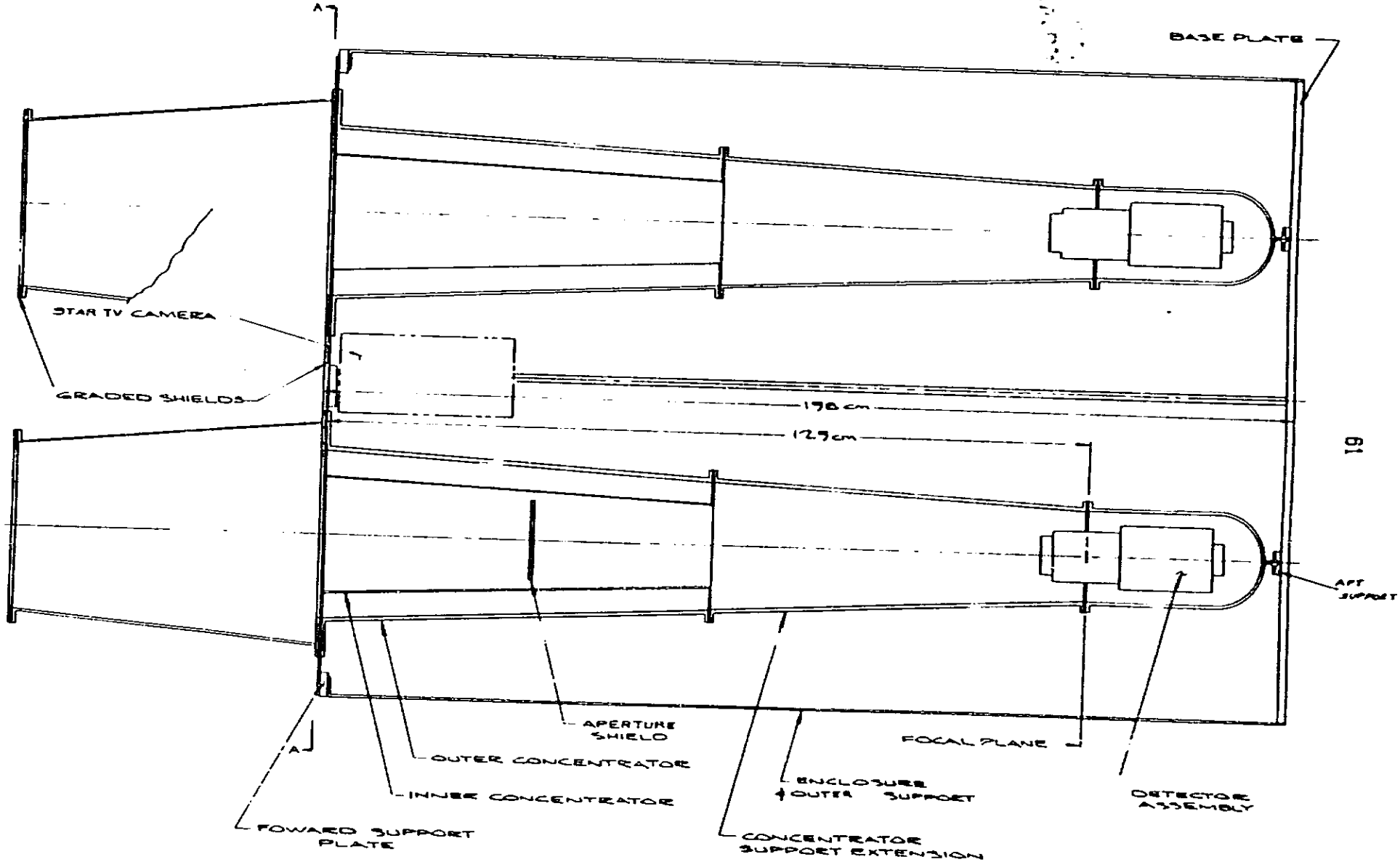

Figure 5.1 Sectional view of a proposed hard X-ray diffraction telescope.

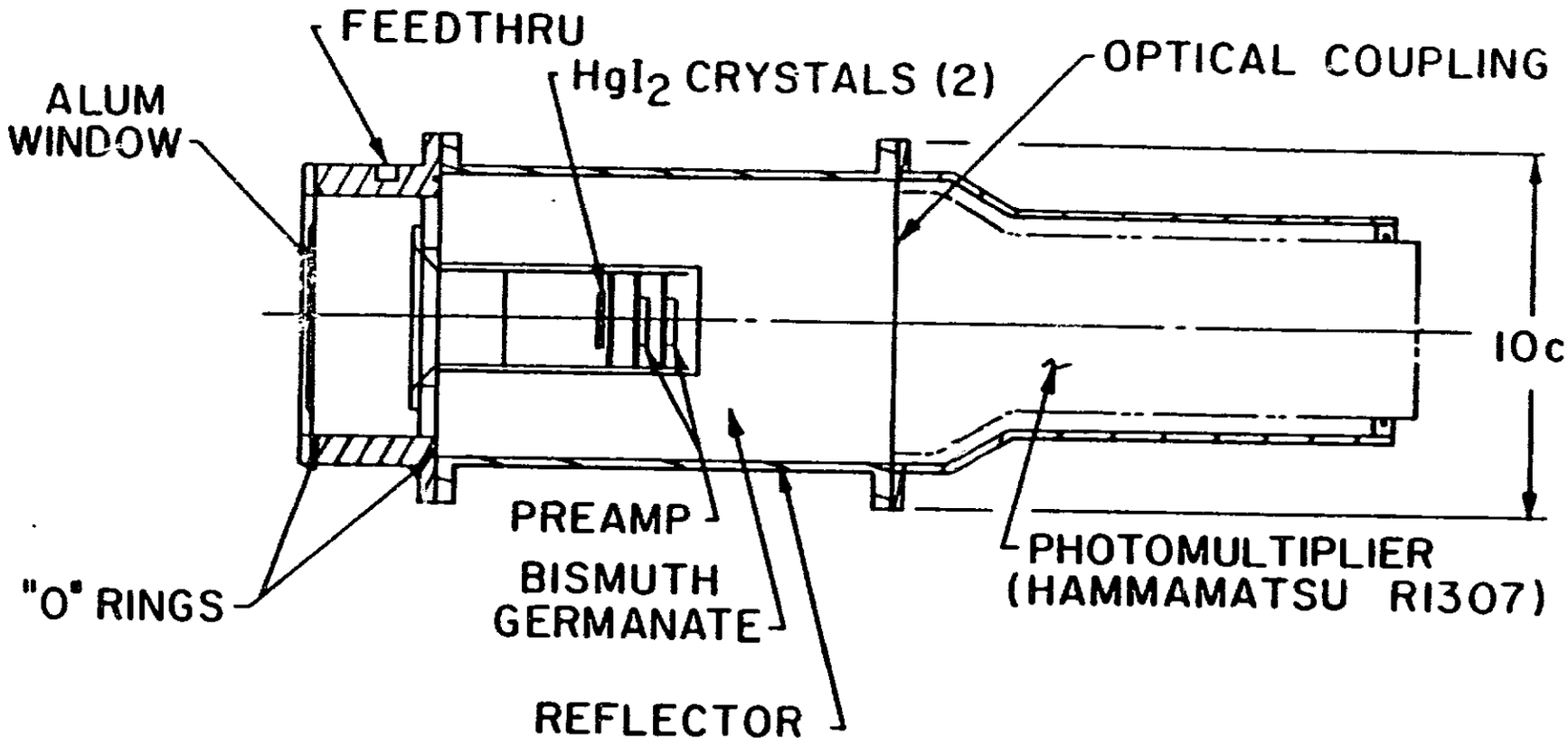

Figure 5.2 A schematic cross section of the bismuth germanate shielded detector assembly. The mercuric iodide detectors are positioned inside the gas tight, axially symmetric well.

state detector.

To limit the size of the concentrator (and therefore a possible balloon gondola), two nested paraboloids optimized over 1 octave in energy (40-80 keV) has been the basis of a new gondola design. This energy range was chosen because it lies above the energy of significant atmospheric absorption at balloon altitudes. The upper energy boundary is limited by the size of the paraboloid. For a small, lightweight balloon gondola, 80 keV seemed a reasonable compromise. Some interesting astrophysical processes that have signatures in this energy range include cyclotron emission or absorption features from magnetic neutron stars and spectral turnovers in active galactic nuclei power law spectra. Gamma-ray line emission from long lived radioactive isotopes such as ^{44}Ti is expected to be observed in supernova remnants in this energy range. Observing these narrow line features will require excellent energy resolution.

The detector system behind these concentrators consists of thin HgI_2 detectors surrounded by a large bismuth germanate scintillator operated in anticoincidence (Fig. 5.2). A prototype detector system has been designed, constructed and integrated into a small balloon gondola (Fig. 5.3) to measure the actual counting rate background at balloon altitudes. This background counting rate, B(cts/sec cm^2 keV) will be used in the sensitivity calculation as well as a check on background models of the detector systems. This will allow further modification and improvements in background rejection and overall gondola design.

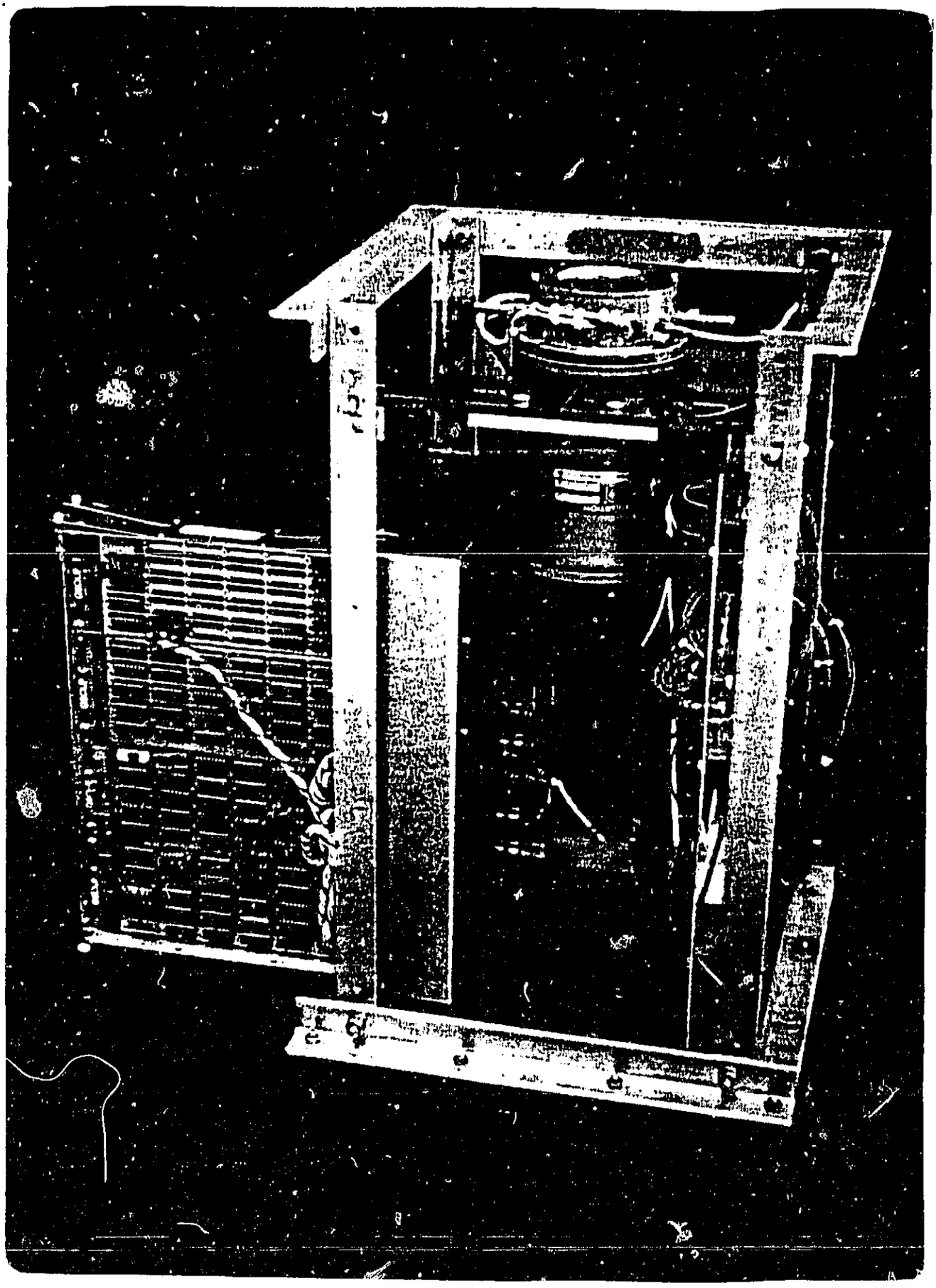

6.0 SHIELDED MERCURIC IODIDE BACKGROUND MEASUREMENT EXPERIMENT

In research work leading to this thesis, a small gondola (Fig. 5.3) containing a prototype detector for a hard X-ray diffracting telescope was designed, constructed and flown at balloon altitudes. Its purpose is to measure the background counting rate at the eventual telescope operating environment (>40 km altitude, balloon or satellite). The radiation environment (X- and gamma rays, high energy charged particles, neutrons) is quite different at ground level due to atmospheric shielding and ground radiation. The measurements are compared with predictions made by a detector Monte Carlo simulation. Once the simulation is checked, design parameters (geometry of detectors, shielding components and discriminator settings) can be varied in the simulation to optimize (lower) the expected background counting rate.

The small gondola can be conceptually divided into two subsystems: the prototype detector consisting of a bismuth germanate shielded mercuric iodide detector (Fig. 5.2) described in Section 6.1; and the detector support systems consisting of electronics, power systems, data recording, and temperature control all described in Section 6.2. The radiation environment and detector computer model is described in Section 7.

6.1 Prototype Detector System

The overall design goal for the detector behind the X-ray concentrator was to minimize the number of background events in the energy range of 40-80 keV while keeping the response to the concentrated signal X-rays as high as possible. The proposed concentrator requires

a detector with an area equal to the size of its focal "spot" (~1 cm^2 for a lithium fluoride concentrator optimized for 40-80 keV). The detector must also have a field of view larger than the solid angle subtended by the concentrator to "see" all diffracted signal X-rays ($\Omega \sim .12$ steradian for same concentrator). The active anticoincidence shield should surround the detector except the aperture and if not stop incoming radiation then at least detect and veto it. Passive mass viewed by the detector (i.e., structural material such as aluminum that cannot be used to detect radiation) should be minimized because secondary radiation generated in this mass might not be vetoed.

The prototype detector system consists of two HgI_2 detectors mounted back to back and operated in anticoincidence. The two detectors are placed inside a bismuth germanate ($Bi_4Ge_3O_{12}$ or "BGO") scintillating shield along with two hybrid charge sensitive preamps. The BGO shield is also operated in anticoincidence with the main (top) detector. The axially symmetric "well" containing the detectors is gas tight (.5mm Al entrance window) to retain one atmospheric pressure at balloon altitudes. Such a gas tight enclosure eliminates the problem of high voltage corona breakdown encountered at low atmospheric pressures and avoids the need for potting the detector assembly.

6.1.1 Primary Mercuric Iodide Detector

The "main" HgI_2 detector that will eventually be used to detect X-rays from a celestial X-ray source is the top detector in the back to back geometry (Fig. 6.1). The actual HgI_2 detector used in the test flights has an effective area of 0.8 cm^2 (defined by the size of the palladium electrode) and is 390 microns thick. The bottom detector has

HgI_2 DETECTOR ASSEMBLY (DETAIL)

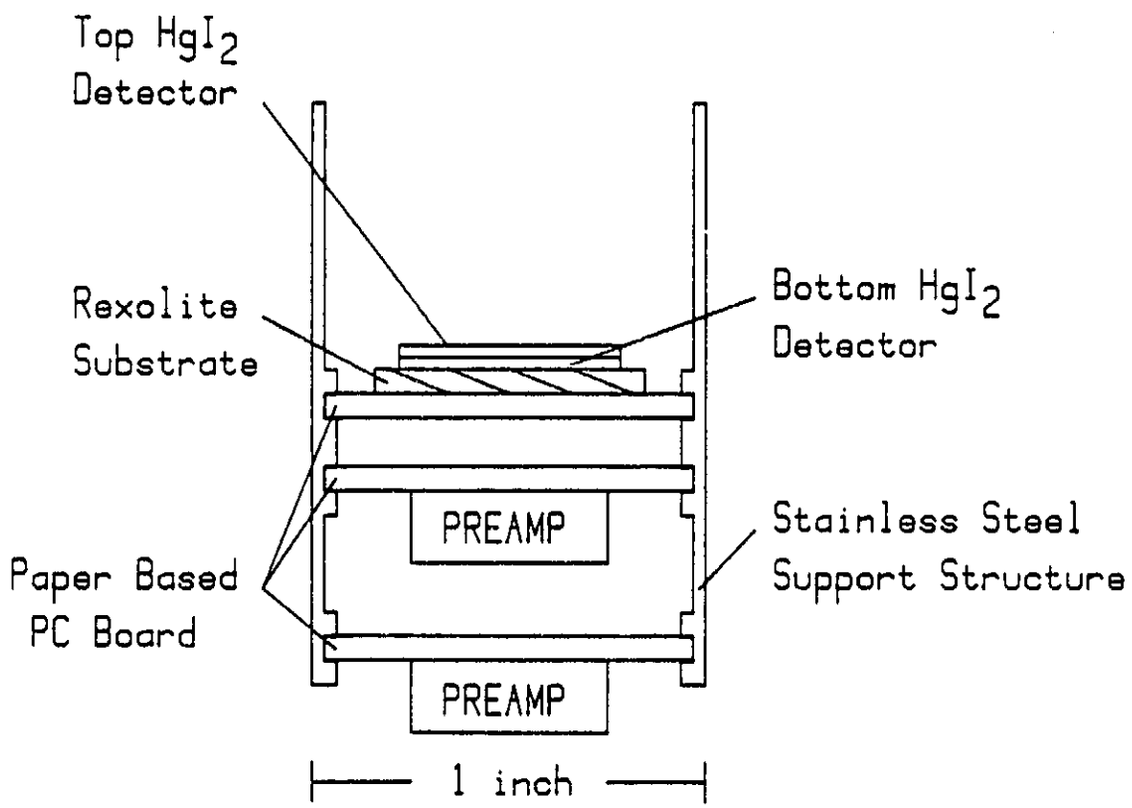

Figure 6.1 Detailed view of mercuric iodide detector assembly showing the components that fit in the axially symetric well inside the bismuth germanate shield.

the same area and is ~1000 microns thick. The bottom detector's main purpose is to provide active shielding from radiation generated in the passive material underneath (printed circuit boards and preamps) as well as better protection from aperture charged particle flux. The HgI_2 detectors are separated by a thin (13μm) mylar insulator and mounted on a Rexolite substrate. The HgI_2 crystals are grown and then fabricated into the "back to back" units by EG&G, Inc., Santa Barbara.

The charge sensitive preamps are mounted on paper based printed circuit boards and are held in place underneath the bottom detector by a low mass stainless steel structure. A glass epoxy based printed circuit board was avoided because of the high concentration of potassium 40 in natural glass (Knoll 1979, pg. 775). The preamps were based on a low power design for SAS-C (Goeke 1975) and were modified and hybridized by EG&G, Las Vegas. They were placed close to the detectors to minimize input capacitance and noise pickup. These preamps were chosen because of availability but future designs might consider placing just the input field effect transistor (FET) in the well to reduce passive mass. Small copper wires bring preamp power, high voltage, and ground down the well to the detector assembly and the top and bottom signals out of the well. The well is lined with electrically grounded aluminum (.25 mm) to provide electromagnetic shielding. Outside the well and field of view of the detectors but inside the pressure container are RC filters for the high voltage and preamp power.

6.1.2 Bismuth Germanate Shield

Bismuth germanate was chosen as the shield material because of its

very high photoelectric cross section and density. In terms of its stopping power it can almost be considered "active lead". The crystal is 7.5 cm in diameter and 12.5 cm long with a machined 7.4 cm deep x 2.5 cm diameter axially symmetric well in which the HgI_2 detectors are placed. The outside surface of the crystal is coated with reflective paint and encased in aluminum to protect the crystal and prevent light leaks. A Hammamatsu R1307 photomultiplier is mounted on the unpainted bottom of the BGO crystal opposite the well (Fig. 5.2) and surrounded by a μ metal shield to protect it from magnetic field induced gain changes.

At the time when the BGO was ordered from Harshaw Chemical Co. the 7.5 cm diameter was the largest size available. The 2.5 cm inner diameter of the well was determined by the preamp size and ease of construction. In the energy range where BGO has the smallest attenuation coefficient (~1 to 3 MeV), non-aperture gamma rays that intersect the HgI_2 must traverse at least 2.5 cm of BGO (~1 attenuation length). At lower and higher energies the attenuation is much greater. The top HgI_2 detector is placed 2.6 cm deep into the well measured from the top of the BGO. The BGO then acts as the collimator with a flat topped response and an effective circular field of view of ~.12 steradians.

With such a large field of view the diffuse atmospheric and cosmic X-ray background would dominate the background count rate. For the diffracting concentrator concept to work, X-rays that can reach the HgI_2 detector directly through the aperture must be stopped so that only diffracted X-rays from a celestial X-ray source are detected. The "direct" (undiffracted) field of view must be blocked using a graded

shield of lead, tungsten, and tin. The lower atomic number materials are included to stop the characteristic K X-rays of the higher. For the test flight of the prototype detector this passive shield was placed directly over the entrance window though in actual use with a concentrator it would be further from the detector so as not to block the diffracted X-rays. This is shown schematically in Fig. 6.2. The transmission of 1 mm of Pb + 1 mm of W + 2.5 mm of Sn is shown in Fig. 6.3.

6.2 Balloon Gondola and Associated Electronics

The detector prototype (BGO shield and HgI_2 detectors) is contained in a small (30 cm x 30 cm x 45 cm) aluminum framed package along with its support electronics (Fig. 5.3). Power for the electronics and heaters is supplied by lithium batteries while the high voltage for the HgI_2 crystals comes from a charged 0.2 microfarad capacitor. The capacitor stays within 30% of its original voltage for ~30 hours because of the small leakage currents of the detectors, cables and capacitors themselves. This detector biasing method also removes noise contributions from low to high voltage converters. The detectors are kept biased continuously before and during launch of the balloon to avoid "cold start" problems (see Section 3.1). Low voltage power is turned on at approximately 6 km altitude by parallel pressure switches operating a relay. This conserves the batteries and protects against electrical shorting at launch and landing.

Once power is turned on, data collection begins. The main part of the electronics takes random, asynchronous voltage pulses from the detector preamp, converts these pulses into synchronous, 8 bit digital

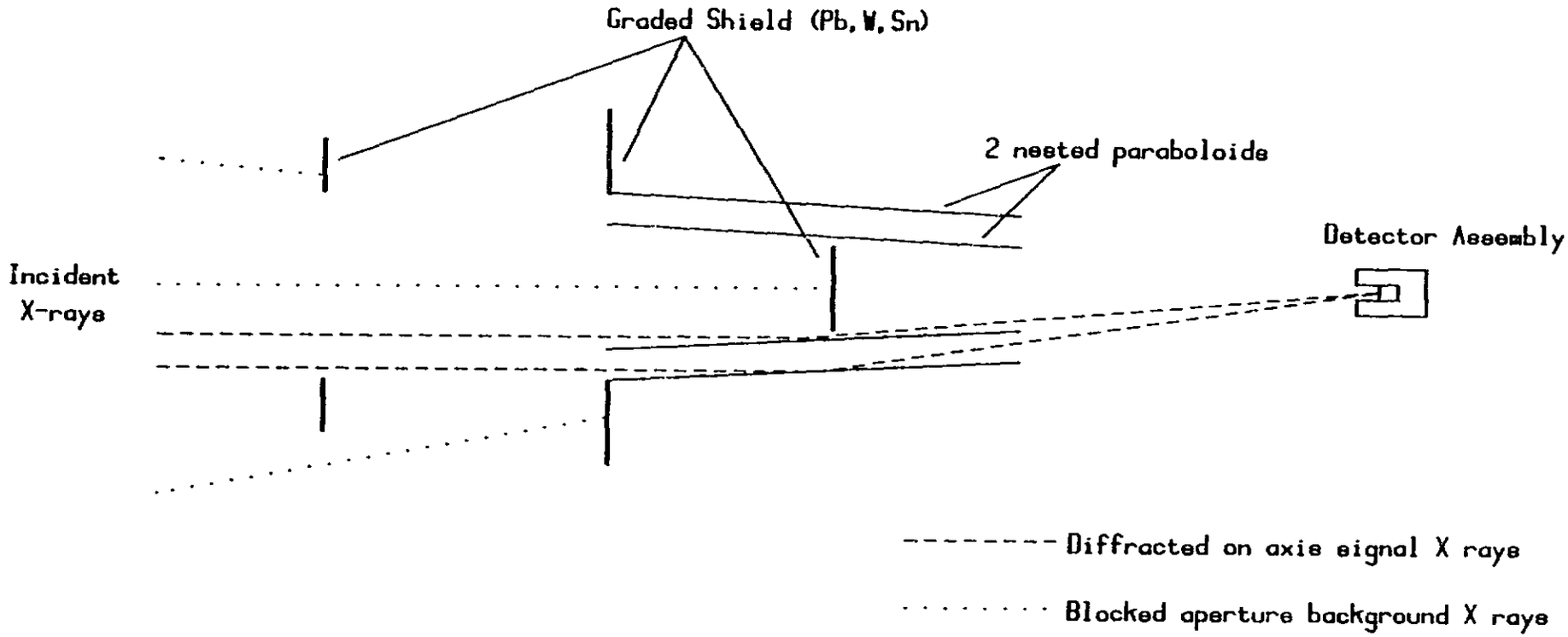

Figure 6.2 Schematic of the diffraction concentrator showing the passive graded shields (lead, tungsten, and tin) stopping background aperture X-rays that would normally impinge on the mercuric iodide detector. Only on-axis X-rays that are diffracted by the concentrator reach the detector.

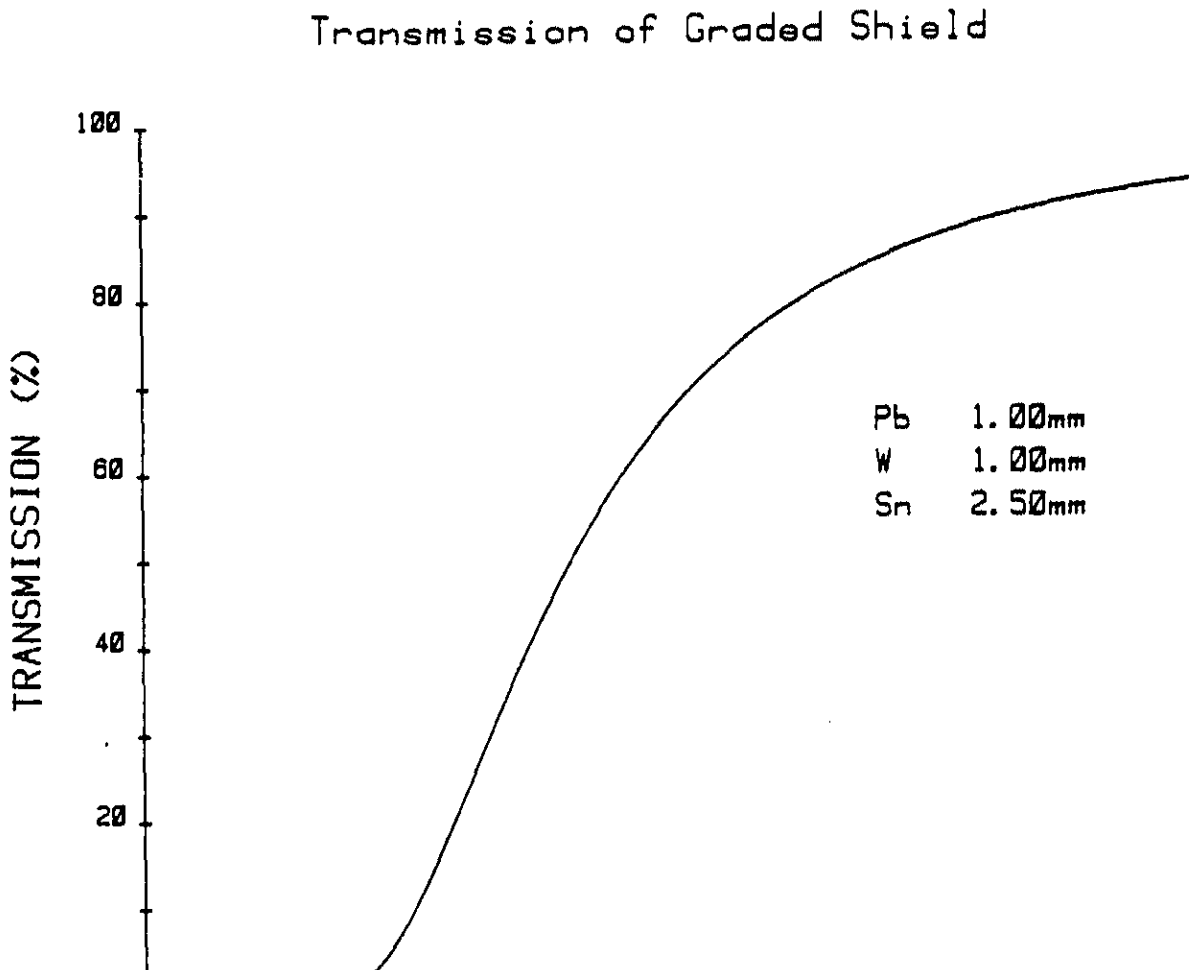

Figure 6.3 Transmission of photons vs. energy through a graded shield of 1mm of lead, 1 mm of tungsten and 2.5 mm of tin. The lower Z metals act to stop the fluoresced K X-rays of the higher Z metals.

words and routes these words to an appropriate magnetic tape track. The remainder of the electronics monitors the condition of the gondola (temperatures, voltages, currents, etc.) and records this housekeeping data on a separate magnetic tape track. The gondola is self contained during flight (i.e., no telemetry, no commands, no interface). However, it is essential that the cassette tape be recovered!

6.2.1 Event Logic Electronics

Pulse height spectra are recorded for both top and bottom HgI_2 detectors. Output pulses from the BGO photomultiplier are fed into an Amptek A-101 logarithmic amplifier/discriminator which produces a digital pulse if the charge pulse amplitude is above a set threshold. Only the BGO shield count rate is recorded; no pulse height information is retained.

Small voltage pulses from both HgI_2 detector preamps are brought to pulse shaping voltage amplifiers (time constant ~15μs). The last stage of these amplifiers is a "peak stretcher" which retains the maximum voltage attained by the pulse and holds it at the input of an analog to digital converter until reset. If the pulse height triggers the lower level discriminator, the pulse height will be converted 22 μseconds later to an 8 bit digital word. For the top HgI_2 detector, the event logic determines if an event occurred in the BGO crystal or the bottom detector in the time interval from 13μS before the top event to 9 μS after. If no "veto" event occurred then the 8 bit digital word is shifted to the "valid" buffer for tape track #1. If a "veto" event occurred in either the BGO or the bottom crystal then the 8 bit word is shifted into the "veto" buffer for tape track #2. All events occurring

Figure 6.4 EVENT LOGIC DIAGRAM

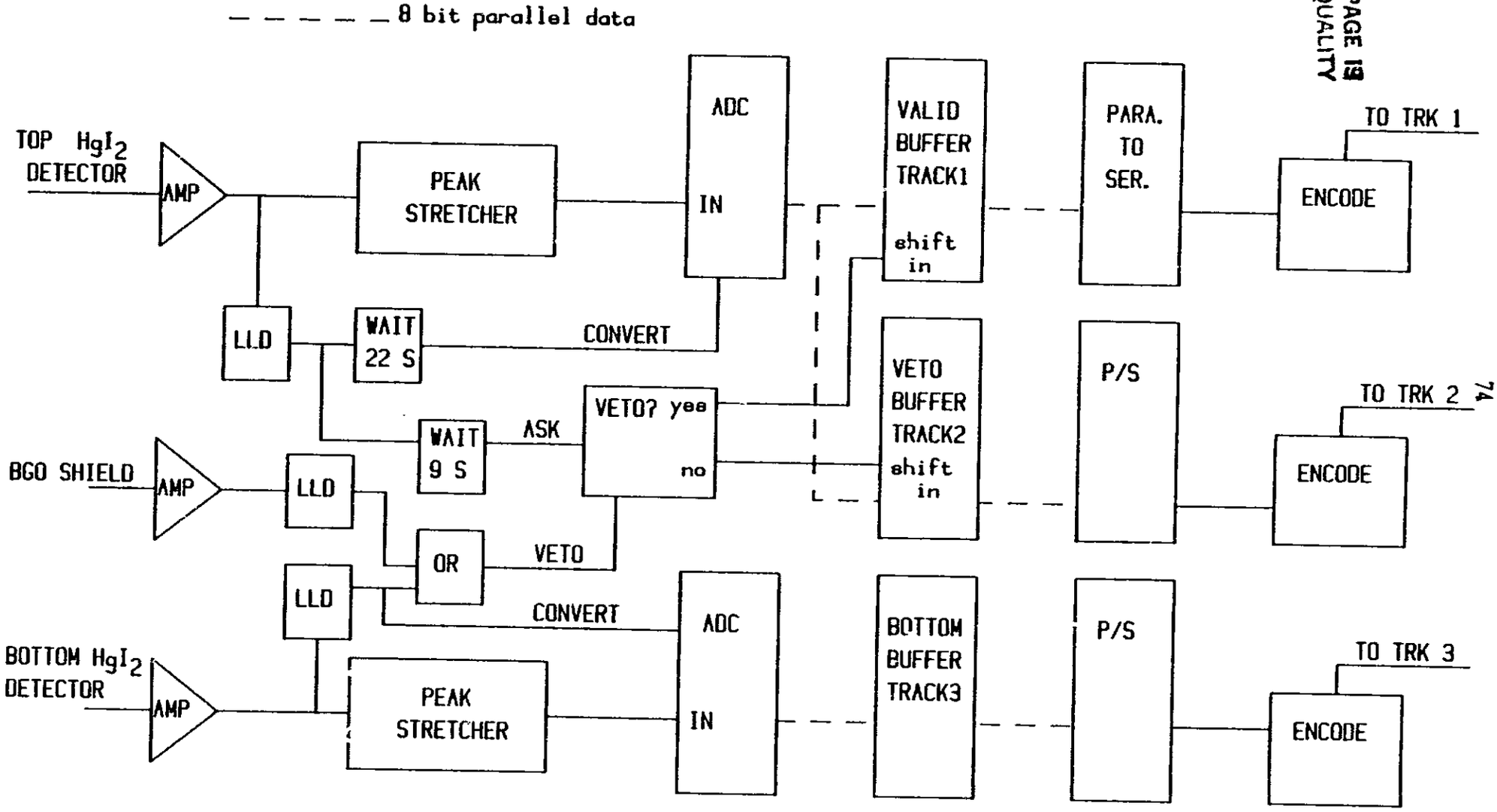

in the bottom crystal are converted and shifted into the "bottom" buffer for tape track #3. Once the shift into the buffer takes place, the peak stretcher is reset and ready for a new pulse. Total time from event to reset is approximately 50 microseconds. The event logic diagram is shown in Fig. 6.4.

Because of the very low count rates in the HgI_2 detectors at float (~1 ct/sec) the dead times due to the finite conversion time are negligible. The BGO count rate of ~1000 cts/sec plus the veto flag duration of 22 microseconds gives a 2% probability that a valid event will be vetoed by accident.

6.2.2 Data Recording

Events arrive at the 8 bit wide x 16 bit deep buffer asynchronously but are read out synchronously at 8 bytes per second (slow mode) or at 1024 bytes/sec (fast mode). The fast mode is used on the ground for calibration and testing purposes while the slow mode allows recording on tape for flight or long term background runs.

Separately for all three data tracks (valid, veto and bottom) the 8 bit pulse height is read out of the buffer and inserted into a serial bit stream 515 bytes (≡1 block) long. The bits are Manchester phase encoded (Rooks 1979) and sent to the tape head amplifiers. The tape recorder is a 4 track LTD 800, a long term data logger constructed by Braemar Inc., and uses standard Phillips cassettes. The tape speed is .08 inches/second and a 560 foot cassette tape (size 120) will run for 23.4 hours. The maximum bit density allowed is 800 bits/inch which determines the 8 byte /second recording rate.

The tape is formatted (Fig. 6.5) into blocks of 515 bytes separ-

FIGURE 6.5 TAPE FORMAT

DENSITY..... 100 bytes/inch
SPEED..... .08 inches/sec.
ONE BLOCK..... 515 bytes
SIZE 120 CASSETTE... 1350 blocks

TRACK 1 .... Top detector valid events
TRACK 2 .... Top detector vetoed events
TRACK 3 .... All bottom detector events
TRACK 4 .... Housekeeping data

TRACKS 1 to 3:

INTER-RECORD GAP	PREAMBLE	BLOCK NUMBER	X-RAY DATA	EVENT#	CHECK SUM	POSTAMBLE	INTER RECORD GAP
0.1 inch	01010101 1 byte	1 byte	ONE BYTE/ EVENT TIME = POSITION ON TAPE 511 bytes	511 1 byte	1 byte	01010101 1 byte	

TRACK 4:

IRG	PRE	BLOCK	HOUSEKEEPING DATA	CHECK	POST	IRG
			32 ONE BYTE WORDS 17 ASSIGNED (repeat 16 times)			

ated by an inter-record gap of 0.1 inch. Each block starts (and ends) with a preamble (postamble) of 10101010. The next byte is a block number that is incremented every block and is the same for all 4 tracks. For tracks 1, 2 and 3 the remainder of the 511 bytes are pulse heights (mostly zero). Position on the tape corresponds to the event arrival time. Events that arrive during the inter-record gap and post and preamble are not lost but kept in the buffer until readout after the block number.

Track 4 has the same tape format as tracks 1-3 but instead of pulse heights the digital words correspond to various housekeeping data. Temperatures, currents, and voltages are all converted to a voltage between 0 and 10 volts using linear transducers, amplifiers or simple resistive dividers. These voltages are multiplexed to another analog to digital converter and the 8 bit digital word is again inserted into a serial bit stream, encoded, and recorded. Also recorded is the 16 bit clock/counter and the 16 bit BGO event counter that is reset every 2.91 seconds.

6.2.3 Ground Support and Data Analysis

Pulse height spectra from the top or bottom HgI_2 detectors are accumulated by a Hewlett Packard HP85 desktop calculator via an interface that can read a track from the cassette tape or directly from the gondola. A CS400A data reader built by Braemer Inc. reads and decodes 1 tape track at a time at 10 inches per second and sends this serial bit stream to the interface which directs this data onto an IEEE 488 interface bus connected to the HP85. The HP85 can analyze up to 30 blocks at a time and will bin all events by their 8 bit pulse height

(256 bins). An arbitrary number of these spectra may be summed together. A 23 hour tape requires 20 minutes to reduce into a spectrum.

For calibration and testing, the interface can take data directly from the gondola using the serial bit stream just before it is encoded. This method can use either the slow or fast mode (8 bytes/sec or 1024 bytes/sec; manual switch selectable). The fast mode is used when the count rate exceeds 8 cts/sec as it does using ordinary radioactive sources. Overnight runs to measure laboratory background use the slow mode with tape as does the actual balloon flight.

C-2

7.0 BACKGROUND SOURCES AND MONTE CARLO ANALYSIS

The background counting rate of an X-ray detector at high balloon altitudes and in orbit is due to high energy radiation at the detector. The components of this radiation include: the primary cosmic rays and their secondaries (including neutrons) produced in nearby matter; atmospheric gamma rays from bremsstrahlung and decay of the secondaries; the diffuse cosmic X- and gamma ray background; and induced radioactivity of the detector and its surroundings. The physics of interaction of each type of radiation are quite different. Shielding systems that work on one type of radiation sometimes fail to notice (or even worse) enhance another type. Regardless of the type of radiation, if 40-80 keV of energy is deposited in the top HgI_2 detector it looks like a signal X-ray unless vetoed by a simultaneous event in a shield.

The radiation environment at balloon altitudes (40 km or 3 gm/cm^2 atmospheric column density) are summarized in Table 7.1. These fluxes are not always what the main detector sees because the transmission of the shield varies with energy and type of radiation. Each must be treated separately using measured ambient fluxes to determine the individual contribution to the X-ray background counting rate and then summed together. Secondary radiations created in the detector are treated along with the original radiation (i.e., electron bremsstrahlung is treated under the charged particles contribution while positron annihilation is treated under the gamma rays' contribution).

A note on terminology: the detector is considered to be oriented with the aperture pointing at the zenith so the primary HgI_2 detector is referred to as the "top" detector while the HgI_2 detector below it

Table 7.1

Integrated Radiation Flux at 3 gm/cm^2 and
Magnetic Latitude = 42°N (Palestine, Texas)

Radiation Type	Flux	Reference
Gamma rays photon energy >70 keV >200 keV	7.6 photons/cm² sec 4.8 photons/cm² sec	Ling 1974
Protons (E>3 GeV)	.3 protons/cm² sec	Meyer 1969
Electrons (E>1 MeV)	1.0 electron/cm² sec (possibly factor 2-5 to high)	Verma 1969 Daniels 1974
Neutrons (E>.1 eV)	1.2 neutrons/cm² sec	Armstrong 1973

is the "bottom" detector. Events in the top detector are "vetoed" if there is a coincident event in the BGO or bottom detector or they are "valid" if there is no coincident shield event.

7.1 Gamma Ray Induced Background

Gamma ray induced background in some ways is the most straightforward to understand yet the most difficult to calculate. The physics of interaction with matter are well understood and the cross sections can be expressed as analytical functions (McMaster, 1969). Yet the complex geometry of the BGO shield combined with the high probability of large angle scatters that are random in nature required the use of a Monte Carlo simulation. Before describing the details of the analysis some general conclusions can be stated. The gamma ray spectrum at float altitude has been modelled by Ling (Ling 1974) and is shown in Fig. 7.1 for 3 gm/cm^2 altitude. The transmission of gamma rays through 2.5 cm of BGO is plotted on the same graph. There will be a certain energy range where the transmission becomes non-negligible and the flux of photons is still appreciable. This "shield leakage" must then be folded with the detector response. A typical valid event would be a 2 MeV gamma ray penetrating through the BGO, Compton scattering in the HgI_2 detector leaving a 50 keV Compton electron and then escaping without being detected again, all improbable events. From Fig. 7.1 the need for an aperture shield is evident to stop the direct flux of low energy (20-200 keV) X-rays.

7.1.1 Monte Carlo Simulation

The Monte Carlo simulation of the gamma ray interactions with the detector assembly (BGO, HgI_2 detectors, passive aperture shield) used

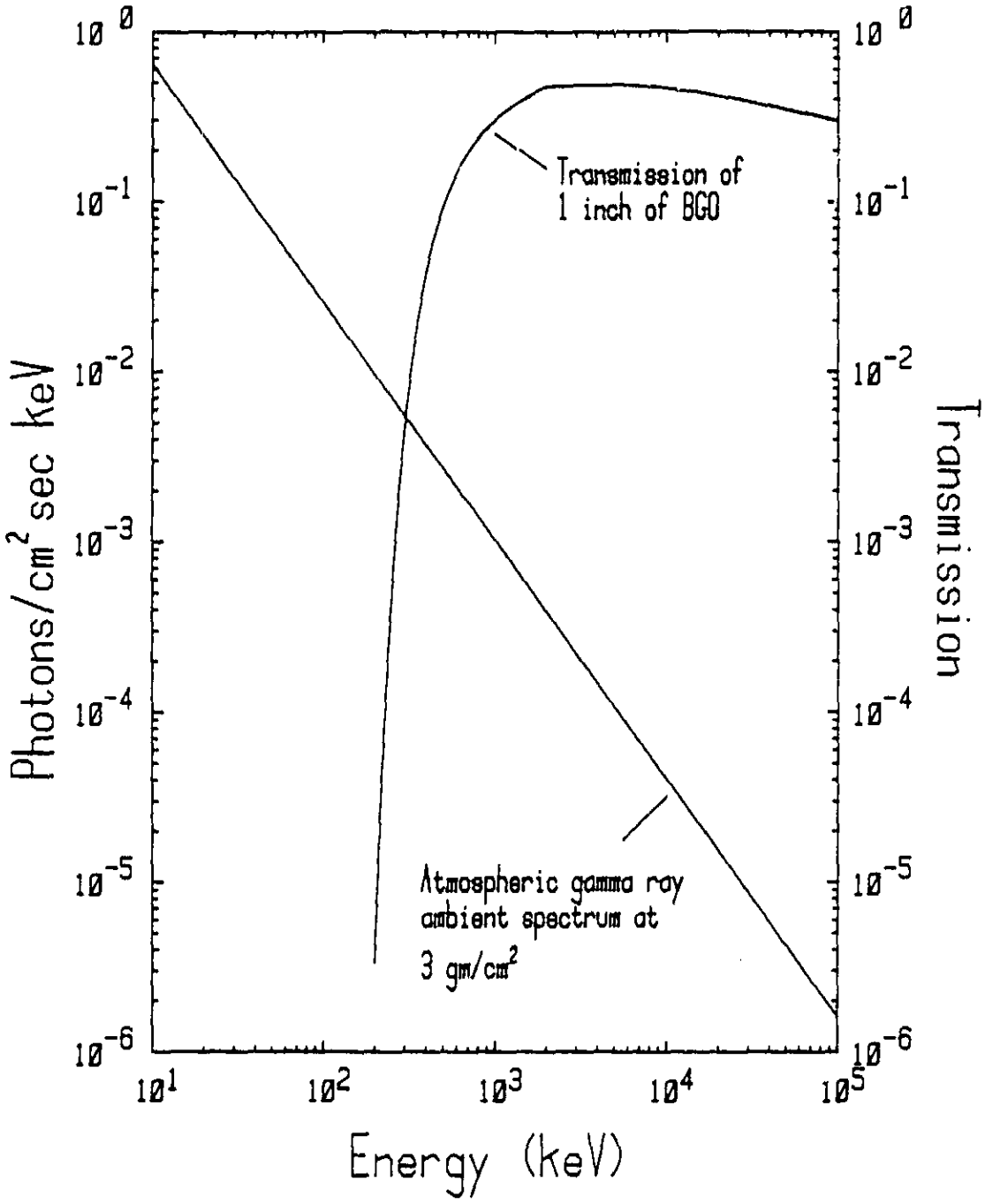

Figure 7.1 Plot of ambient gamma-ray spectrum at 3 gm/cm² taken from Ling (1974). Also plotted is the photon transmission of 1 inch of bismuth germanate to show the effectiveness vs. energy of the shield crystal where the minimum thickness is 2.5 cm. The shield leakage will be a maximum between the energies of ~.5 MeV to 3 MeV, where the atmospheric flux is still appreciable

as an input an assumed atmospheric photon flux density (function of energy and direction and the geometry of the detectors). The output consists of the resulting energy spectra of valid, and veto events for the top detector, as well as the spectra in the bottom and BGO detectors. Details of the technique and computer code can be found elsewhere (D. Wood, MIT Senior thesis, 1982).

The simulation employed a ray tracing technique and can be summarized as follows:

(1) A photon is generated from the input distribution with an energy, direction, and starting point.

(2) With the attenuation coefficient of the material in which the photon is travelling (HgI_2 or BGO), the position of next interaction is calculated based on the geometry of the detector and direction of travel.

(3) The type of interaction is determined based on the different calculated cross sections (photoelectric, Compton scatter, pair production). The energies and direction of any secondary photons are generated if needed for the interaction and the energy deposited is calculated.

(4) Secondary photons are traced from the interaction site starting with step (2) until the photon escapes entirely from the detector or until its energy drops below a set discriminator level.

(5) When the incident and all secondary photons are completely traced the energy deposited in each detector is separately accumulated and the appropriate energy bin in the bottom and

BGO spectra are incremented. A deposit in the top detector will increment the valid spectrum unless a concurrent deposit occurs above a discriminator level in the other two detectors. In that case the veto spectrum would be incremented.

(6) All energies are cleared and the number of incident photons is incremented and another photon is generated in Step (1).

Three types of photon interaction were used in the simulation: photoelectric absorption, Compton scattering and electron-positron pair production. The attenuation coefficients used for the different detector materials are shown in Fig. 3.1 and 3.3.

For the photoelectric interaction the simulation would generate a K-alpha X-ray photon if the energy absorbed was greater than the binding energy of the K shell in the material absorbing the initial photon. The K alpha photons were assigned the K-alpha-one energies of 77.1 keV and 70.8 keV for bismuth and mercury, respectively. The K escape photons of iodine, germanium and oxygen were ignored because of their low escape probabilities. The strength of these line features are very important for determining the contribution of gamma rays to the detector background. K fluorescence is a "signature" of photon interaction and should scale as the gamma ray continuum. All other radiations produce a continuum background in the 20-200 keV range which cannot be separated from that produced by gamma rays. The line features supply a measurable test for the simulation's prediction.

The Compton scatter cross sections and angular distributions are based on the Klein-Nishina formula (Knoll 1979, pg. 69). In the energy range where this cross section dominates (.5-2MeV), the Monte Carlo

simulation is most needed to follow the mulitple scatterings. Fig. 7.2 is a two dimentional visual representation of the Monte Carlo program showing the various scatters and interactions.

Pair production, although relatively infrequent because it requires a photon with an energy greater than 1022 keV, generates the positron annihilation line at 511 keV which could also be a measurable prediction of the simulation. However, the dynamic range of the electronics (10-250 keV) did not allow this measurement.

The gamma ray spectral distribution that was input to the simulation was adapted from Ling (Ling 1974) and can be expressed as

$$\frac{dN}{dE} = 16E^{-1.4} \text{ photons/cm}^2 \text{ sec keV}$$

at 3.5 gm/cm^2 along with a line feature at 511 keV of strength .3 photons/cm^2 sec. The directional distribution was assumed to be isotropic in the upper and lower half spaces. The ratio of upward to downward flux at different energies was estimated from Ling's angular distribution and was fitted by the function:

$$\frac{\text{upward flux}}{\text{downward flux}} = 1.7 \ln (E/87 \text{ keV} + 1.84)$$

During an actual flight the balloon cannot be expected to arrive exactly at a desired altitude used in the simulations. Fortunately the variation with depth of the photon flux is slight for lower energies. Descending from 3 gm/cm^2 to 5 gm/cm^2 there is a 10% increase in flux at 300 keV while effectively no variation occurs at higher energies (>1 MeV) (Ling 1974).

2-Dimensional Ray Trace

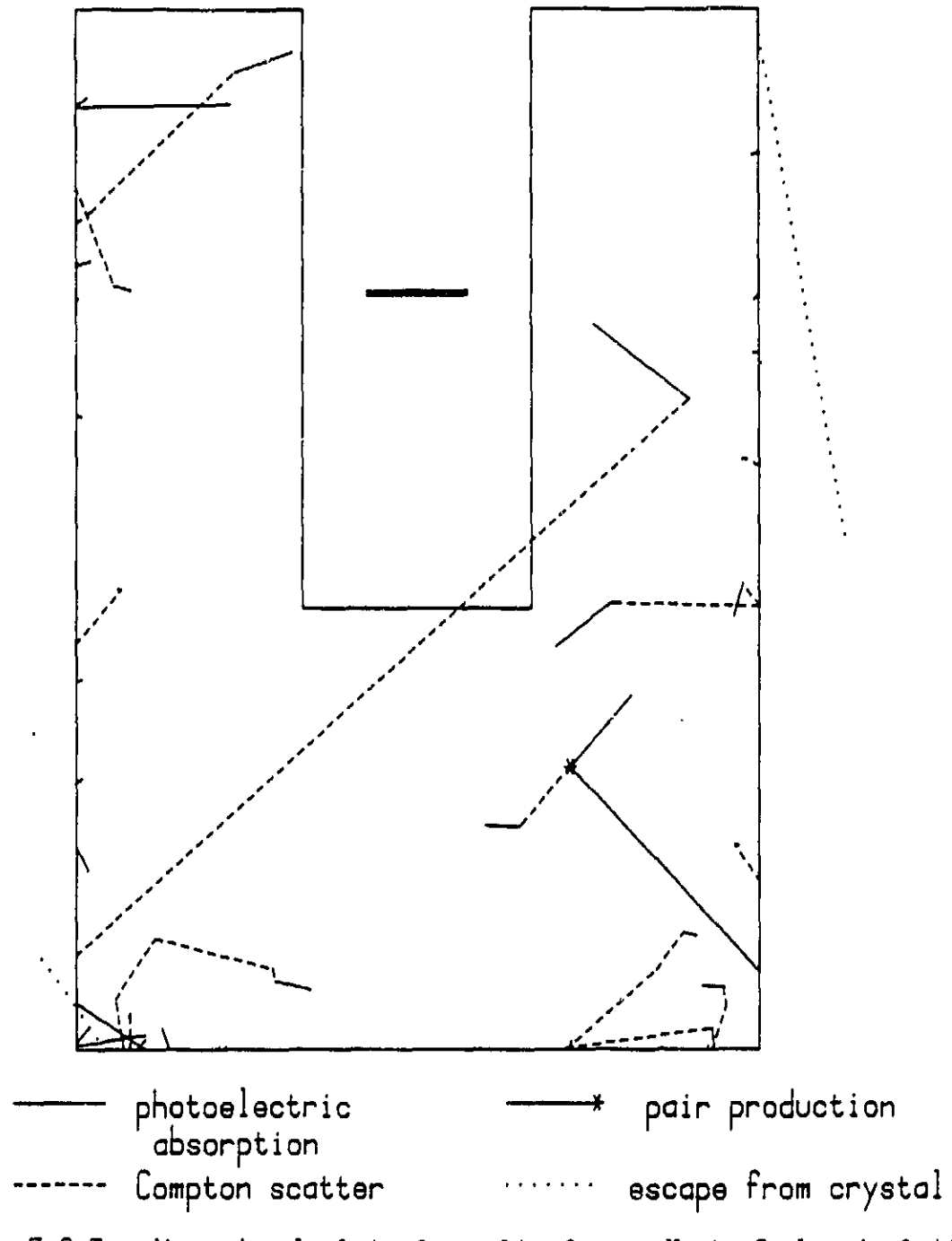

Figure 7.2 Two dimensional plot of results from a Monte Carlo simulation of gamma-ray interactions in the shielded HgI_2 detector assembly. The simulation followed 50 photons generated on the outside of the bismuth germanate shield until they were absorbed or escaped from the shield. The photons were distributed in energy according to the ambient gamma-ray spectrum at 3 gm/cm^2 (Fig. 7.1). Therefore, most of the interactions occur near the outside surface of the BGO shield.

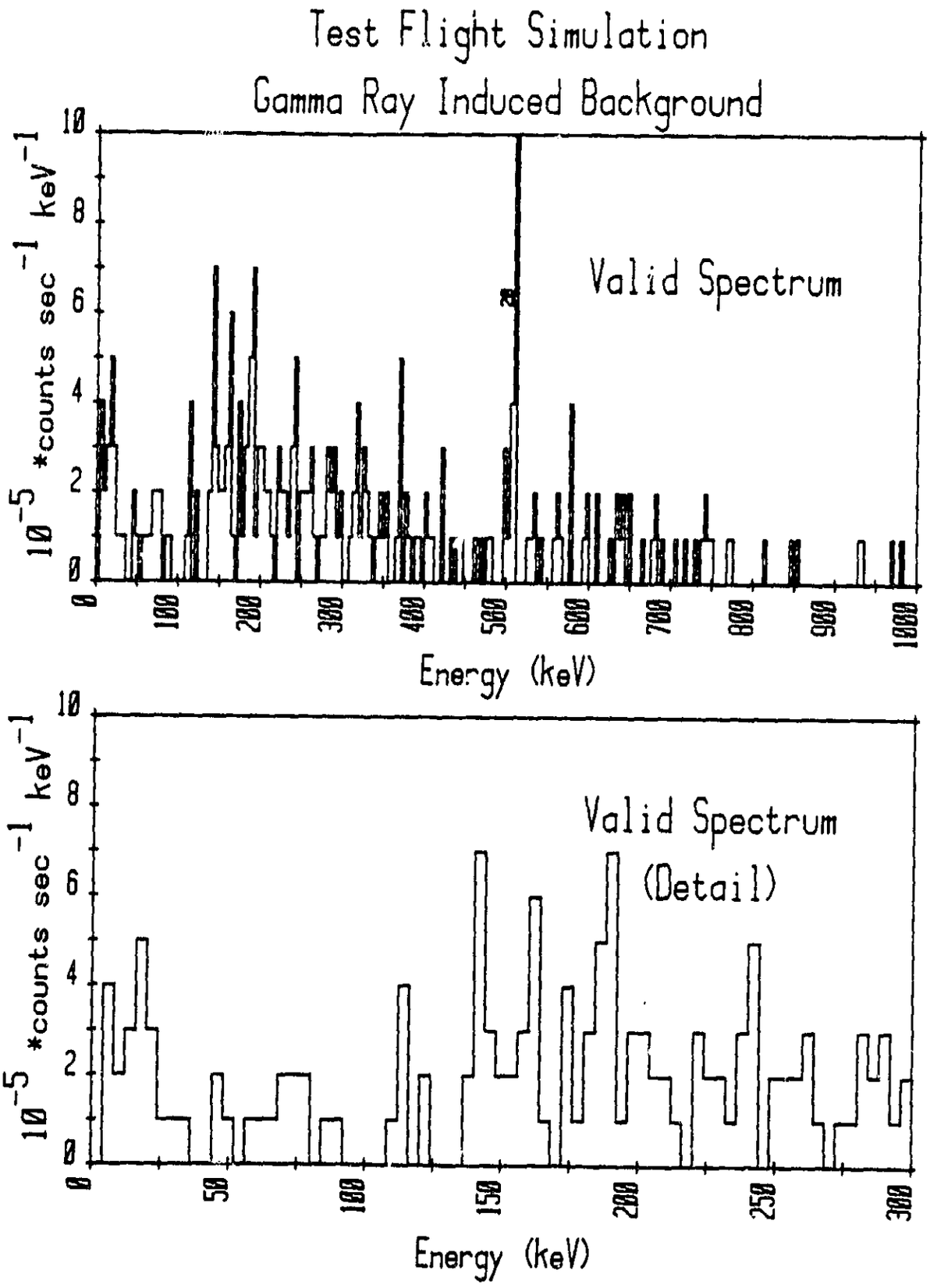

Figure 7.3 Predicted valid background spectrum due to gamma-rays for the top mercuric iodide detector at 3 gm/cm² float altitude. The small excess between 100 and 300 keV is due to the leakage through the passive aperture shield. The atmospheric positron annihilation line at 511 keV is also apparent.

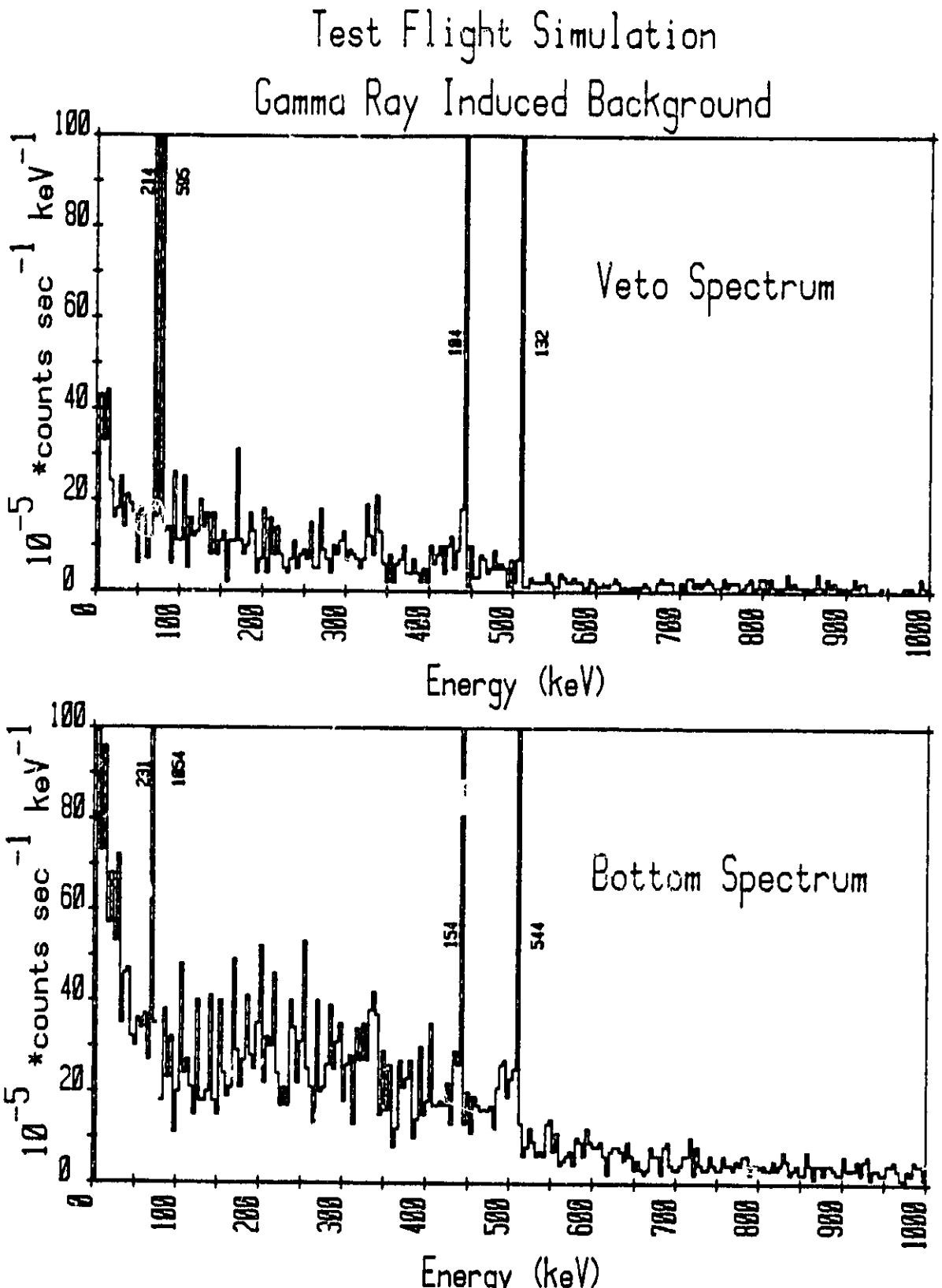

Figure 7.4 Predicted vetoed (top detector) and bottom detector spectra at 3 gm/cm² due to gamma-rays. The spectra are featureless except for the Hg and Bi K X-rays and the positron annihilation line along with its Hg K escape feature, 70 keV lower in energy.

7.1.2 Results of Simulation

The results of the Monte Carlo simulation are shown as energy spectra for the top (valid and veto) and bottom detectors in Figs. 7.3 and 7.4 and are taken from the thesis of D. Wood (Wood 1982). The valid spectrum attained a broad general maximum at an energy of ~200 keV and a local minimum between the energies of 25 to 140 keV. A strong line feature exists at 511 keV due to the atmospheric line feature. Aside from the 511 line, the valid spectrum exhibited no other resolvable line features. However, the processes which produced line features in the bottom and veto spectra were not expected to contribute to the valid spectrum because the detection of K-α photon and positron annihilation photons required concurrent interactions in either of the anticoincidence detectors that produce such photons. These events are always vetoed if the energy deposited in the veto detectors exceeds the discrimination level. The simulations verified this condition.

Predicted integrated count rates of the continuum background and line features due to the gamma ray flux are tabulated in Table 7.2. Only the K fluorescence line features can be compared directly to the flight results (Section 8) because the continuum background must be summed with background produced by neutrons and charged particles.

7.2 Neutron Induced Background

A significant contributor of background events in the HgI_2 detector are neutrons generated by primary cosmic ray interactions with oxygen and nitrogen nuclei in the atmosphere. The event rate in the HgI_2 detectors is significant because the shielding schemes for suppressing gamma rays and charged particles are not effective at atten-

Table 7.2

Predicted Background Count Rates in BGO-Shielded Top HgI_2 Detector Due to Atmospheric Gamma Rays at 3^2 gm/cm^2 and Magnetic Latitude 42°N

Continuum:

Energy (keV)	Valid† Backround Rate (10^{-5} cts/sec cm^2 keV)
40 - 80	1.3 ± .4
80 -120	.8 ± .3
120-160	.3 ± .1
160-200	1.3 ± .2
200-240	1.2 ± .3
240-280	1.4 ± .4

Line Features††:

Bismuth K Xray	2.6×10^{-2} cts/sec cm^2
Mercury K Xray	1.0×10^{-2} "

† A "valid" event is an event not accompanied by a coincident event in either veto shield detector.

†† Present only in vetoed spectrum

uating the neutron flux. The mean free path for diffusion and absorption of fast neutrons (E_n>1 MeV) in BGO is approximately 6 cm which is comparable to the thickest part of the shield. The only advantage of this situation is computational in that the effect of the neutron background can be calculated analytically assuming a slab detector in an isotropic flux of neutrons. The complexity enters in the types of neutron interactions and their corresponding cross sections: elastic scattering, inelastic scattering, and neutron capture with a prompt gamma ray and delayed beta decay. Errors in these calculations will result more from extrapolated neutron cross sections and fluxes rather than the simplified geometry.

The upper atmosphere neutron flux has been measured and modelled by a number of authors (Armstrong 1973; Merker 1973; Klumpar 1973) at various atmospheric depths and magnetic latitudes. From thermal energies to 20 MeV the flux at 3.5 gm/cm^2, magnetic latitude λ=42°N (Palestine, Texas) can be expressed as $F(E_n)=.1E_n^{-.83}$ neutrons/cm^2 sec MeV. The spectrum remains flat from 20 to 50 MeV and than falls off as E^{-2} above 50 MeV. In the energy range 10 to 100 MeV, 80% of the flux at 3.5 gm/cm^2 is upward moving neutrons. To calculate the event rates in the HgI_2 crystal for the different types of neutron interactions, the physics of the interaction as well as the tabulated cross sections (Hughes 1964) determined the energy range of interest of the incident neutrons. For example, only neutrons with energies greater than 1.3 MeV could elastically scatter off iodine and leave 40 keV in the detector due to simple conservation of momemtum.

The maximum energy transferred in an elastic scatter of a neutron

and an atomic nucleus is proportional to $4A/(A+1)^2$ where A is the atomic weight (Knoll 1979, pg. 571). This fact gives HgI_2 an advantage over most other X-ray detectors due to the high atomic weight of Hg and I (200.5 and 127, respectively). The elastic event rate at a given energy, E, will be due to neutrons with energies, E_n, greater than $E(A+1)^2/4A$. Using tabulated elastic scatter cross sections (extrapolated as a constant to higher energies) with the incident neutron flux the event rate was separately determined at 40 and 80 keV in cts/sec cm^2 keV for Hg and I_2 and a power law was fit to these points. The results are shown in Table 7.3 and in Fig. 7.5.

Inelastic scattering from a nucleus by a neutron leaves the nucleus in an excited state which will decay by emitting a gamma ray. This is an important process because even though the cross sections are samll, the detector sees the events in a small energy bandwidth. But with a high resolution detector, these line features can be "resolved out" (i.e., the signal in this small bandwidth is ignored). The line features of interest are the 59 and 203 keV gamma rays of ^{127}I and the 160 keV line of ^{199}Hg. Higher energy gammas have a higher probability of escaping the crystal and a lower production probability due to small cross sections and fewer neutrons above the required threshold energy. Starting with the neutron flux above the threshold energy (~inelastic gamma energy) and tabulated cross sections, the number of gammas produced is calculated. This is multiplied by the probability that the gamma will escape the detector without interacting. The line strengths (cts/cm^2 sec) are given in Table 7.3 and plotted in Fig. 7.5 folded with a Gaussian energy response with 5 keV FWHM. The 59 keV line

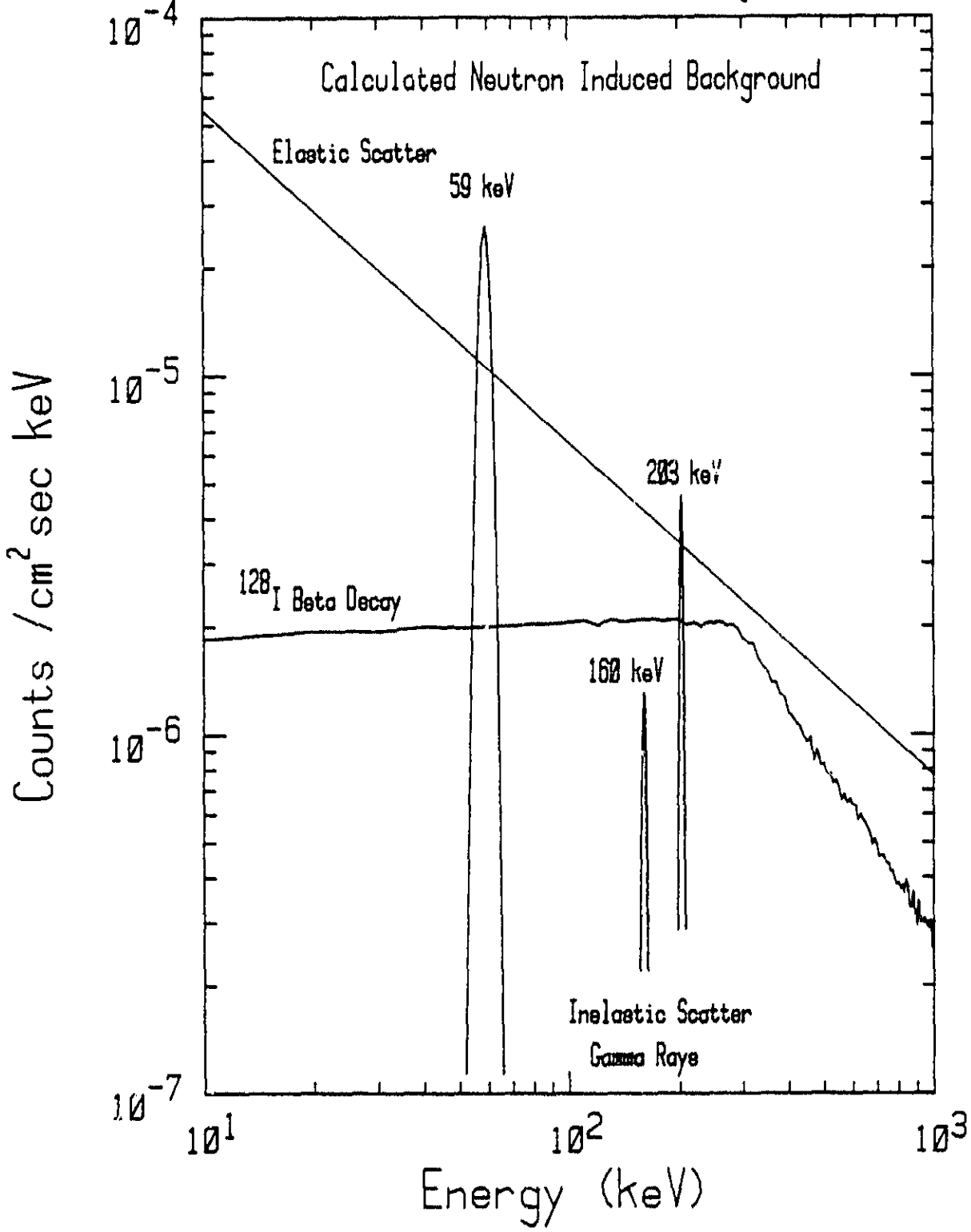

Figure 7.5 Predicted neutron induced valid background showing the three types of interactions. The elastic scatter power law results from the power law energy spectrum of the fast neutron flux. The gamma-rays are the result of nuclei being excited to higher energy states by inelastic collisions with fast neutrons. The ^{128}I beta decay induced energy spectrum results from the capture of 20-100 eV neutrons by ^{127}I and then beta decaying (half life = 25 minutes).

Table 7.3

Predicted Background Count Rates in BGO-Shielded Top HgI_2 Detector Due to Atmospheric Neutrons at 3 gm/cm^2 and Magnetic Latitude 42°N

Continuum:

	Valid Background Rate (10^{-5} cts/sec cm^2 keV)		
Energy (keV)	Elastic Scatter	^{128}I beta decay	Total
40 - 80	1.00	.20	1.20
80 -120	.64	.20	.84
120-160	.46	.21	.67
160-200	.36	.21	.57
200-240	.30	.21	.51
240-280	.26	.20	.46

Line Features (inelastic scatter):

59 keV	1.40×10^{-4} cts/sec cm^2
160 keV	$.07 \times 10^{-4}$ "
203 keV	$.25 \times 10^{-4}$ "

feature has been observed in all balloon-borne NaI and CsI detectors (-Matteson 1977; Peterson 1975) and is unfortunately right in the middle of the energy range of interest (40-80 keV).

Neutrons can be captured, (n, γ) reaction, by the ^{127}I nuclei or the seven stable isotopes of Hg. The prompt effects of the capture are the emission of many gamma rays up to the binding energy of the neutron ~8 MeV. The small probability that these photons will be absorbed in the thin HgI_2 crystal combined with the high probability that the associated photons will be absorbed in the veto crystal leads to an insignificant valid contribution from these prompt events.

The decay of the daughter products of this same neutron capture may produce delayed gamma, X and beta rays. ^{128}I has a half life of 25 minutes and quickly comes to equilibrium at balloon altitudes emitting a beta ray with maximum energy of 2.2 MeV. The beta rays that leave energy in the 40-80 keV range are the initial low energy betas and the high energy betas that are created near the surface and deposit 40-80 keV before escaping the HgI_2 crystal. The deposited energy spectrum is calculated assuming the beta emitters are distributed evenly throughout the detector using a Monte Carlo technique. The resulting spectrum is plotted in Fig. 7.5 and the contribution to the valid spectrum is given in Table 7.3.

Neutron capture in the Hg isotopes usually leads to another stable Hg isotope with prompt γ-rays. The unstable daughter products are ^{197}Hg, ^{203}Hg, ^{205}Hg with half lives of 65 hours, 46 days, and 5 minutes, respectively. Only ^{205}Hg, which emits a beta particle, has a short enough half-life to be noticed in a balloon flight, though all

must be of concern for possible long duration space applications. ^{197}Hg decays by electron capture giving a 77 keV gamma ray. Though the thermal cross section is high for the $^{196}Hg(n,\gamma)^{197}Hg$ reaction, the natural abundance of ^{196}Hg is only 0.15% and therefore its contribution is negligible. Based on the thermal cross section for Hg as a whole and assuming 6% (natural abundance of ^{204}Hg) of the Hg undergoing neutron capture end up as ^{205}Hg, the beta decay response spectrum is a factor of ~8 less than that produced by ^{128}I.

Elastic scattering of neutrons is the main contributor to the neutron induced valid background in the energy range 40-80 keV. Though this rate is less than an equally photon efficient NaI detector due to the higher atomic mass, it is an intrinsic background limit and only large amounts of neutron shielding would decrease this background source.

7.3 Charged Particle Induced Background

High energy charged particles will also contribute to the background count rate of an astronomical X-ray detector. The source of the particles are the primary cosmic rays, (mostly protons and alphas) and the secondaries they produce in the atmosphere and nearby matter (mostly electrons and mesons). Due to the geomagnetic cutoff, only protons greater than ~3.5 GeV reach the upper atmosphere above Palestine, Texas (magnetic latitude λ=42°N; cutoff rigidity 4.5 GV; Peterson 1975). Almost all of the charged particles are highly relativistic ($E>>M_0c^2$) and therefore highly penetrating, resulting in geometric simplifications. Protons directed at the HgI_2 crystal will reach it and deposit ~400 keV (minimum ionizing) as well as depositing

20-50 MeV in the BGO on the way in or out. The total count rate in the HgI_2 is therefore determined by the charged particle flux though veto efficiency approaches 100%. The effects of charged particles that can increase the valid background are decays of spallation products and bremsstrahlung photons.

The flux of high energy primaries in near earth space is isotropic and to first order the effective solid angle Ω, for a detector close to the earth, is 2π steradians. Of the primaries, 15% are alphas by number and a few percent are CNO and heavier elements, the rest are protons. Above 3.5 GeV the flux can be modelled as a power law (see Meyer 1969 for review).

$$\frac{dN_p}{dE} = 6.3xE^{-1.6} \text{ protons/cm}^2 \text{ sec sr MeV}$$

$$E > 3500 \text{ MeV}$$

This leads to an expected integrated count rate in the HgI_2 of .28 cts./cm^2 sec due to primaries including the cosine θ dependence of the effective area (plus .03 cts./cm^2 sec due to alpha particles).

The electron flux at high balloon altitudes (~3 gm/cm^2) is dominated by albedo electrons produced by primaries in the atmosphere below. The downward moving electrons are just the re-entrant albedo electrons and to a good approximation can be set equal to the upward moving flux (Daniels 1974). Again a power law fit to this omnidirectional differential spectrum above Texas is (Verma 1967):

$$\frac{dNe}{dE} = .05E^{-1.3} \text{ electrons/cm}^2 \text{ sec sr MeV}$$

$$10 \text{ MeV} < E < 1000 \text{ MeV}$$

Using the range of electrons in BGO to determine the lower energy bound (33 MeV from sides and 80 MeV from bottom) leads to an integrated count rate in HgI_2 due to electrons of .32 cts/sec cm^2. The integrated count rate is not very sensitive to the assumed low energy cutoff (i.e. geometry) while the measured fluxes have disagreed by factors of 2-5 (Daniels 1974).

All charged particles reaching the HgI_2 detector must pass through the BGO and be vetoed except those that pass through the passive Pb-W-Sn shield over the aperture. The high energy particles will continue through the top detector and interact in the bottom HgI_2 and probably the BGO as well. The only particles that will leave energy between 40 and 80 keV in the top detector alone are electrons in a small bandwidth with initial energy of ~8 MeV. The estimated count rate between 40 and 80 keV is .06 cts/hr, a negligible contribution. Though charged particles dominate the total count rate of HgI_2 at float, their valid prompt contribution is nil.

7.3.1. Spallation and Bremsstrahlung

Though prompt charge particle interactions will be vetoed, the spallation daughter products with their delayed decay can be a problem, especially in orbit where the trapped protons and long flight duration can lead to a significant background (Peterson 1975). The geomagnetic cutoff and short duration (~24 hours) of balloon flights combine to decrease this contribution to a small fraction of the valid background. The thin HgI_2 crystals will be most sensitive to the radiation of daughters that decay by beta emission (plus and minus) and electron

capture. Most of the high energy gammas will escape and/or interact in the BGO.

The spallation of iodine has been well studied due to the many detectors containing iodine (NaI, CsI) flown in orbit as well as irradiation experiments (Dyer 1980). A quick order of magnitude calculation can be done using geometric cross sections and assuming (worst case) every proton interaction with an iodine or mercury nucleus decays later by electron capture. These crude assumptions give background features at 30-34 keV (iodine daughters) or 76-80 keV (mercury daughters) with intensities of .8 cts/hr and .5 cts/hr, respectively. To reach this equilibrium rate would take weeks in orbit (Dyer 1980). Most of the electron capture decays also emit gamma rays that have a high probability of interacting in the BGO shield and being vetoed. Though not required for a short balloon flight, a detailed analysis of the proton induced spallation, peripheral, fission and evaporation cross sections of the seven stable isotopes of mercury should be attempted to determine the equilibrium counting rate for HgI_2 in orbit. A cursory look at the semi-empirical cross section formulae (Silberberg 1973) shows that the most probable product isotopes (mercury and tellerium) are either stable or have relatively long half lives (~days) so that this possible background source cannot be measured in a "standard" balloon flight.

An indirect method for an electron to deposit energy in the top HgI_2 crystal without being vetoed is by bremsstrahlung in the passive graded shield and then stopping or backscattering. To estimate this effect, the active volume used is the area of tin "seen" by the HgI_2

times one attenuation length of the emitted photon. Photons created above this volume are self-absorbed in the passive shield. Using the relativistic bremsstrahlung cross section (Jackson 1975, pg. 713) and electron flux in the field of view gives .06 cts/hr between 40-80 keV due to electrons between 8 and 9 MeV. Higher energy electrons will continue through to the active shields and veto their own bremsstrahlung radiation.

Because relativistic charged particles interact strongly with matter they are easily detected and vetoed though not easily stopped. Only through indirect means (spallation) can they deposit energy in the top HgI_2 crystal without being vetoed. A typical balloon flight is not long enough for these reactions to build up though longer duration satellite flights must be concerned with this source of background.

8.0 RESULTS OF BACKGROUND MEASUREMENTS AT SEA LEVEL AND AT B'LLOON ALTITUDES

8.1 Sea Level Background

The radiation envirionment on the ground consists mostly of high energy gamma rays due to the decay of naturally occurring radioactive isotopes such as potassium 40 and uranium and thorium daughter products. Primary cosmic rays and neutrons are shielded by the atmosphere but secondary muons do reach ground level. The gamma ray intensity is a strong function of the type of building where the measurements take place. Wood frame buildings are usually less active than concrete buildings due to the amount of radionuclides in sand and cement.

Long term background spectra were accumulated with the prototype detector gondola in many locations and many configurations. Fig. 8.1 shows the normalized count rates for spectra obtained in: Building 37, 5th floor, MIT; a ground floor preparation room at the National Scientific Balloon Facility in Palestine, Texas; and the iron cave in the basement of Building 2 at MIT. Integrated count rates are compared in Table 8.1 along with the BGO shield count rate. The iron cave results provide an upper limit to the intrinsic background of the prototype detector (background due to radioactive material used in the construction of the detector assembly itself) though extrinsic muons are more likely to be the cause of this background. The gamma ray contribution can be scaled with the bismuth K line observed in the veto spectrum. The veto ratio (the number of vetoed counts divided by the total counts) increased in the iron cave as the bismuth line decreased. This would be expected if the iron cave background is dominated by

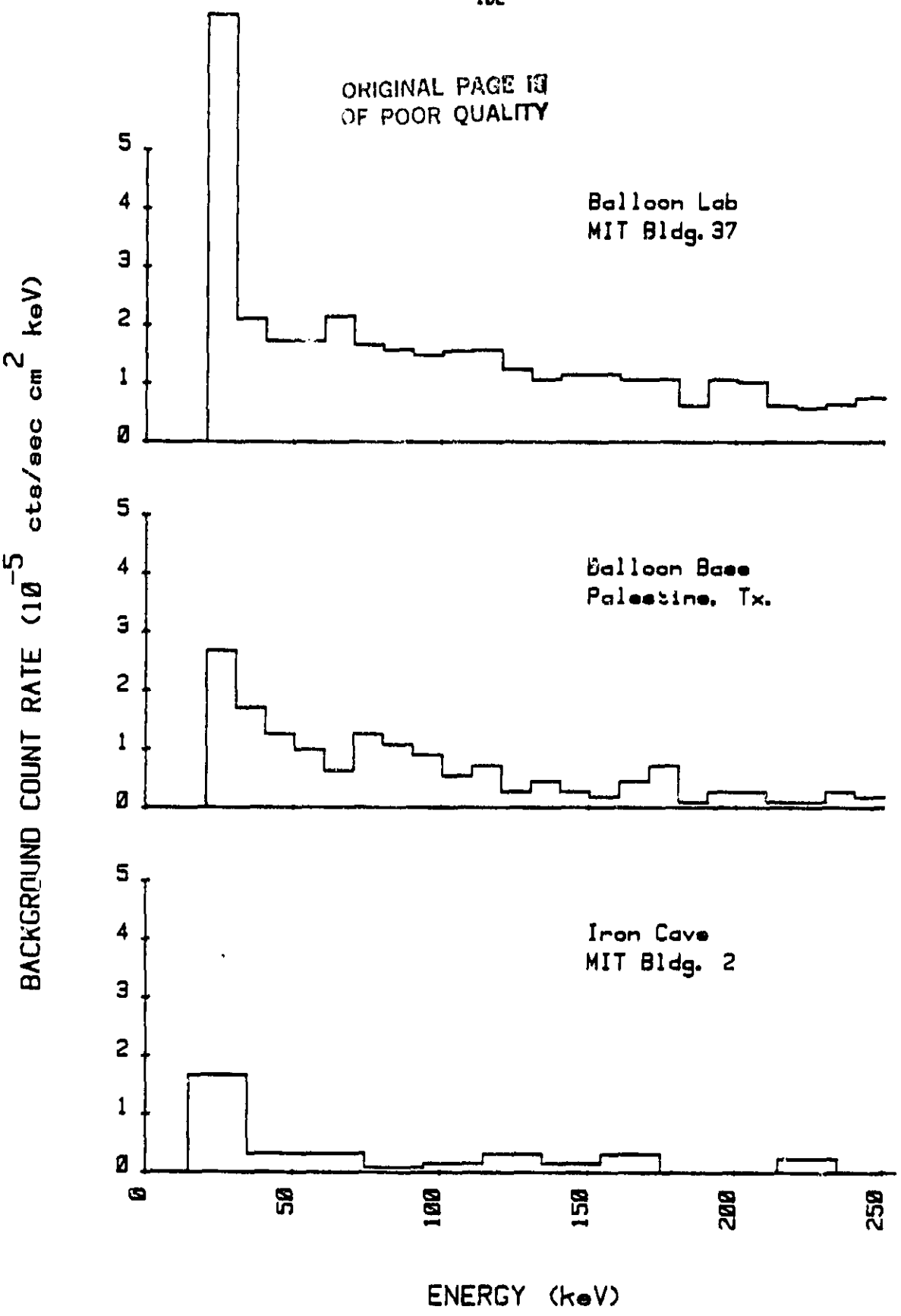

Figure 8.1 Sea level valid background spectra in top mercuric iodide detector for various experiment sites.

Table 8.1

Measured Background Count Rate of BGO-Shielded Top HgI_2 Detector for Various Surface Locations

Location	Valid Count Rate$_2$(40-80keV) (cts/sec cm^2 keV)	Veto† Ratio	Bismuth†† K X-ray	BGO Count Rate
Balloon Lab MIT Bldg. 37	1.8×10^{-5}	91%	14×10^{-4}	1231 cts/sec
Balloon Base Palestine, Tx.	1.0×10^{-5}	89%	5×10^{-4}	791 cts/sec
Iron Cave MIT Bldg. 2	$.2 \times 10^{-5}$	94%	1×10^{-4}	527 cts/sec

† Ratio of number of vetoed counts to total counts (veto + valid) over the energy range 40-160 keV

†† Counts/sec cm^2 observed in the vetoed spectrum

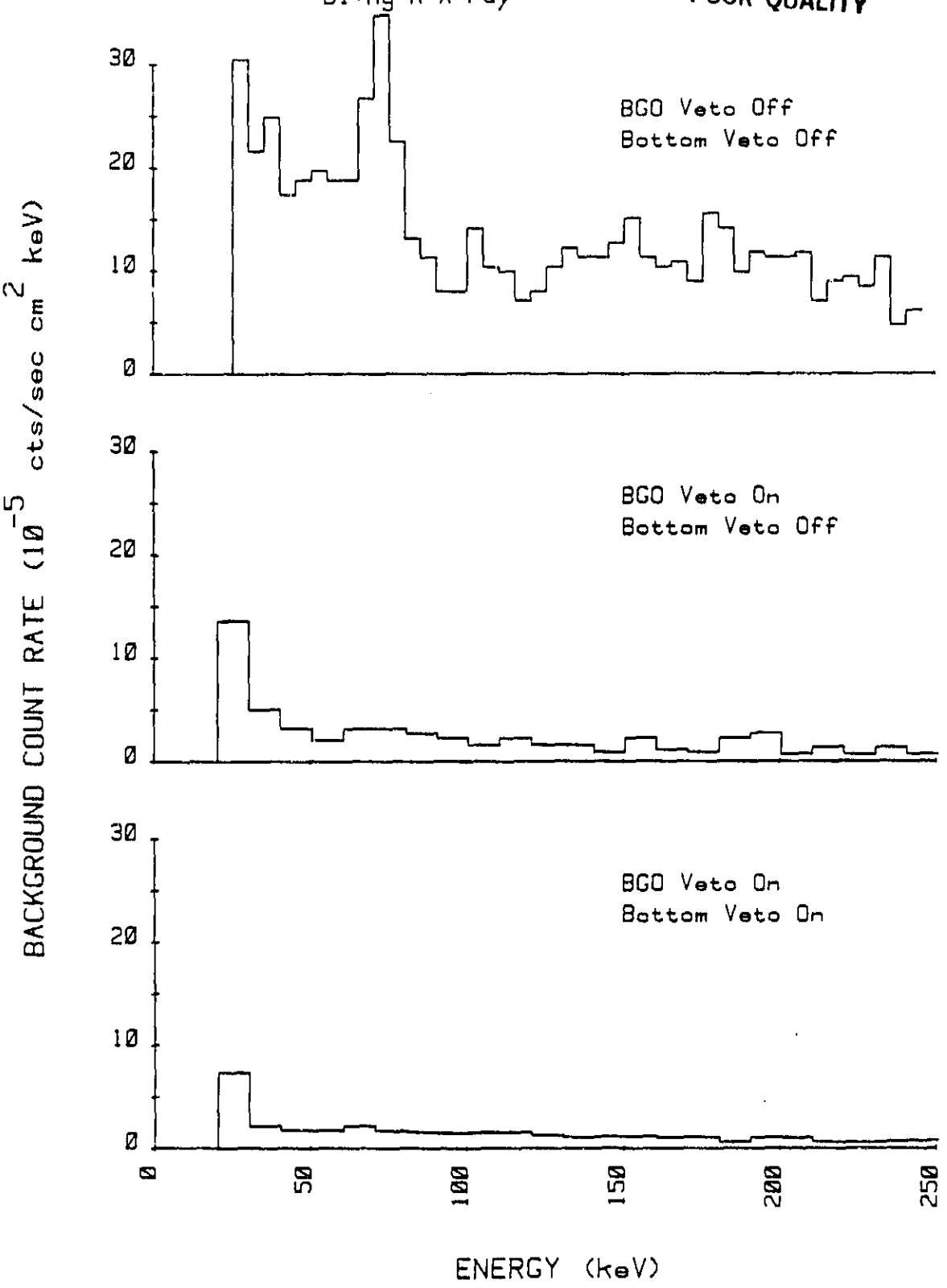

Figure 8.2 Valid background spectra in top mercuric iodide detector showing the effectiveness of the anticoincidence shields.

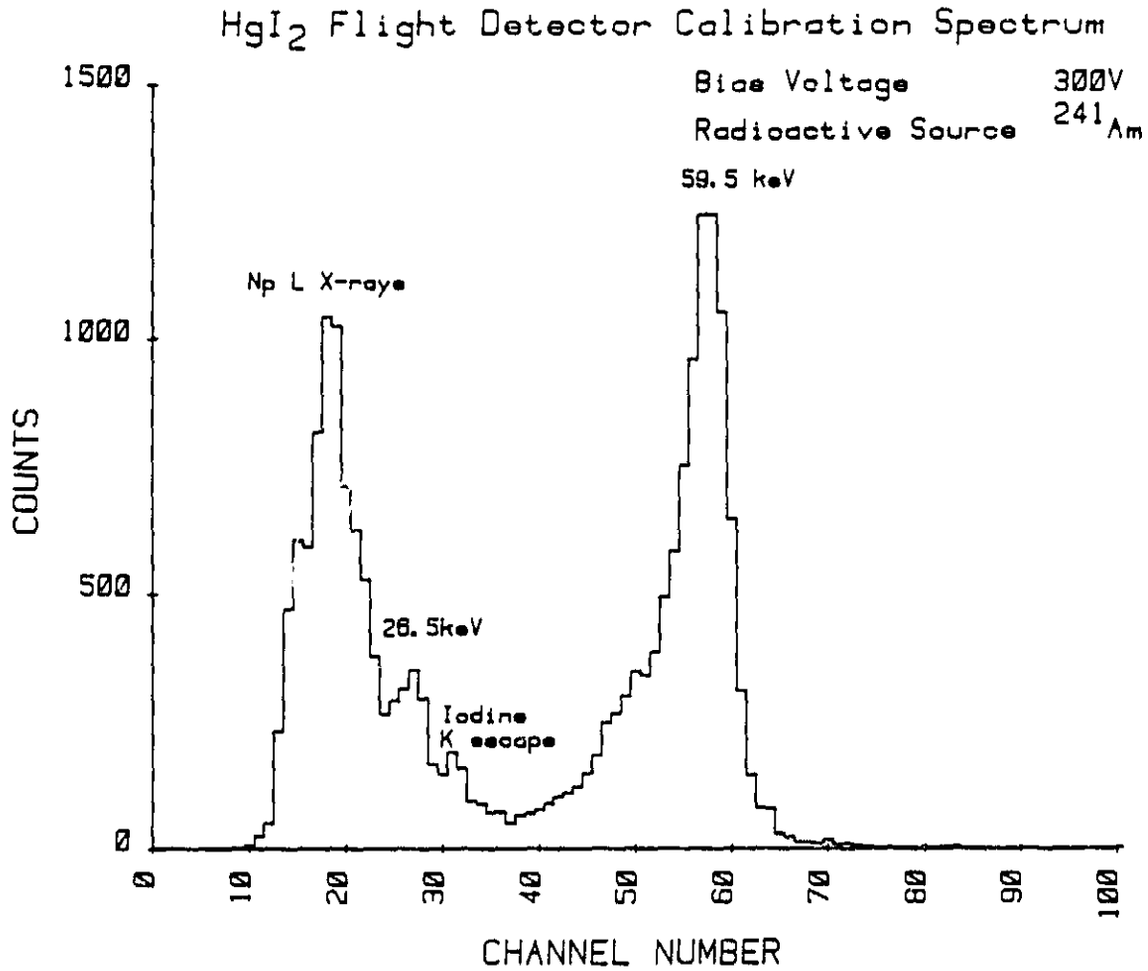

Figure 8. Actual mercuric iodide flight detector calibration spectrum using a ^{241}Am radioactive source. The energy resolution at 300V (flight bias) was 5.5 keV FWHM at 60 keV.

so the quantization error of one channel/keV was negligible. This detector was chosen for its stability and size and operated at 300 volts to decrease leakage current "bursts" that mimic background counts. Some energy resolution was sacrificed since the dominant background contributors produce a continuum of counts vs. energy.

8.3 Balloon Flights

The small prototype detector gondola was flown twice from Palestine, Texas. The first time, flight 1282P, was a "piggyback" flight in which the small gondola was strapped on the side of a large (1400 kgs.) payload flown by Martin Isreal's group at Washington University, St. Louis. The first flight was launched at 12:25 UT, May 8, 1982. It reached float altitude at 14:48 UT at an altitude of 38 km (3.8 gm/cm^2 vertical atmospheric column density). The flight lasted 35.5 hours and was successfully recovered in Mississippi. Analysis of the housekeeping data showed that the batteries began to fail after 13 hours, probably due to a defective lithium cell since they were expected to last 35 hours.

Another problem observed in the first flight was multiple triggering on energetic events due to extreme saturation of the voltage amplifier. The extra events had a characteristic signature of preferentially occurring with a channel number of 4N-1. This effect was duplicated in the laboratory by applying large pulses to the input of the voltage amplifier as would have occurred during flight if a very energetic particle interacted in the detector. This was a small effect in the veto and bottom spectra but it dominated the valid spectrum, increasing the count rate by a factor of 5. Two modifications were

made to the electronics. Diodes were placed at the input and on the feedback loops of the voltage amplifier so that large pulses from the preamps would only slightly saturate the last stage. In addition, a time constant was changed in the event logic so that the analog to digital converter would not accept another pulse for 750μsec after it converted a pulse. Despite this lock-out period, the additional dead time was negligible (.07% for a count rate of ~1 ct/sec). The change in the voltage amplifier required a new energy calibration (see above).

The second flight, 1296P, was a solo flight for the small gondola using a small (62×10^3 m^3) balloon. The launch was at 12:00 UT on June 21, 1982 and a float altitude of 40.2 km (2.8 gm/cm^2 vertical atmospheric column density) was reached at 14:01 UT. The flight was terminated at 21:00 UT and reached ground 43 minutes later ~60 km Northwest of Pecos, Texas. The payload struck a 130,000 volt power line, resulting in the parachute being ripped apart and the payload free-falling the last 15 meters. Though the styrofoam burned on the outside, the payload received only minor mechanical damage and the data tape was recovered intact. The free fall also demonstrated the ruggedness of BGO which operated flawlessly on its return to the laboratory.

8.4 Flight Results and Comparison to Predictions

The background spectra of flight 1282P for both HgI_2 detectors, top and bottom, are shown in Fig. 8.4. Only the vetoed spectrum of the top detector is presented because the valid spectrum was contaminated with spurious events due to multiple triggering of the event logic by energetic paticles. The spectra from flight 1292P are presented in Figs. 8.5 and 8.6. The electronic modifications made between flights

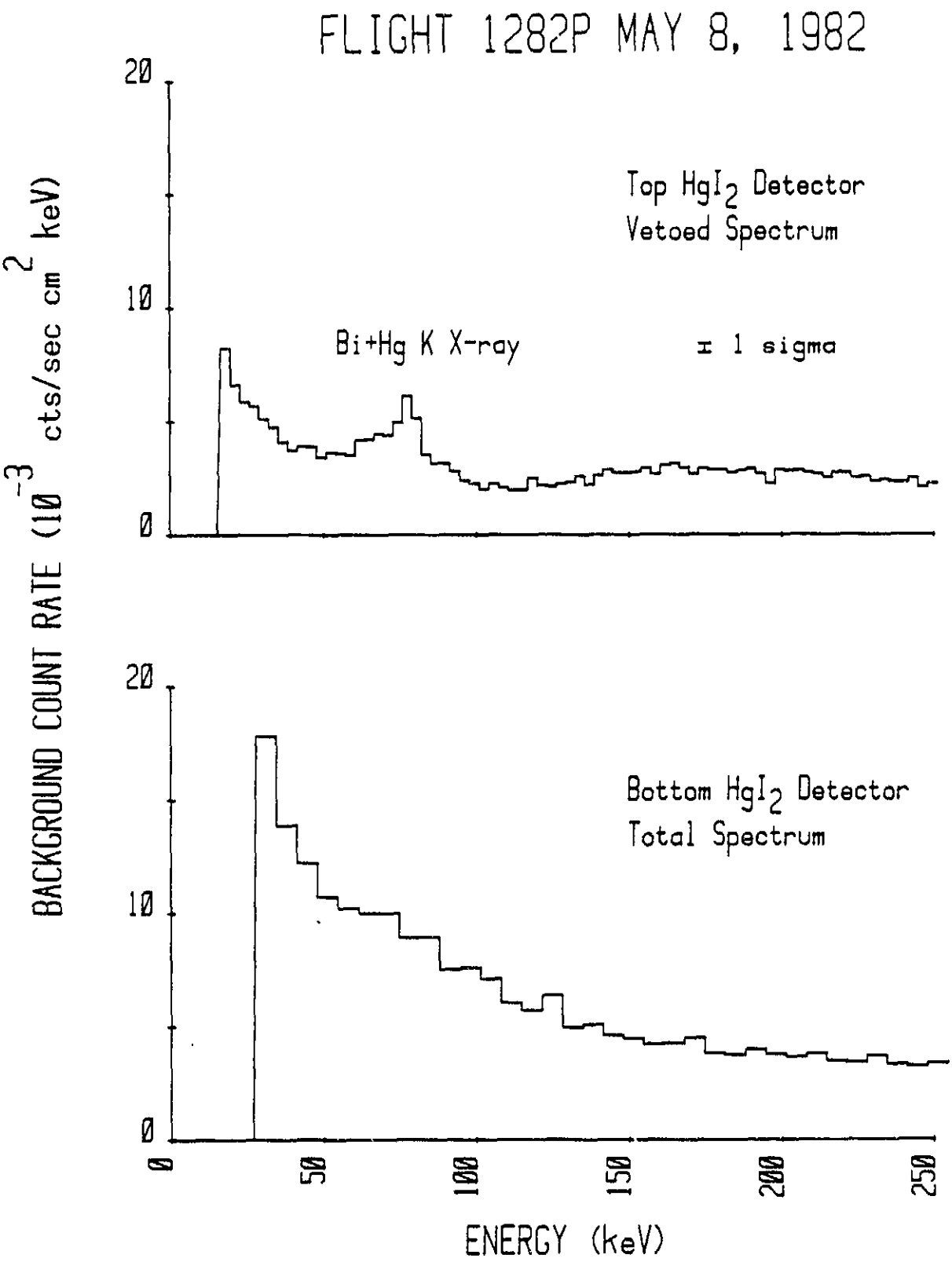

Figure 8.4 Vetoed and bottom spectra from flight 1282P. The veto rate of the top detector was .15 counts/sec over the energy range 40 to 80 keV. As can be seen, the energy resolution of the bottom detector (used as an anticoincidence shield) was substantially broader than the top detector.

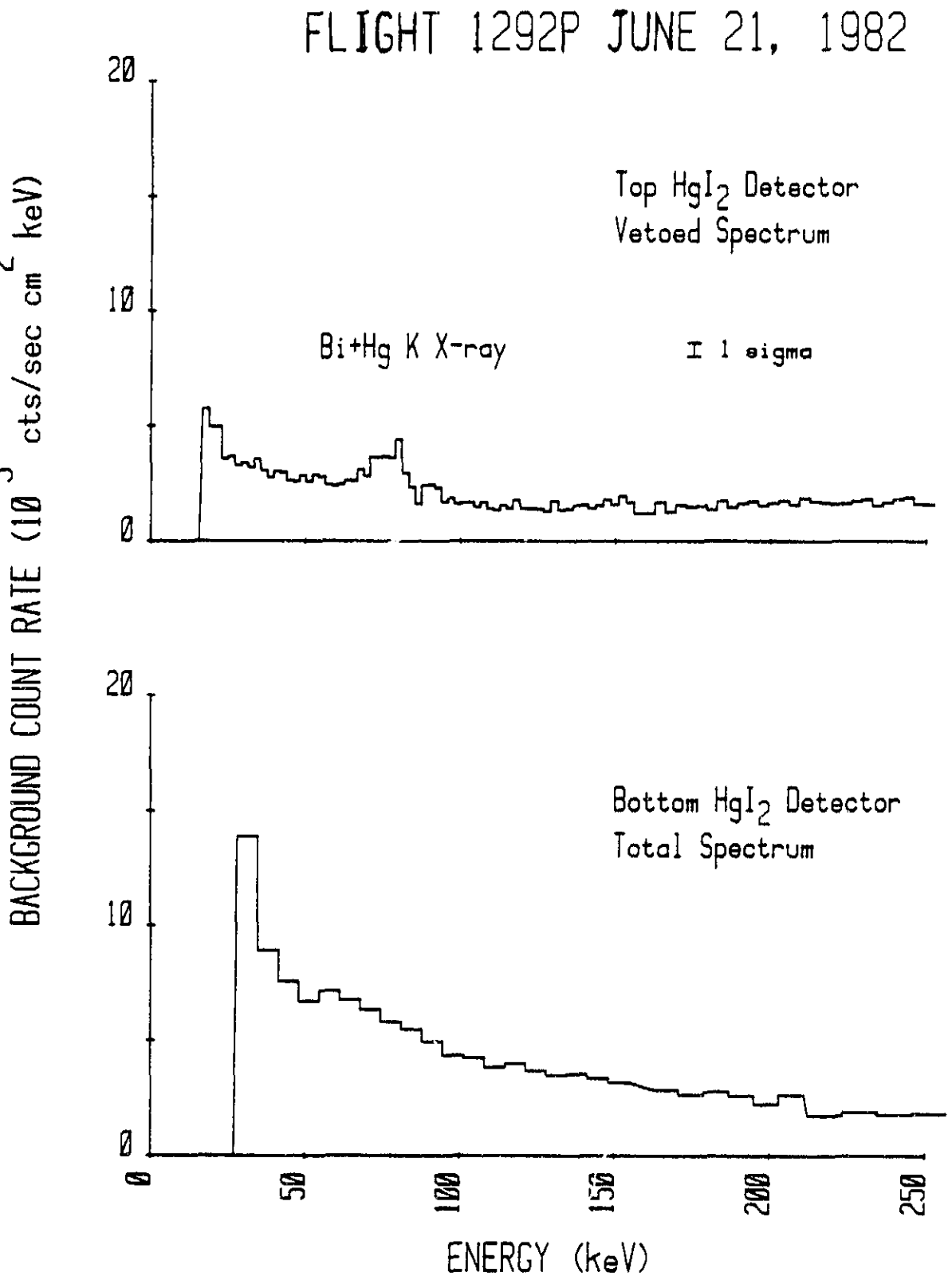

Figure 8.5 Vetoed and bottom spectra from flight 1292P. Note the decrease in count rate from the previous flight as well as the resolved bismuth K-beta X-ray at 87 keV in the vetoed spectrum.

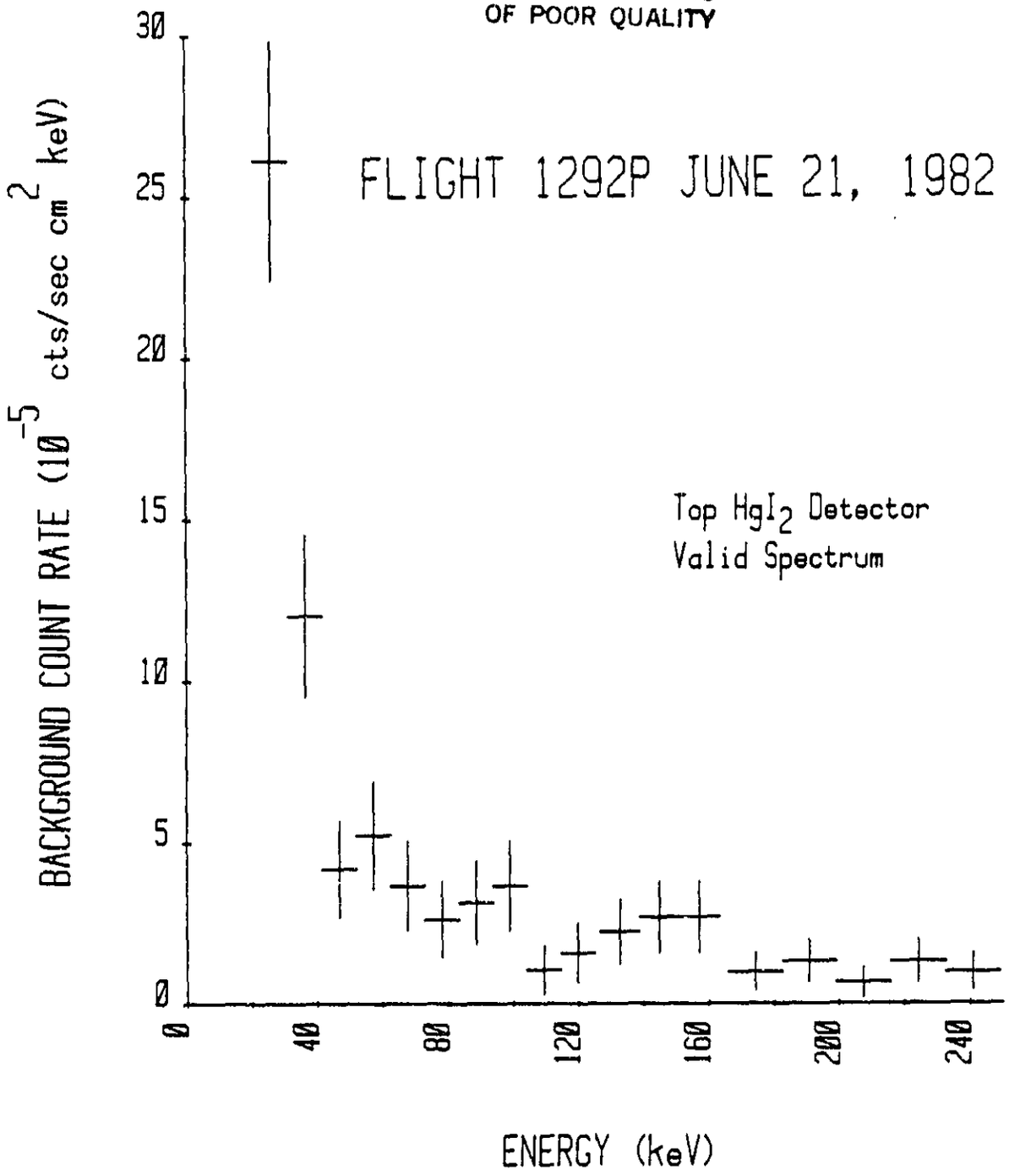

Figure 8.6 Valid spectrum from flight 1292P. The measured background rate was 4.2×10^{-5} counts/sec cm^2 keV (40-80 keV). There is a possible feature at 59 keV (see text). The increase in count rate below the 40-80 keV range of interest was due to detector "bursts" (see text).

were successful in suppressing the multiple triggering and the valid spectrum (Fig 8.6) is free of the single channel peaks.

All these spectra were integrated over time starting at float and ending at flight termination (or power failure for flight 1282P). Arrival at float altitude was determined by when the count rate versus time stabilized as shown in Fig. 8.7. The two maxima in the count rate vs. time plot are due to the Pfotzer maximum, the altitude (~17 km.) at which the flux of cosmic ray secondaries reaches its peak. The payload passed through this region slowly on the way up and quickly on the way down.

The vetoed spectra for both flights are very similar in that they are featureless except for the bismuth and possibly mercury K X-ray line features. The K beta X-ray of bismuth was also resolved in the second flight. The overall count rate decreased by about 25 to 35% from the first flight to the second. This occurred in both detectors, top and bottom. Changes this large cannot be explained by the differences in altitude between the two flights. As can be seen in Fig. 8.7, the count rate was 30% higher ~20 minutes before float which corresponds to a difference in altitude of 6 km. in contrast to the actual difference of 2 km. in float altitude between the flights. The only other differences between the two flights was the change in the event logic electronics and the absence of the adjacent 1400 kg. payload in the second flight. Multiple triggering only accounted for a small part of the higher count rate in the first flight based on the number of events in the single channel peaks. A massive payload above the detector as in flight 1282P, however, would produce an increase in the

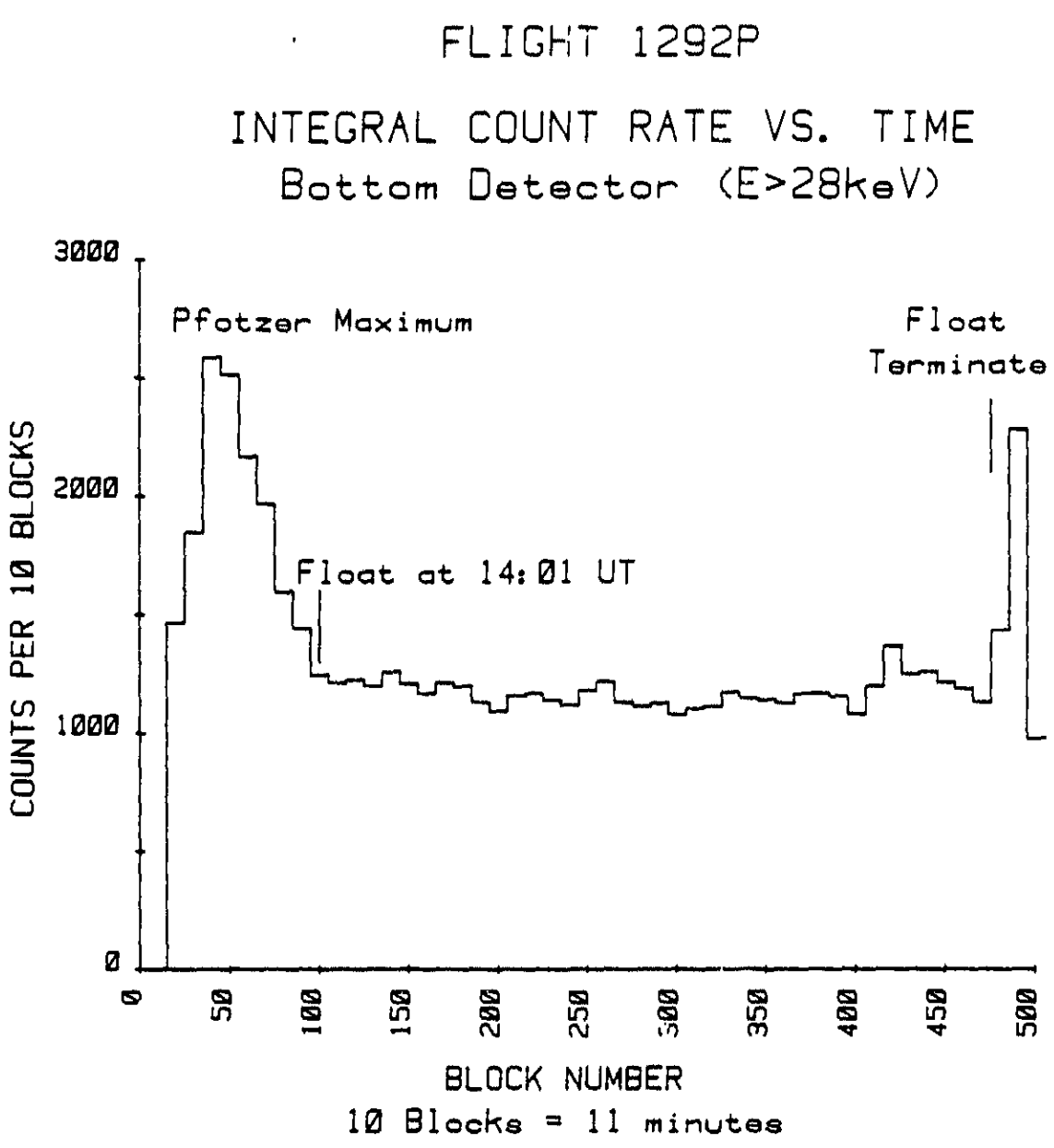

Figure 8.7 Count rate vs. time of the bottom detector during flight 1292P showing both ascending and descending passages through the Pfotzer maximum and the steady count rate at float altitude.

local radiation flux due to interactions with the primary cosmic rays. If the massive payload is responsible for the higher count rate in the first flight it would be equivalent to an atmospheric slab of 9 gm/cm^2 vertical column density.

As expected, the total number of valid background counts accumulated during the second flight was small (31 counts, 40 to 80 keV) and the spectrum is featureless. There are a few extra counts (6 cts. total) close to 59 keV. For a flight of this duration, 2.6 counts would be expected at this energy from inelastic neutron scattering from the ^{127}I nucleus. Unfortunately, the tungsten K-alpha X-ray energy is also 59 keV so this barely significant feature might also be fluorescence of the passive graded shield or a combination of both. Based on their timing signature (many simultaneous low energy events), the excess number of counts at very low energies are due to leakage current "bursts".

Table 8.2 contains the float background count rate predictions of Section 7 as well as the measured values. The valid count rate agrees surprisingly well. The gamma ray prediction of the Monte Carlo simulation (Wood 1982) can be directly tested against the strengths of the K alpha and beta line features of mercury and bismuth in the vetoed spectrum. During flight 1292P, the measured value was 25% smaller than predicted, which might indicate that the gamma ray contribution was overestimated. This is also indicated in the energies above 160 keV. If the gamma ray prediction is scaled down to match the measured results for the line features and the higher energies then the discrepancy at lower energies would be enhanced. This discrepancy

probably indicates that the neutron contributions at lower energies were underestimated, which could easily be the case, considering the uncertainties in the neutron fluxes and cross sections.

Table 8.2

Comparison of Measured and Predicted Count Rates at Float in the Top HgI_2 Detector for Flight 1292P

	Valid Count Rate (10^{-5} cts/sec cm^2 keV)	
Energy (keV)	Predicted†	Measured
40 - 80	2.9	4.2 ± .7
80 -120	1.6	2.6 ± .6
120-160	1.0	1.9 ± .5
160-200	1.8	1.5 ± .5
200-240	1.7	1.0 ± .4

Bismuth and Mercury K X-ray line feature††:

Predicted†	Measured
3.6×10^{-2} cts/sec cm^2	2.7×10^{-2} cts/sec cm^2

† Sum of predicted background due to gamma rays and neutrons (Tables 7.1 and 7.2 respectively). The gamma ray contribution was determined by a Monte Carlo simulation while the neutron contribution was calculated analytically.

†† Present only in vetoed spectrum

9.0 CONCLUSIONS

Previous to the research work described in this thesis, HgI_2 showed great theoretical potential for use in hard X-ray astronomy. The combination of high energy resolution at room temperature plus a high photon quantum efficiency seemed ideal for many balloon and satellite detector applications. Yet, experience in the field operation of HgI_2 was minimal and background count rate information at high altitudes did not exist. Development of HgI_2 specifically for use as an astronomical X-ray detector here at MIT over the last 3 years has changed this situation. Procedures for handling and packaging detectors have been developed that produce stable and dependable HgI_2 detectors for use in the field. HgI_2 detector assemblies have been constructed and flown at balloon altitudes and the detectors operated flawlessly on all occasions.

A major limitation to the application of HgI_2 in X-ray astronomy is the inability to fabricate individual detectors larger than ~ 1 cm^2. A scheme to overcome this limitation involves the use of X-ray concentrators to increase the effective area of a shielded, low-background HgI_2 detector. The concentrator consists of a paraboloid shell lined with lithium fluoride crystals that Bragg diffract on-axis incoming X-rays to the focus of the paraboloid, where a small area detector is located. To establish the expected sensitivity of this concentrator /detector design, the background counting rate of the shielded HgI_2 detector at balloon altitudes had to be determined. A balloon-borne gondola containing a prototype detector assembly was designed and constructed to measure this background rate. The prototype detector

consisted of thin HgI_2 detectors surrounded by a large bismuth germanate scintillator operated in anticoincidence. This gondola was flown twice in the spring of 1982 from Palestine, Texas.

The second flight of this prototype instrument established a background counting rate for a bismuth germanate-shielded mercuric iodide detector of $4.2 \pm 0.7 \times 10^{-5}$ counts/sec cm^2 keV over the energy range of 40-80 keV. This measurement was within 50% of the predicted value. The prediction was based on a Monte Carlo simulation of the detector assembly in the radiation environment at float altitudes (~40km). The Monte Carlo simulation can now be used to investigate the detector design parameters (geometry, discriminator levels, etc.) to attempt to lower the background rate even further.

Based on a background rate of 4.2×10^{-5} cts/sec cm^2 keV, calculations indicate that with 4 concentrators and 4 detectors systems a celestial X-ray source with 1/100 the intensity of the Crab Nebula could be detected in 1.5 hours. This excellent sensitivity is achieved by simultaneously reducing the background by BGO shielding a HgI_2 detector, and increasing the effective area using hard X-ray concentrators.

The prescription for reducing the background rate by a factor of ~10 over previous balloon-borne hard X-ray detectors can be summarized very simply: use very high quantum efficiency detectors shielded by dense, high Z active scintillators. Because they are well suited to this experimental approach, HgI_2 and BGO are both likely to become major detector materials in X-ray astronomy. Furthermore, their ease of handling and improved performance at moderately reduced temperatures

enhance their desirability for balloon and satellite use.